DYNAMIC TESTING TO DETERMINE SOME MECHANICAL PROPERTIES OF ALUMINUM, COPPER, AND DRY EGLIN SAND USING SPLIT HOPKINSON PRESSURE BAR (SHPB), HIGH SPEED PHOTOGRAPHY AND DIGITAL IMAGE CORRELATION (DIC)

By

SWAPNIL S SANKAYE

Bachelor of Science in Mechanical Engineering

Government Engineering College

Dr. Babasaheb Ambedkar University

Aurangabad, Maharashtra

2008

Submitted to the Faculty of the
Graduate College of the
Oklahoma State University
in partial fulfillment of
the requirements for
the Degree of
MASTER OF SCIENCE
July, 2011

DYNAMIC TESTING TO DETERMINE SOME MECHANICAL PROPERTIES OF ALUMINUM, COPPER, AND DRY EGLIN SAND USING SPLIT HOPKINSON PRESSURE BAR (SHPB), HIGH SPEED PHOTOGRAPHY AND DIGITAL IMAGE CORRELATION (DIC)

Thesis Approved:

Dr Ranga Komanduri

Thesis Adviser

Dr Sandip Harimkar

Dr Don Lucca

Dr. Mark E. Payton

Dean of the Graduate College

ACKNOWLEDGMENTS

I would like to thank from the bottom of heart Dr. Ranga Komanduri, my thesis advisor, who gave me an opportunity to pursue my M.S. research under his valuable guidance. He has been very considerate and supportive of my work and provided ideas throughout my thesis work. His valuable guidance, patience, knowledge, time, charm and faith made this work possible. I appreciate his valuable time in organizing my research and in reviewing my thesis and making necessary improvements.

I would also like to thank Dr. Sandip Harimkar and Dr. D Lucca for serving as a committee member in my master's program. I thank them for your valuable time in reviewing my thesis and help me improve, refine and expand my thesis.

This project has been funded by Department of Defense through a DEPSCOR grant (FA9550-08-1-0328) and monitored by the Air Force Office of Scientific Research (AFOSR). I would like to thank Dr. David Stargel, Program manager, Multi-scale Structural Mechanics and Prognosis, AFOSR for the support of this work.

Special thanks are due to Dr. Hongbing Lu, Dr. William Cooper and Dr. Hartely for their valuable comments and suggestions as well as valuable inputs time and again. The weekly technical meetings of the SHPB group helped me in achieving what I wanted to accomplish in this research.

I would like to thank my colleagues Vijay Subramanian and Chetan Kulkarni for working with me on this project day and night. I also thank for their friendship and moral support during the project work. Besides the names mentioned above, I would like to thank my friends Hrishikesh, Gaurav, Kumar, Vishvesh, Manish, Dhananjay and Shalaka for their support over the past two and half years.

I owe my deepest and sincere gratitude to Oklahoma State University for giving me the opportunity to work with such great facilities and amenities. Without the support of OSU, the projects I worked on would have been a distant reality. For aspiring engineers OSU is the best place they should opt for.

Finally, I am extremely thankful to my mother, Mrs. Mangala Sankaye, and my family for supporting me and helping me reach this point in my life. It is due to their efforts and backup that I have been fortunate enough to get quality education. I extend my gratitude and a special thanks to my elder sister, Suparna for her love and guidance.

TABLE OF CONTENTS

LIST OF TABLES

LIST OF FIGURES

Figure Page

Figure Page

CHAPTER I

INTRODUCTION

Split Hopkinson Pressure Bar (SHPB) is a commonly used experimental apparatus for determining various mechanical properties at high strain rates. First experiments were performed on the Hopkinson bar in the early 70's and 80's. In our research lab we built an advanced or the modified Kolsky bar, commonly known as Split Hopkinson Pressure Bar (SHPB). The significant advancement in the analysis of data collected from SHPB has only been done in the last couple of decades.

SHPB setups, more often than not, consist of two long steel bars; namely, the Incident Bar (IB) and the Transmission Bar (TB). The specimen/sample to be tested is sandwiched between these two bars, for compression tests. Earlier, SHPB was also used for the tensile testing of the specimen. In the working of this apparatus the end of the IB is struck with a striker bar. Due to this, a compressive wave is introduced and propagated within the steel bar, and allowed to traverse towards the specimen. The specimen is sandwiched between the bars as shown in Figure 1.1.

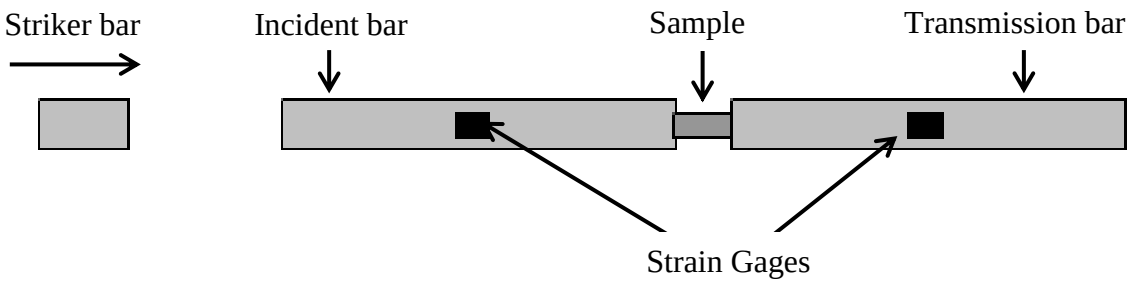

Figure 1.1: Main components in SHPB setup showing sample between the incident and transmission bar

At the other end of the incident bar and the specimen face, due to impedance mismatch, the wave partially reflects back towards the striking end, while part of the wave is transmitted through the specimen. Then the wave passes from the specimen onto the second bar, causing plastic deformation in the specimen, which is irreversible. It has been shown that the stress and strain rates of the specimen are proportional to the reflected and transmitted waves. Specimen mechanical behaviour, such as stress-strain properties can be determined by analysing the strain in both steel bars using strain gauges.[1]

There have been numerous studies using SHPB apparatus. Some of them used foam, aluminium, copper, plastics, clay, glass beads etc. as the samples material but currently extensive research is being carried out on sand. This thesis deals with the tests carried out on aluminum (Al 2024) and copper (C360), coupled with high-speed photography and Digital Image Correlation (DIC) analysis. These tests were carried out to calibrate the SHPB setup at OSU, and to compare the results with those reported in the literature. Most of the tests were performed on dry Eglin sand to determine its dynamic

mechanical properties. Several issues affect the accuracy of the results. They include longitudinal wave dispersion, mismatch of the impedance between the bars and the specimen, strain gauge precise measurement and proper mounting of it on the respective pressure bars. A specific area of advancement is one of the new ways to determine the bars dispersive nature, and hence minimizing the distorting effects.

In this investigation, the compressive response or the dynamic mechanical behavior of aluminum, copper (coupled with high-speed photography and DIC analysis) and dry sand (Eglin sand) was investigated. Variable parameters for the sand samples are the specimen initial mass density, particle size, and pulse shapers used at conditions of approximately constant strain rate and applied pressure. An advanced or modified SHPB has been used; employing a pulse shaping technique to produce controlled dynamic loading pulses that allows the specimen to deform uniformly under dynamic equilibrium conditions at constant strain rate. During each dynamic test, the stress equilibrium conditions are maintained. The pulse-shaping technique was found to be independent of the confinement. Pulse shaping enables systematic variation in strain rates in the specimens [2]. Experimental results show negligible strain-rate effects on the compressive response of sand within the strain-rate range covered. The compressive response is significantly differed and stiffer if high density specimen was used. Adding moisture definitely alters the relative movement of sand, and has an effect on the stress-strain behavior of sand. This area of addition of moisture to grains at various percentages has to be explored even further. The axial stiffness is found to increase with confining pressure. These results contribute in creating a quality database of dynamic properties to be used for the development of physics-based constitutive models for sand.

1.1 Basic principle of SHPB

The split Hopkinson pressure bar tests are commonly used for determining material properties at high strain rates. Significant advancements in the areas of testing techniques, numerical methods, and signal processing have improved the accuracy and repeatability of high strain rate testing. Constant strain rate tests can be performed consistently at strain rates approaching $10^3 s^{-1}$. In the split Hopkinson pressure bar tests, a short cylindrical specimen is sandwiched between two long steel bars, as shown in Figure 1.1. The bars are generally made of high strength steels, with diameters of 0.75 in. and a length of 5 feet. The ends of the steel pressure bars and the specimen are machined flat precisely to ensure prescribed boundary conditions. Typically, a striker bar is shot into the end of the input bar generating a compressive stress pulse. As soon as there is an impact of the striker and the incident bar, the pulse generated travels along the bar towards the incident bar-specimen interface, at which location the pulse is partially reflected back into the incident bar and partially transmitted through the specimen and into the transmission bar. The reflected pulse is reflected back as a wave in tension whereas the transmitted pulse remains in compression. The strain histories in the two pressure bars are recorded using strain gages mounted on the incident and transmission bars, respectively. So long as the pressures in the bars remain within their elastic limits, specimen stress, strain, and strain rate can be calculated from the recorded strain histories. Under certain deformation conditions, qualified later, only two important strain pulses need be identified. These are the reflected pulse and the pulse transmitted through the specimen. Kolsky [3] developed a relationship for calculating the specimen stress which is discussed in Chapter 3.

1.2 Difficulties in testing and analyzing

The pulses acquired from a given sample are the time dependent transmitted and reflected pulses. For a sample to homogeneously deform, the specimen strain rate and stress have to be proportional to the amplitudes of these pulses. The specimen strain is easily calculated by integrating the strain rate which will be described in Chapter 3. Producing a stress-time and strain-time plots are not that tedious, but they are not very useful. Hence, these time dependent pulses must somehow be combined to generate a dynamic stress-strain plot which is quite familiar to the engineering field. Also, determining the first point of each pulse is not a simple or precise matter. Since we are considering the impact events occurring on the order of a few hundred microseconds, alignment of the stress and strain pulses becomes difficult. Often, investigators align these pulses based on the time it takes for the pulses to travel in the bar and sample. This requires that the velocity in each sample be known prior to testing. Furthermore, the pressure bar–specimen interfaces must be perfect for this timing scheme to work effectively. By applying certain numerical methods, these pulses can be aligned without relying on perfect interfaces and knowledge of sample wave velocities. A major concern in longitudinal wave propagation is dispersion. Dispersion is a result of a bar's phase velocity dependence on frequency, which in effect distorts the wave as it propagates. Since it is the properties of the specimen that we are interested, the dispersive properties of the pressure bars needs to be known in order to accurately predict what the pressure pulses look like at the pressure bar-specimen interfaces [4]

1.3 Topics included in the thesis

Chapter 2 covers literature review on the influence of different parameters used in sand samples in the split Hopkinson pressure bar tests. It also discusses the importance of sand testing under quasi static testing and review of that literature relevant to the current investigation. Current areas of research interest in this investigation are also discussed.

Chapter 3 introduces and explains the concept of one dimensional wave theory in a split Hopkinson bar testing. This chapter begins with a schematic description of SHPB setup and then describes the SHPB apparatus used in the present investigation. Descriptions of as to how to test materials under compressive loading at high strain rate and integrate the theoretical models into the data processing method are presented in the wave propagation theory sub-title. The basis for choosing strain transducers, determining signal conditioner characteristics, and implementing numerical analysis procedures are given. It also describes the development of one-dimensional equation of motion governing vibrations in a long, slender, elastic bar. Wave behavior is then described as the wave encounters various discontinuities including step changes in area and material. Herein the equations for calculating the specimen stress, strain and strain rate are derived. The explanations for all assumptions are given.

Chapter 4 presents aims of the proposed work including the problem statement based on the prior work reported in the literature.

The aims of Chapter 5 are to combine the theory with the practice, as well as to present experimental results. Also insights towards improved testing procedures are given. A statistical analysis of the mechanical properties of aluminum and copper are presented, that is applicable to other material types. Further work of creating a speckle pattern on the copper sample for the DIC analysis is presented to compare with the stress-

strain values obtained analytically. Comparisons of the dynamic and DIC stress-strain characteristics of copper are given. This chapter also includes various parameters used for the tests to be performed on Eglin sand such as the effect of initial mass density, effect of pulse shapers at a given constant density of dry Eglin sand and effect of particle size at the same density. The results of the initial mass density on stress strain relationship are compared with Luo *et al's* [5] work done on the same dry Eglin sand (unsorted) last year.

The thesis is concluded in Chapter 6. Recommended areas of continual research and work to be done in future are suggested in this chapter.

CHAPTER II

LITERATURE REVIEW

There are numerous procedures developed to test soil dynamics, along with which there are different kinds of associated problems. In the field of soil dynamics, unfortunately there is no specific approach to investigate various problems such as:

- earthquake engineering
- pile driving
- dynamic compaction

Sand is one of the most easily available and abundant materials in nature. It has been widely used for construction in both civil engineering and military applications. Structural response and damage under high-rate loading are often assessed by numerical simulations, as it is of great concern considering its broad range of applications. Hence, it is mandatory to understand the mechanical properties of the geo materials including sand, specifically under impact and compression loading conditions. The data analysis of the sand on the high rate mechanical and dynamic response of the sand is also considerably useful in many other applications, such as mining, earthquake engineering, and containment of underground explosion [6]. There are two major approaches presented: one of them is the direct analysis of dynamic response of soils [7, 8] and the

other is the study of wave propagation theory in soils [7, 9]. In this thesis, we focus on experimental studies dealing with dynamic response of Eglin sand.

The dynamic response of sand has not been well understood and interpreted even though sand is one of the readily and most available materials in nature and in construction engineering. Extensive research has been conducted on the quasi-static behavior of sand [10]. Strain-rate effects have also been studied, but mostly within quasi-static range [11]. Dynamic response of sand has also been explored under vibratory conditions [12]. Over the past two to three decades sand has been investigated periodically to characterize its high-rate behavior. For efficiently modeling the dynamic behavior of sand one should understand better the effects of moisture content in sand, effective particle size, effects of initial density, hydrostatic pressure besides the strain-rate effects under various loading conditions.

Using the conventional Kolsky bar apparatus, Bragov *et al* [13] conducted experiments and performed analysis on plasticine and clay confined within a rigid steel jacket. Composite striker bars provided both loading and unloading of the specimen to be investigated. These experiments synthesized the mechanical properties in compression at a strain-rate of $4x10^{3}s^{-1}$. Further work by Bragov *et al* [14] investigated the dynamic response of dry sand using the same conventional Kolsky bar method. The dry sand was loaded at stress amplitudes of 80 MPa, 150 MPa, and 500 MPa. In these experiments, the specimens were confined in aluminum or steel jackets allowing the specimen to be in a state of nearly uniaxial strain. Using the conventional Kolsky bar apparatus, Ross *et al*. [15] evaluated the effect of a single short pressure pulse propagating through long specimens of dry sand, silica flour, clay, glass beads, and steel balls. Varying the

percentage of moisture content in dry sand, the static and dynamic compaction methods were characterized. Pierce [16] investigated the effects of moisture content and different confining methods using a conventional Kolsky bar for 20 and 30 grit size Ottawa sand and Eglin sand. These materials have particle size of majority between sieve size #20 and #30, which is about 600 to 850 μm.

Felice *et al.* [17] conducted tests to investigate the behavior of clayey sand at high strain-rates. Variables include the percentage of water contents, dimensions of the specimen and loading conditions. The uniaxial stress-strain behavior of compacted moist Eglin sand, Tyndall sand and Ottawa sand were conducted by Veyera [18] at strain rates of ~ $10^3 s^{-1}$ and $2x10^3 s^{-1}$ The humidity was varied from 0% to 100% of saturation. Specimens at 20% saturation, showed similar response as dry sand, whereas 40% saturation showed a stiffer response. These tests were conducted using a conventional Kolsky bar apparatus. The research efforts, specifically that of Bragov *et al*, Veyera *et al*, and Felice *et al* [14, 17-19] have contributed towards the understanding of the dynamic behavior or the mechanical response of sand. It has been shown that there has been an increase in the stiffness of the samples in the material response due to various methods of compaction of specimens. Sometimes, this compaction method also makes results appear contradictory. For example, the results and conclusions presented on loose or uncompacted sand show opposite trends in moisture effects as compared to the results by Veyera [18]. Bragov *et al* [14] also investigated the dynamic behavior of dry sand. Ross *et al*., Charlie *et al*. and Pierce *et al* [6, 15, 16] used samples with larger aspect ratios. Due to low longitudinal wave speed of sand, the dynamic stress equilibrium during the early stages in the specimen was doubted.

Despite extensive research efforts, the high strain-rate response of sand is still not well interpreted and understood. There is a need for a systematic research considering the effect of moisture, initial mass density, particle size and strain-rate effects on sand response which is identified as technology gap. One of the reasons why sand is not characterized dynamically is the complex nature of the sand specimen. Apart from that, another reason is the lack of standardization of the dynamic experimental methods. Due to the complex nature of the material, variations of the testing conditions inherent in the characterization methods need to be minimized in order to reveal the intrinsic material response. Recent advancements in Kolsky-bar technique have significantly improved the ability to control the testing conditions the specimen experiences. For example, the conventional Kolsky-bar produces a trapezoidal incident pulse with very fast initial loading rates. The fast loading rates can be used to accelerate a metallic specimen to high velocity but for the geo-materials the longitudinal wave speeds are slower, and requires slower loading rates to allow the specimen to acquire stress equilibrium and constant strain-rate [14].

Till now, the high-rate mechanical behavior and properties of the sand have not been investigated extensively due to the difficulties and hurdles of dynamic experimental setups and techniques. In addition to this, the complex nature of the sand has made it less exciting to perform extensive research. Split Hopkinson pressure bar (SHPB) is employed to obtain stress–strain response of engineering materials at high strain rates since 1949 [3]. SHPB has recently been utilized to characterize dry and unsaturated sands at high strain rates [13, 14, 17-20]. Since sand is rather a unique and distinct material compared to most engineering materials, the regular assumptions in the SHPB experiment may need

to be revised. A fraction of the air-filled void volume in a dry sand specimen makes a considerable change in its wave speeds. The wave speed is low and the rate of wave attenuation is very high which can significantly affect the results acquired from SHPB experiments. One can understand a sand specimen with low density, low rigidity, and low wave speeds. All of these characteristics are great challenges to overcome for dynamic testing. When the wave speed is very low, a compressive wave may propagate in the specimen, making the specimen deform progressively instead of uniformly along the axial direction [21]. This violates a basic assumption of uniform deformation in SHPB experiments because of non-uniformity in specimen deformation [3].

The stress-strain data for the sample can be obtained if the dynamic stress equilibrium in the specimen is reached once the incident, reflected and transmitted waves signals are measured. The equilibrium state may not be reached and satisfied automatically, especially when the sample used in the experiments are soft [22]. It has been found that it is nearly impossible to achieve dynamic stress equilibrium in a conventional Kolsky bar apparatus on soft materials, for example, rubbers. The reason behind that is due to the very high initial loading rate in the incident pulse. Also, it is valid even for very thin specimens [22]. Hence, it is mandatory to make advancements in the loading part of the incident pulse. An efficient and proven method to control the loading pulse is to use a pulse shaper. It is employed at the impact end of the incident bar (Figure 3.1). The pulse shaper is commonly a punched small disk made of metal, e.g.: copper, aluminum or plastic, rubber or even paper. The selection of appropriate pulse shapers may depend on specimen material and strain-rate. Varying the material and size of the pulse shaper controls the loading profile of the incident pulse. The dynamic stress

equilibrium and constant strain-rate deformation in a specimen would depend on striker bar velocity, striker length, and material. It is of great importance to collect precise and reliable stress-strain data at various constant strain rates to investigate the strain-rate effects of materials and to develop strain-rate-dependent mechanistic models.

The amplitude and duration of the incident compressive wave can be controlled by (a) varying the geometry of the copper disc (b) changing the striker bar velocity, and (c) changing the length of the striker bar. A well-shaped incident pulse produces dynamic stress equilibrium and constant strain-rate within the specimen. In a conventional SHPB test, e.g., on dry sand by Veyera *et al* [18], the incident pulse is nearly trapezoidal. This generates a decreasing reflected pulse indicating a constantly changing strain-rate in a specimen that may have become non-uniform through the initial rapid loading. In this research we load the specimen with controlled pulses that allow the specimens to acquire stress equilibrium at nearly constant strain-rates. The specimen length is limited due to the low longitudinal wave speed in sand. On the other hand a long specimen delays stress equilibrium and causes initial non-uniform deformation. Prior to evaluating the sand a study was conducted by Song *et al.* [21] to determine the specimen thickness required to ensure dynamic stress equilibrium within the specimen.

It is well known that longer the specimen, longer is the time it takes for stress equilibrium to reach. Furthermore, sand is considered as a typical attenuating material. When propagating through the sand specimen the amplitude of stress wave is significantly attenuated or disturbed. This attenuation of the stress wave, results in more severe non-uniform deformation and stress, along axial direction in the specimen. A modified Lagrangian analysis procedure, usually used in data reduction for plane shock

wave experiments was developed by Felice *et al*. [17, 19], to compute the dynamic stress–strain response for soils using SHPB setup and experiments. However, to reduce the physical effect of stress wave attenuation careful consideration of sand specimen length should be taken into account. The dimensions of the sand specimen thus need to be carefully chosen to satisfy the requirement of dynamic stress equilibrium, which has been addressed by Felice *et al* [19]. An aspect ratio of less than or equal to 0.2 was proposed for dynamic testing of the soil. However, it has been shown that reducing only the specimen thickness or length does not suffice to satisfy the stress equilibrium particularly in soft specimens, such as sand. Hence it requires further modification and advancements to the conventional SHPB technique and setup [2, 21]. To facilitate the specimen to reach stress equilibrium quickly there has been considerable studies conducted on pulse shaping techniques and methods to generate a relatively-low rate of loading [23, 24]. Also, the pulse shaping techniques are capable of producing constant strain rate deformation in the specimen by producing different shapes of incident pulses. This is always desired to study and analyze the strain-rate effects.

Big hurdle is to pack the sand specimen carefully prior to testing. The packing material has a significant role to play in the mechanical response of the confined sand. Different packing materials provide different confinement in the radial direction of the specimen which in turn results in different axial stress response in the specimen. Previous work showed that compliance of the confining tube and friction between the sand specimen and the inner surface do not have a significant effect on the measured characteristics of the sand. Later work by Bragov et al. [14, 25] showed that friction force between the sand and the inner surface affects the inner surface of the confining tube at

pressures in sand from 50 to 100 MPa. A thin layer of a lubricant, in our case grease, is used on the inner surface of the confining tube as well as on the end surfaces of the incident and transmission bars to reduce friction. The importance of lubricants was presented by Bragov *et al* [13].

Uniaxial strain state is achieved with a rigid confinement, whereas using a very soft confinement makes the sand sample in a nearly uniaxial stress state. The sand specimen confined with a steel or hard aluminum alloy jacket has been mostly characterized with a conventional SHPB [6, 13, 14, 17, 19]. The dynamic response of the sand confined with different materials has been less investigated. Furthermore, the loading conditions on the sand specimens have not been actively controlled in the previous investigations. In this research, we have made advances and modified the SHPB apparatus to conduct dynamic characterization of the Eglin sand at approximately same strain-rates. The strain-rate effects on the compressive response of the Eglin sand are yet to be more explored or examined. When subjected to high loading rates, the mechanical properties of geo-materials, such as soils, sand, and concrete compared to metals are less characterized and consequently less understood. A better understanding of the dynamic response of sand is necessary to better describe the response of soils by incorporating associated physics into the constitutive models. Predictive capabilities of current sand constitutive models are limited due to the complex nature of the material. In particular, parameters, such as loading rates, density, and moisture contents need to be considered as variables. For example, partially saturated soils under loading exhibit a multiphase behavior due to four different constituents interacting to give the overall material response

(1) Soil skeleton

(2) Pore water

(3) Grain stiffness

(4) Pore air

Constitutive models will have to account for the mechanical response of these constituents and the interactions between them. The main aim is to determine if the basic assumptions used in SHPB techniques can be verified and if the data is repeatable. Bragov *et al*. [14] investigated the dynamic behavior of dry sand. Recent developments in SHPB techniques have significantly improved the ability to control the testing conditions the specimen experiences.

CHAPTER III

PROBLEM STATEMENT

The mechanical behavior of metals such as aluminum and copper cylindrical samples are investigated in this investigation. The main aim of testing these metals is to calibrate the setup and make sure the stress equilibrium is achieved while comparing the results with those reports in the literature. A new approach of DIC analysis on deformation of cylindrical copper sample was introduced to verify the stress-strain values obtained from the strain gages were in fact precise. This work was done so as to make sure that the tests to be performed on dry Eglin sand would have less dispersion effects and human errors.

From the literature review it was found that the response of sand to mass density, moisture content in the sand, the confinement used, and use of high pressures was actively investigated. Factors, such as grain shape, size, strength, and moisture content contribute to the complexity of the model. Processes, such as grain interactions and grain fracture need to be investigated for the development of a model. Experimental characterization of the mechanical behavior of sand under compression is essential for the development and verification of such a constitutive model.

Based on the literature review, presented in Chapter 2, it can be seen that even though the mechanical behavior of sand has been investigated for almost a century, much of it has been for unsorted sand at pressure of 100 to 400 MPa. For testing of sorted sand, i.e. choosing a particular size of sand at a certain density, very few investigations were reported. This experimental investigation is aimed to characterize the behavior of Eglin sand of certain grain size at a given density. Also, the effect of different pulse shapers at constant density of sand at a particular size is investigated. Using the technique of confined compression, the mechanical behavior of sand under uniaxial compression is investigated. The primary factors considered are initial mass density, effect of particle size at constant density, and effect of pulse shapers. Three different initial mass densities of sand namely, 1.51, 1.57, and 1.63 g/cm^3 are investigated. The effect of particle size at constant density of 1.57 g/cm^3 on the mechanical behavior is investigated at four grain sizes, namely, particle size = 850 μm (sieve size 20), particle size = 425-500 μm (sieve size 40), particle size = 212 μm (sieve size 70), and particle size = 150 -180 μm (sieve size 100). The results of this investigation are presented in this thesis.

CHAPTER IV

EXPERIMENTAL SETUP, CONDITIONS AND TEST PROCEDURES

Uniaxial compression tests were conducted under dynamic as well as quasi-static loading conditions using a Split Hopkinson Pressure bar (SHPB) also known as the modified Kolsky bar. SHPB was used in this investigation for dynamic compression testing only, which is shown schematically in Figure 4.1. It shows the main components of the SHPB apparatus as well as the advancements made, namely, use of pulse shapers, momentum trapper, data acquisition unit etc.

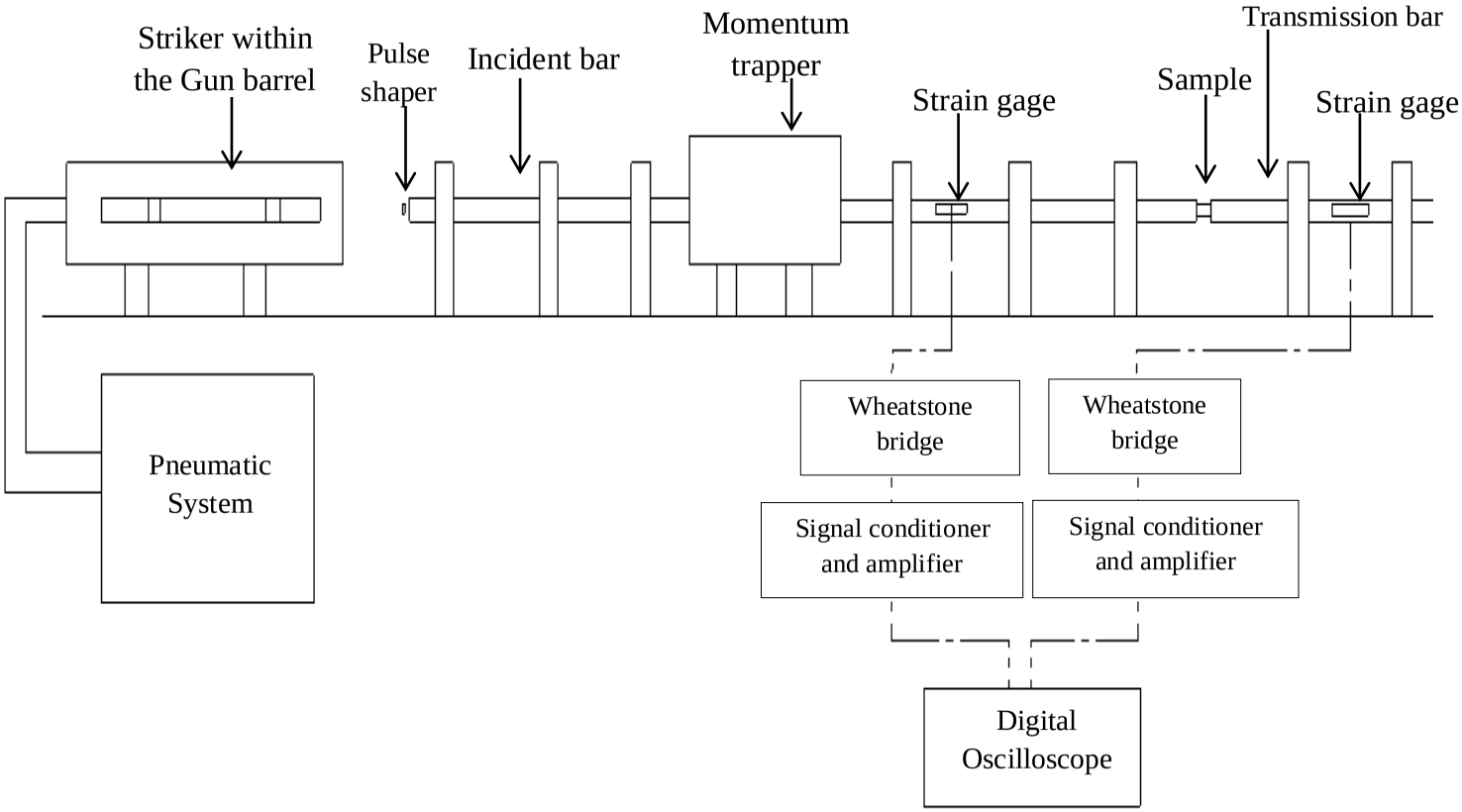

Figure 4.1: Schematic of the SHPB apparatus

4.1 Components of a SHPB setup

As such, there is no hard and fast rule or a standardize design for SHPB setup, but still the apparatus has some common elements in it.

a) Two long, symmetrical and uniform cross section pressure bars are used. The uniformity is generally achieved by precision center less grinding. The length to diameter ratio of these bars is between 20 and 100 and they are generally made (preferred) from the same material. Different materials used are aluminum (E= 90 GPa), titanium (E= 110 GPa), magnesium (E= 40 GPa), maraging steel (E= 210 GPa). The ends of the bar are machined flat and orthogonal to the bar axis with high accuracy to make sure that the good contact is established between the sample and the bar and also between the striker and the bar.

b) A solid base and a bearing and alignment fixture for precise alignment to satisfy 1-Dimensional wave propagation conditions.

c) A pneumatic or a compressed gas launcher/gun barrel so as to shoot the striker bar towards the incident pressure bar made from the same pressure bar material.

d) Strain gages which are mounted on both the bars in order to measure the stress wave propagation in the bars.

e) Required instrumentations and data acquisition system to control, record, and analyze the data obtained from the strain gauges on the bars.

The original apparatus was by Kolsky in 1949 [3] and is named after him. It primarily consists of three rods: a striker bar, an incident bar, and the transmission bar. The striker bar is driven by a pneumatic pressure to apply an impact load on the specimen. To record

the deformation and loading-unloading data in the specimen, the incident and transmission bars are introduced with sensors and load carriers. The one dimensional stress waves in the bars carry information characterizing the loading conditions to the bar ends [26]. Over the years the original setup of Kolsky bar has been continuously improvised, with the enhancement in instrumentation for measuring stress waves and the increase in experience for conducting such instrumented experiments [27-30]. Apart from the standard and basic components in a conventional Kolsky bar, a pulse shaper at the impact end of the incident bar was employed in the modified Kolsky bar used in this investigation (Figure 4.1). This modification was done to control the loading profile, which in turn allows sand specimens to deform at a nearly constant strain-rate under approximately uniform stress state. The pulse-shaping technique was initially developed over three decades ago by Duffy *et al* (1971), and then was extensively used at Los Alamos National Laboratory by Follansbee *et al* [31]. The technique was later quantitatively modeled by Nemat-Nasser *et al*. [29], and Frew *et al* [24].

4.2 Dynamic compressive experiments

The SHPB description of the apparatus for compression test is given in the following: Figure 3.1 shows a schematic diagram of the SHPB setup and Figure 4.2 shows a photograph of the actual SHPB apparatus. Dynamic compression tests were conducted using the modified SHPB apparatus built at Oklahoma State University (OSU). Both the incident and transmission bars are made of maraging steel with Young's modulus of 210 GPa, density 8100 kg/m^3, and bar wave speed 5055.25 m/s. The incident, transmission, and striker bars are 24, 12, and 2 feet long, respectively. The outer diameter

of the bars is 0.75 inch. Figure 4.2 is a photograph of the actual SHPB setup viewed from the transmission bar side and Figure 4.3 shows the photograph of the setup from incident bar side.

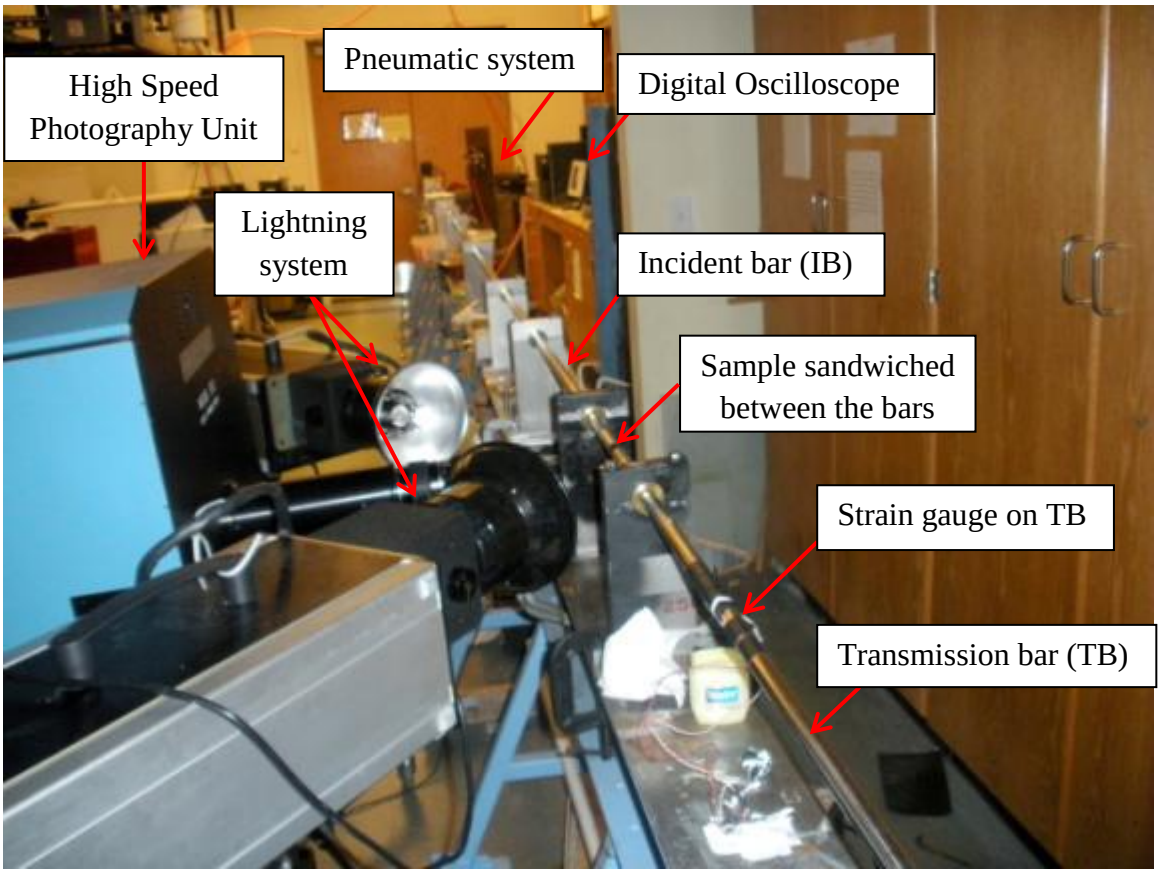

Figure 4.2: SHPB experimental setup from the transmission bar side

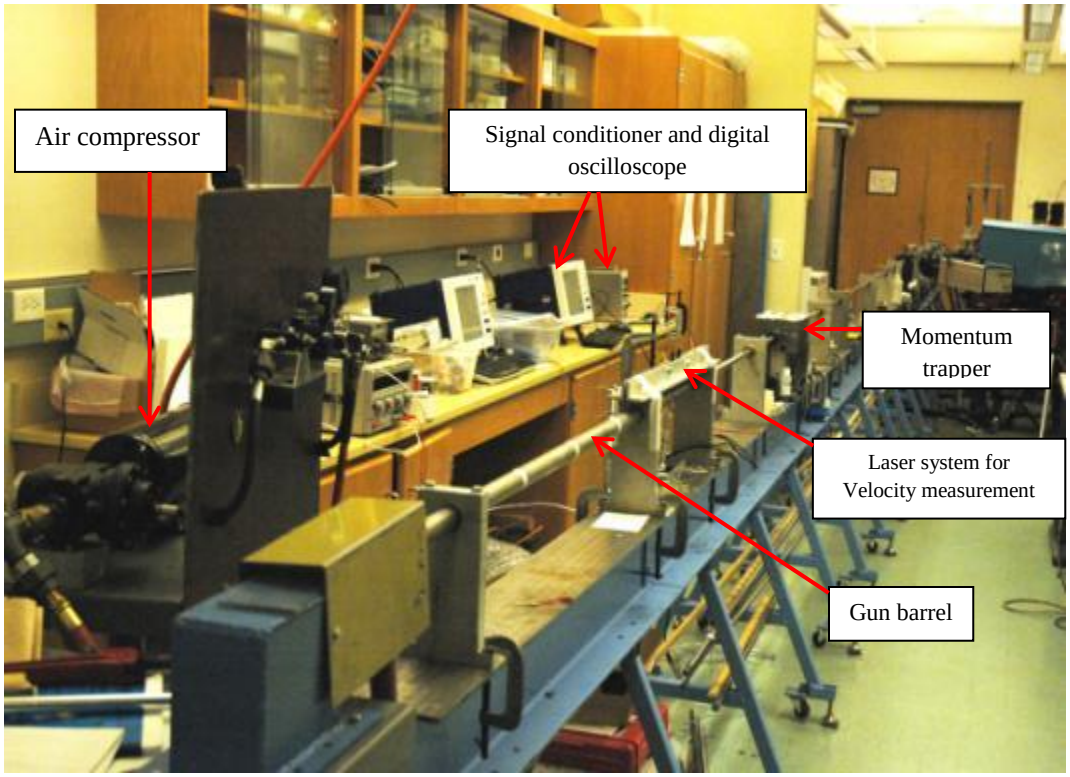

Figure 4.3: SHPB experimental setup from the Incident bar side

A Pneumatic launcher is used to launch the striker bar as shown in Figure 4.4. At certain pressurized air measured by the digital pressure gauge, the gun barrel launches a striker bar as soon as the pressure is released with the help of a pressure relief valve. This forces the striker bar to impact on one end of the incident bar. A stress wave is generated as a result of it, which travels through the incident bar and is recorded accordingly by the first and second strain gages mounted longitudinally on the bar. The stress wave then approaches the other end of the bar at the interface of the bar end and the specimen. The wave then propagates through the specimen causing the specimen to compress. Some part of the stress wave is reflected back as a tensile pulse, and is recorded sequentially by the second strain gauge. Part of the stress wave energy is absorbed by the specimen and the remainder is transmitted to the transmitter bar. There is the third strain gauge mounted on

the transmitter bar which measures the transmitted wave. These three readings are used to determine the time dependent stress state of the specimen. From the time dependent strain state data, a stress-strain plot is obtained. A pneumatic valve was employed to control the compressed air to launch the striker bar.

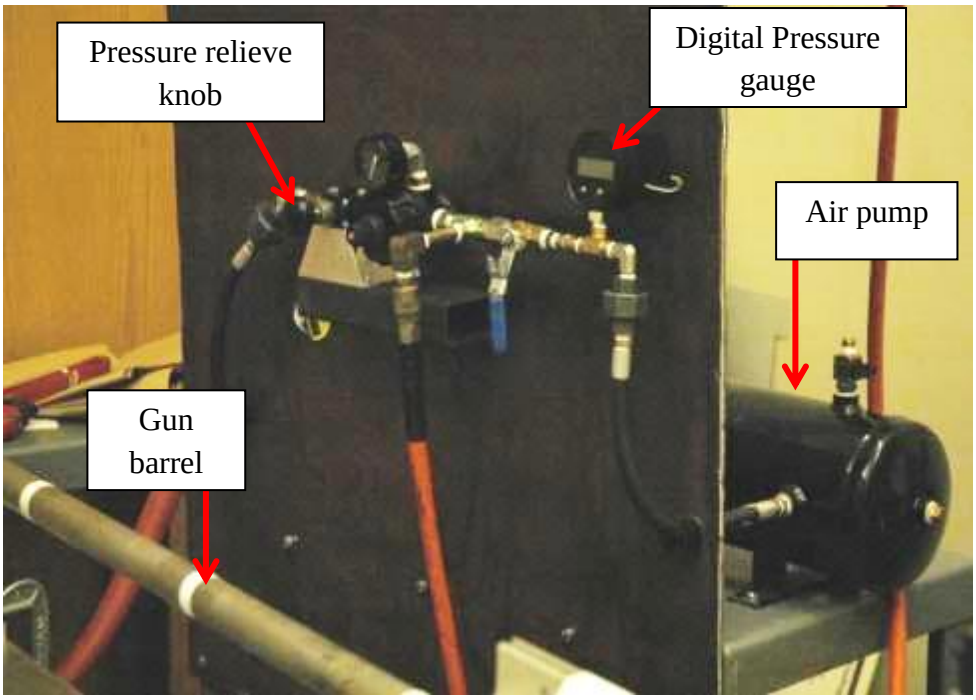

Figure 4.4: Pneumatic system for the SHPB setup

Different pulse shapers namely, aluminum (Al 2024, 6061-651), annealed copper (C360) and lead (Pb) were used in the experiments. These pulse shapers were punched out of a disk to ~2 mm in thickness and ~ 0.25 inch in diameter. The pulse shaper was placed in a coaxial/concentric arrangement with respect to the axis of the SHPB during impact. This facilitates dynamic stress equilibrium and constant strain rate over a sustained period. The velocity of the striker at impact was critical for precise pulse shaping and was determined by using the striker traveling distance divided by the time

interval when the striker moves close to the incident bar. The distance was measured between two parallel laser beams as shown in the Figure 4.5. When the striker bar travels towards the incident bar, the laser beams are blocked successively from the two New Focus 1621 nanosecond photo detectors, which have a wavelength range of 350–1000 nm and 1 ns rise time. The time interval of two signals from two photo detectors was measured using a Nicolet Sigma-30 digital oscilloscope.

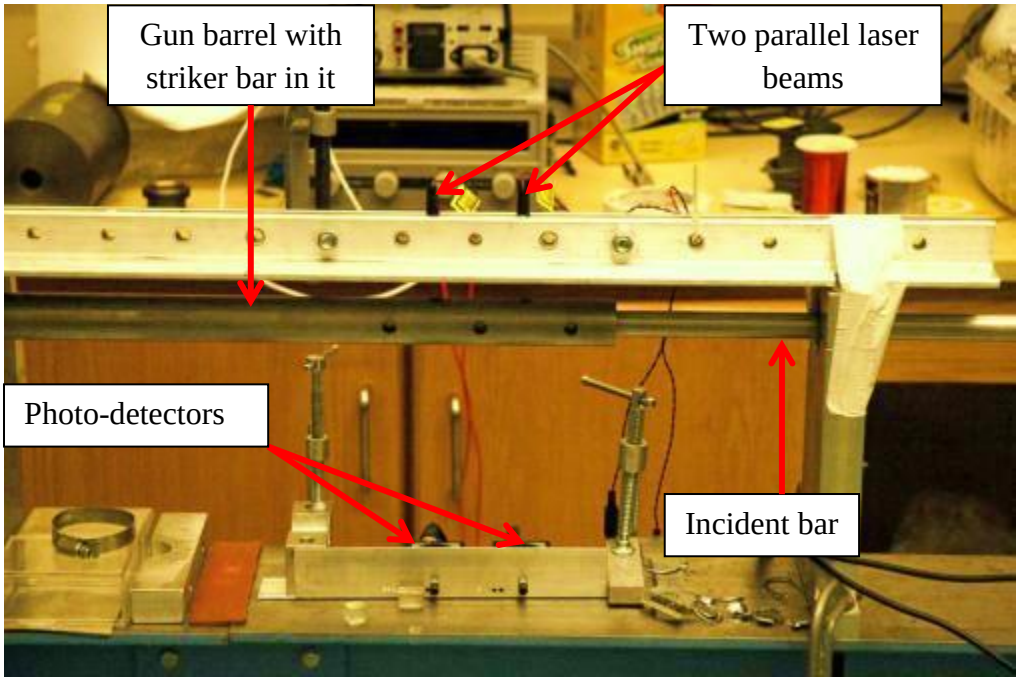

Figure 4.5: Laser system used for the velocity measurement of the striker bar on the SHPB setup

All dynamic compression tests were conducted under ambient conditions with room temperature 20 ± 1°C and relative humidity 22 ± 3%. Cylindrical samples were used in the case of metals and dry Eglin sand was used as the other sample compacted in a hollow steel tube to determine the stress-strain relations at strain-rates within 500-

$1100s^{-1}$. In each SHPB experiment, a minimum of three or more specimens were tested to ensure repeatability and accuracy under the same test conditions.

4.3 Mechanical Properties of the bars used in SHPB setup

Tables 3.1 to 3.3 shows the various mechanical properties of the three main bars used in SHPB, namely incident, transmission, and striker bar.

Table 4.1: Mechanical properties of the incident bar in the SHPB setup

Diameter (φ), in	0.75
Length (l_b), ft	24
Young modulus (E), GPa	210
Density (ρ), kg/m^3	8100
Velocity (C_0), m/s	5055.25

Table 4.2: Mechanical properties of the transmission bar in the SHPB setup

Diameter (φ), in	0.75
Length (l_b), ft	12
Young modulus (E), GPa	210
Density (ρ), kg/m^3	8100
Velocity (C_0), m/s	5055.25

Table 4.3: Mechanical properties of the Striker bar in the SHPB setup

Diameter (φ), in	0.75
Length (l_b), ft	2
Young modulus (E), GPa	210
Mass (M), Kg	3 kg
impact speed, m/s	5 to 20

4.4 Instrumentation used for the tests.

In this investigation the specimen is sandwiched between the incident bar and the transmission bar. The striker is launched by compressed air in the gas gun barrel under certain pressure. The impact of the striker bar on one end of the incident bar generates an elastic wave commonly known as the incident wave, which propagates through the incident bar. The incident wave reaches the specimen and travels through, compressing it. The incident wave is partly reflected back into the incident bar as a reflected wave and partly transmitted into the transmission bar as a transmitted wave. This happens because of the mechanical impedance mismatch between the bars and the specimen. The incident and reflected waves are recorded by a strain gages (Vishay Micro measurements specifications WK-13-125BZ-10C, 1000, and 2.08 gage factor). Strain gages were mounted on the incident bar and transmission bar, to measure the incident, reflected, and the transmitted wave respectively. A 15 volts DC power supply along with a half Wheatstone bridge (two strain gages on each bar) was employed to power the strain gages and measure the bar strains. The measured voltages were later converted into longitudinal bar strains and stresses. The recording device is typically a high-speed digital oscilloscope with signal conditioners and amplifiers.

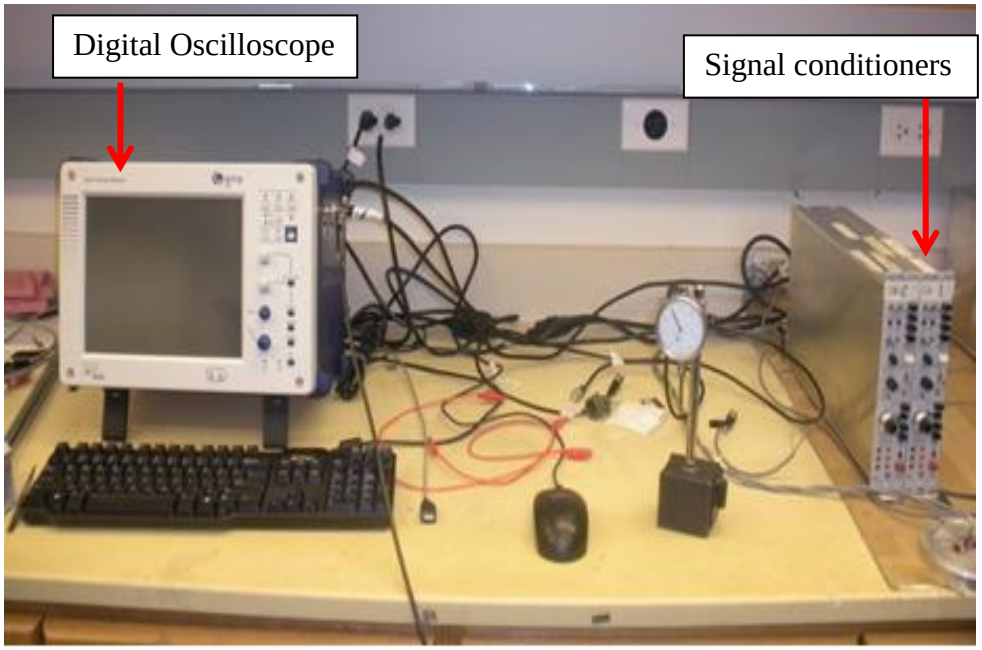

Figure 4.6: Digital oscilloscope and the signal conditioning system used in the SHPB tests

As shown in Figure 4.6, the digital oscilloscope used for the recording of the signals from strain gauges on the pressure bars was a Nicolet Sigma-30 which has specifications as 12-bit resolution, 10 Ms/s sampling rate, 500 MHz bandwidth, and 4 channels. This oscilloscope was coupled via a Wheatstone bridge and a Vishay 2310A signal conditioning amplifier which has a 1–11,000 continuously variable gain; frequency of 125 kHz and −3 dB max frequency response with a bandwidth of 125 kHz.

Strain gauges mounted on the incident bar measure the incident and the reflected pulse, whereas the ones mounted on the transmission bar measure the transmitted pulse. Alignment of the bars is critical. The incident and the transmission bars are supported by a fixture which has bearings in it on the main frame. Each strain gauge forms part of the Wheatstone bridge. When the wave passes the location of the gages, the output voltage change in the bridge is proportional to the resistance change of the gauges. Typically,

high frequency oscilloscopes (≥10 MHz) are used to record the voltage as a function of time. The voltage signal obtained from the Wheatstone bridge is quite small, on the order of a few mV. So the surrounding voltage noise can easily interfere with this voltage. This makes it difficult to determine and identify the actual signal. Hence proper care must be taken to isolate and shield all the electrical devices from such disturbances and interferences. Alignment is one of the biggest issues to tackle and a critical one too. It is worth spending days sometimes on getting the right and accurate alignment of the pressure bars. Because, if a misaligned Hopkinson bar is used for testing, then it gives rise to bending, eventually obstructing the movement of the bars. Also, it damages the interfaces of the bars. This affects the wave's propagation through the bar. Hence alignment has to be thoroughly checked. Also, while performing a test there is a possibility of making some indentation marks on the faces of the pressure bar which disturbs the complete face to face contact. So, a timely check must be performed and requires steps to be taken if such a problem arises.

Narrow gage width and gage length are important to reduce the averaging of strain signals at the measured area. High resistance gage provides increased sensitivity and better signal to noise ratio. The high endurance lead wire in this gage contributes to its high fatigue life. These strain gauges are wired in a full bridge arrangement that takes care of bending and thermal effects. The signal from the full bridge is fed into a VISHAY 2310 amplifier, which is mounted on a custom built platform, with an amplification of 100. The signal is then fed into the NICOLET digital oscilloscope and stored as a 'TXT' file. The data captured by the digital oscilloscope is stored in the form of Excel file. The Vishay 2310A amplifier unit provides strain gage measurement capabilities, namely,

bridge excitation, bridge balancing, shunt calibration, amplification and signal filtering. A 15 V bridge excitation was chosen for maximum source amplification of the measured signal without introducing thermal drift in the measured signals from the strain gage. A gain of 100 was chosen for amplifying the measured signals as it provided a good signal to noise ratio. Prior to testing, the 2310A is switched on for approximately 20 minutes to attain a 'steady-state' condition [32]. The analog output (0-10 V) of the signal conditioner was then connected to a Nicolet Sigma-30 oscilloscope which was digitized (12-bit resolution) and sampled at 50 Hz. Signals from the 2310A controller and the Nicolet oscilloscope were synchronized. The measured strain gage response (V_m in Volts) was converted to equivalent strain (ε) using Equation (1), where 'G_f' is the gage factor of the strain gage, 'V_{ex}' is the excitation voltage in Volts and 'G' is the amplifier gain.

$$\varepsilon = \frac{2 \text{ X } V_m}{G_f \text{ X } V_{ex} \text{ X G}} \tag{1}$$

According to one dimensional (1-D) elastic wave theory [31], to obtain accurate data, the pressure bars must always remain elastic and their lengths should be sufficiently long to avoid overlapping in the elastic waves during the operations of the SHPB setup. Along with this, the ends of the bars in contact with the specimen must remain flat all the time, and should be parallel throughout the dynamic loading experiments. This is one of the mandatory conditions for the specimen to deform under a uniaxial stress condition. Now from the one dimensional wave analysis and recorded bar-surface strain signals, the strain rate, strain, and stress histories in the specimen can be calculated and analyzed [30, 33, 34]

4.5 2-Dimensional Digital Image Correlation (DIC) Analyses.

Strain measurements play a critical role in mechanical sciences, especially when analyzing the dynamic behavior of different samples. A strain in any material can be defined as the ratio of the change in length to the initial length. Strains need to be determined to find out material properties and parameters, such as stress-strain relationship, Young's modulus, Poisson's ratio. More, innovative and extensive investigations are required for strain measurements at any point within or inside an area of interest, to study the mechanical or dynamic behavior of materials and structural components at high strain rates. For this reason, researchers are interested in generating strain maps over the entire specimen surface. Some conventional instruments, which measure strains (i.e. strain gage and LVDT) are capable of creating strain maps, because of low cost and practicality. Owing to the fact that strain maps are needed to perform new investigations, a new technology was developed to obtain these desired results. This technology is the digital image correlation (DIC), which provides a contour map of strains of an entire specimen surface subject to mechanical stresses [35].

The digital image correlation (DIC) is not a new concept and has been used earlier for analyzing strain contours and displacements in the sample [35]. The main aim of DIC analysis is to show the deformation and strain distributed over the sample is uniform. Basically, DIC is an optical method that employs a mathematical correlation analysis to examine digital image data taken while samples are in dynamic mechanical tests. This technique involves capturing consecutive images of the sample under test with a digital camera during the deformation period to evaluate the change in surface characteristics and investigate the behavior of the specimen while it is subjected to compressive or

tensile loads. To apply this method, the specimen needs to be prepared by the application of a random dot pattern, commonly known as speckle pattern, to its surface. This technique starts with capturing of a picture before loading which is called as the reference image and then a series of pictures are taken during the deformation process which are known as the deformed images. All the deformed images show a different random dot pattern relative to the initial non-deformed image (i.e. reference image). With the help of computer software these differences between the patterns can be calculated by correlating all the pixels of the reference image and any deformed image, and a strain distribution map can be created [36].

A Cordin 550-62 high-speed digital camera (62 color frames, 4 million frames per s at the maximum frame rate, 10-bit resolution CCD with 1000 × 1000 pixels per frame) was used to acquire the images of a specimen at a frame rate of 303,118 frames per sec. At a certain time delay after the striker bar blocked the laser, an external output signal from the photo detector that detected the striker would trigger the high speed camera to start capturing a sequence of images of the specimen surface during the entire deformation process. Two Cordin 605 high intensity Xenon light sources with two sets of lenses were used to illuminate the specimen surface at nearly constant amplitude of luminosity as shown in Figure 4.7.

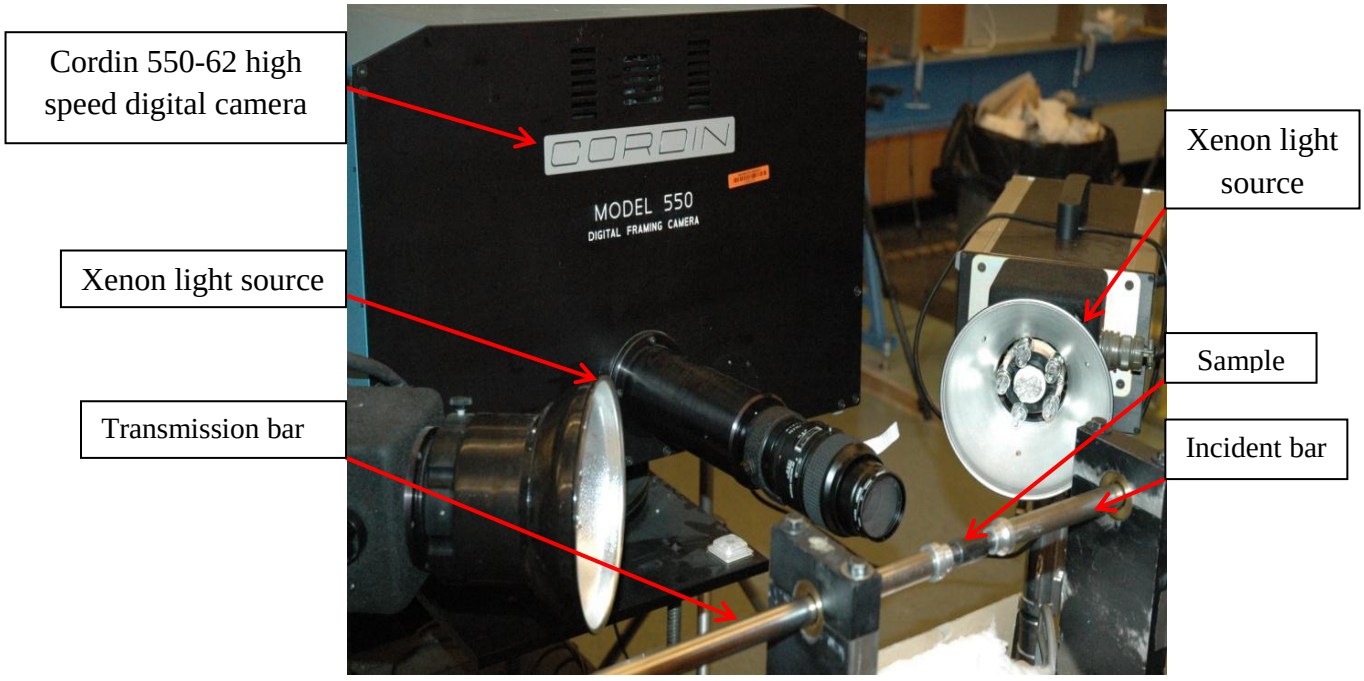

Figure 4.7: High speed camera and lightning setup used for DIC analysis

In order to obtain good focus on a specimen, an aluminum or copper cylindrical specimen (0.25in long and 0.5in diameter) was also used and subjected to compression. The use of such a specimen enabled the sample to yield and bulge, for observation of the failure process and also allowed the measurement of displacement and axial strain. In order to do this measurement, a random speckle pattern was generated on the surface under observation using a quick drying black ink on a white background formed by coating a thin layer of quick drying correction liquid. The digital image correlation (DIC) technique, a non-contact full-field deformation measurement method, was used to measure surface deformations. The method has been previously used in a variety of situations, for example, in measurements of surface deformations of a cylindrical specimen by Lu. H *et al* [37], measurements of second-order displacement gradients again by Lu. H and Gary *et al* [38], and measurements of strains in shear creep by Knauss

et al [39]. In this research work, measurements of surface deformations using DIC in dynamic SHPB experiments were made. In DIC, two images, namely, the reference image and the deformed image are correlated to determine surface deformations. DIC relies on a distinct gray scale pattern in a subset of pixels to track a material point undergoing deformations. In this work, the DIC code developed by Lu and Cary, which has the ability of measuring both the first-order [37] and second order displacement gradients. This methodology and technique was used to determine the surface deformations on an annealed copper cylindrical specimen.

4.6 Wave Propagation Theory

In SHPB, 1D wave propagation principle is used for the stress-strain behavior of a specimen no matter how the testing is carried out, compression or tensile loading [31]. The 1D wave propagation theory in rods is based on certain basic assumptions, namely, the bars used in the system behave linearly and dispersion free. This in turn implies that the pressure bars are homogeneous and isotropic, uniform in cross section and the material of the bar remains in the linear elastic stress state whenever it is loaded with the propagating stress pulses.

The basic split Hopkinson bar test setup includes two pressure bars which have constant cross section areas A_B, an elastic modulus of E and density ρ. The two pressure bars are similar; hence, it is essential to consider only one of them in developing the equation of motion governing axial vibration. Usually in SHPB the length to weight ratio is about 80 or greater. As shown in Figure 4.8; 1 denotes the IB-S interface and 2 denotes the TB-S interface. The displacement at the interface of the bar and the specimen is given

by u whereas the measured strains in the pressure bars are denoted by ε. I, R, T are the subscripts used for incident, reflected and transmitted bar respectively. The arrow heads shows the direction of wave travelling through the bar.

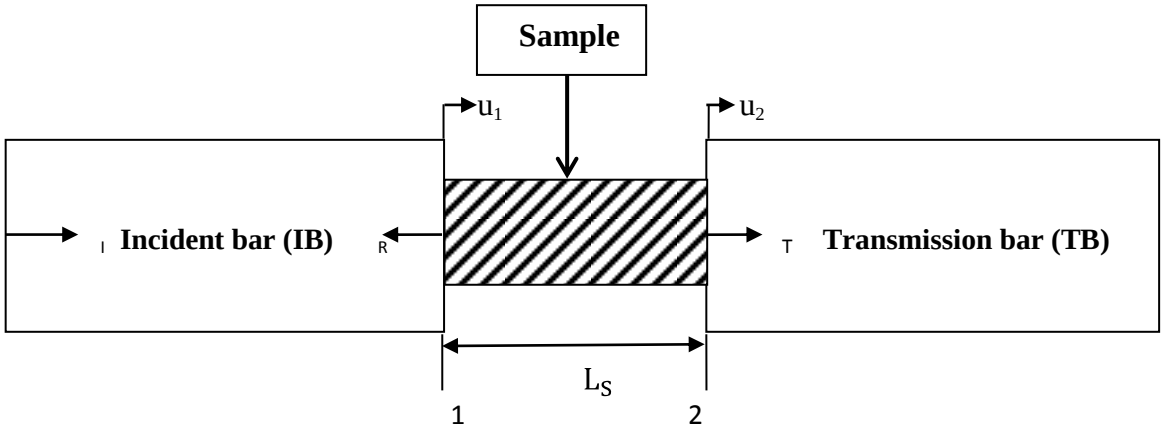

Figure 4.8: Schematic of the SHPB apparatus showing details of the sample, incident, and the transmission bars.

The 1D wave equation is given by the following

$$\frac{\partial^2 u}{\partial x^2} = \frac{1}{C_0^2}\frac{\partial^2 u}{\partial t^2} \tag{2}$$

where $C_0 = \sqrt{\frac{E}{\rho}}$ is the wave velocity (3)

Although the equation of motion in SHPB has no practical use but it does help in getting the theoretical wave velocity for a wave of infinite wavelength. This analysis is later used in calculating the specimen strain and strain rate.

The forces in the two bars are given by

$F_1 = A_B E (\varepsilon_I + \varepsilon_R)$ and (4)

$F_2 = A_B E \varepsilon_T$ (5)

If the assumptions, such as the specimen is in force equilibrium and it deforms uniformly are valid, a further modification or simplification can be done, which is nothing but equating the forces on each side of the specimen: i.e. equating $F_1 = F_2$. Hence, from the above equations we can show

$$\varepsilon_I + \varepsilon_R = \varepsilon_T \quad (6)$$

Considering the force equilibrium, the average specimen strain rate can be written as

$$\varepsilon^* = \frac{2Co\ \varepsilon_R}{L_S} \quad (7)$$

Since there is no change in the volume of the specimen, so $A_0L_0 = A_SL_S$ where A_0 and L_0 represents the initial cross sectional area and length of the specimen, respectively. Similarly A_S and L_S represents the instantaneous cross sectional area and length of the specimen, respectively. The equation used for the calculation of the engineering stress is given as follows

$$\sigma_S\ t = \frac{A_B E}{A_0} . \varepsilon_t(t) \quad (8)$$

And the engineering strain in the specimen is given by the following equation

$$\varepsilon_s = 2\frac{C_0}{L_0}.\ \int_0^t \varepsilon_R\ t\ dt \tag{9}$$

Considering the strain gage signal as shown in figure 4.9, the sign of the transmitted pulse (positive) appears is the same as the incident pulse (positive) but inverse to that of the reflected pulse (negative). This is achieved by keeping the polarity of the recording devices similar for both channels of strain gages on the incident and the transmitted bar. By placing the center of the strain gages equidistant from the specimen-bar interfaces, a relative origin in time can be established if both the pressure bars are made from the same material. Signal shown in Figure 4.9 is a conditioned and amplified signal. The properties of the bar materials, such as the density, modulus of elasticity, wave velocity, and sample dimensions (length and diameter) should be known before conducting data analysis part from the SHPB experiments. For a successful compression test, one has to work with the incident, reflected and transmitted signals as recorded by the strain gages. The signals from the strain gages (volts v/s time) can be converted to stress-strain in the bar. From the mechanical properties and the quantities measured such as the reflected, incident and transmitted pulses or signals an analytical model can be developed. It is known from Kolsky's (1949) derivation that both the average stress and strain of the specimen as a function of time can be calculated from measured quantities [30, 33]

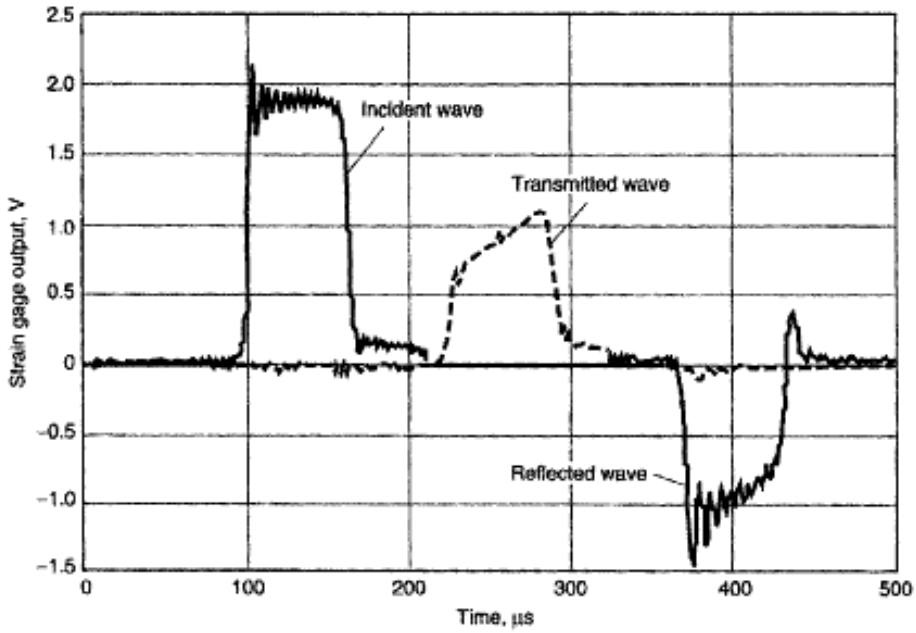

Figure 4.9: Strain gauge signals obtained from a SHPB test of a 304L SS specimen with a maraging steel bar [30]

4.7 Assumptions of a valid SHPB test

Before using the above sets of equations for calculating the average stress-strain behavior of the specimen material under high strain rate loading, from the measured quantities of a SHPB test, it is advised that the validity of the experiments and its assumptions be verified (Gray 2000). Following are the conditions or main assumptions that need to be satisfied for a valid SHPB test [4].

a) Stress wave propagation in the bar is one dimensional.
b) The pressure bars used should be homogeneous and isotropic which can be achieved by suitable choice of bar material.
c) The neutral axes of these bars are straight and uniform in cross section over the whole length.

d) When loaded with propagating stress pulses the stress in the pulse be below the elastic limit of the bar material. This can be achieved by controlling the impact velocity.

e) If L_B/D_B ratio is greater than 20 there should be uniform axial stress distribution over the entire cross section.

f) No dispersion effects.

g) The incident bar-specimen and specimen-transmission bar surface interfaces should be plane all the time during the experiments.

h) There is none or minimum friction and inertia effects involved in the specimen.

CHAPTER V

RESULTS AND DISCUSSION

In this Chapter the dynamic compressive behavior of aluminum cylindrical sample, annealed copper cylindrical sample and dry Eglin sand samples was investigated using a modified split Hopkinson pressure bar (SHPB). For dry Eglin sand samples, further analysis was done by using it at different mass densities and various grain sizes at the same mass densities. A Pb cylindrical disc pulse shaper in concentric axial arrangement with respect to the axis of the SHPB was used. Use of Pb pulse shaper gave a constant strain rate over a sustained period of time under valid SHPB experiments. Also, it was found that Pb pulse shapers gave high axial stress values compared to aluminum or annealed copper pulse shapers at constant density of Eglin sand. This part of the analysis is further explained in detail in the thesis. The stress-strain relationship of dry Eglin sand with different densities was determined at high strain rates (500-1100s^{-1}), and the results were compared with the results of Luo *et al's* [5] on the same parameters. The following flow chart (Figure 5.1) shows various aspects of the research conducted in this investigation.

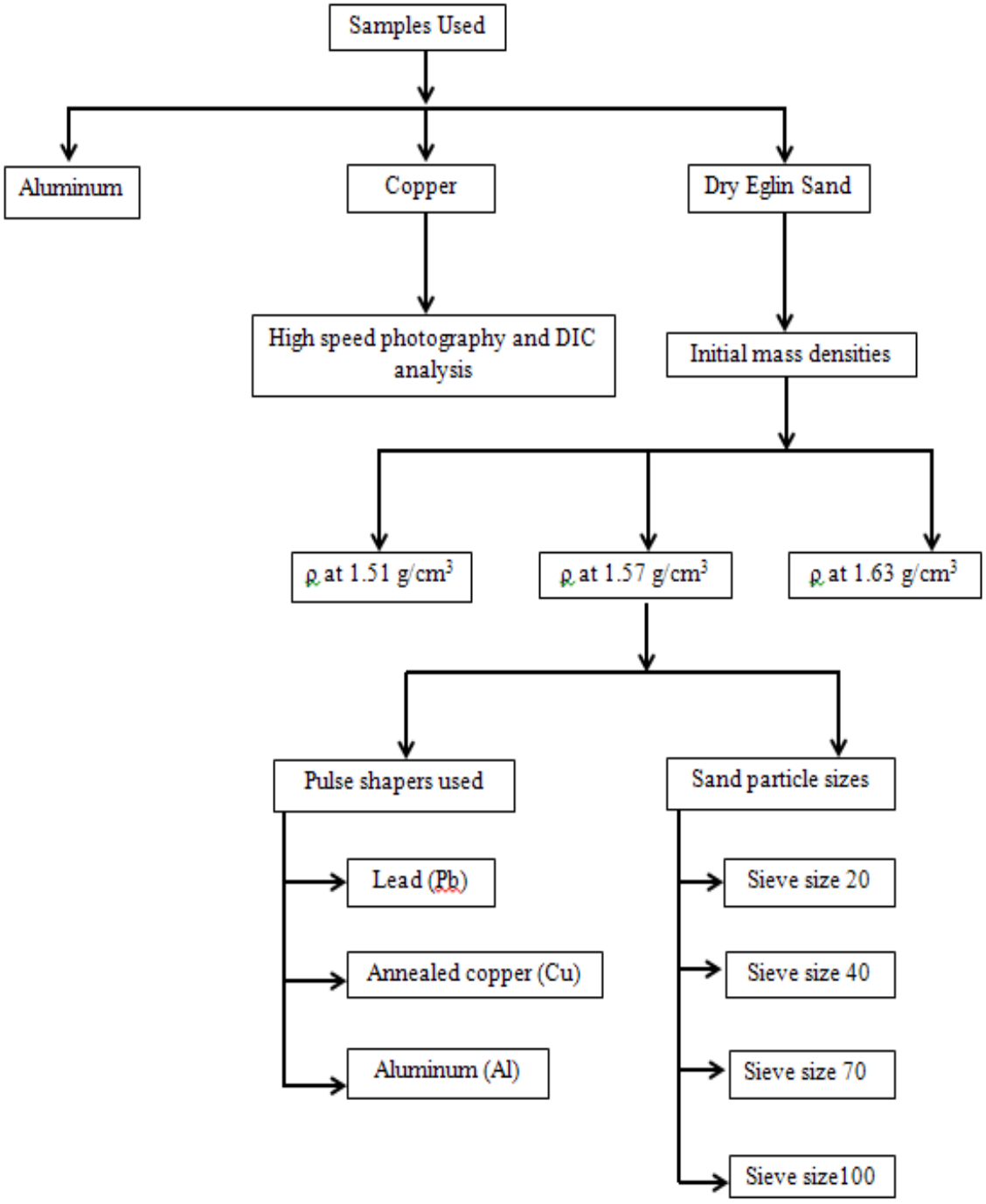

Figure 5.1: SHPB experimental layout

The deformation and failure behavior of aluminum and annealed copper cylindrical samples were observed using a high speed camera. Digital image Correlation (DIC) method was used to analyze the deformation and strain fields at high strain-rates through successive images acquired using high-speed photography. Dry Eglin sand samples of different densities were used in SHPB experiments at high strain rates to determine the effects of initial mass density. Cylindrical samples of aluminum and copper were prepared to calibrate the SHPB setup. The results obtained were compared to the work reported in the literature at high strain rates. The dynamic mechanical behavior of dry Eglin sand was investigated to determine the effects of mass density, particle size, and different pulse shapers at a given density of sand.

Typical data for the incident, transmitted, and reflected signals on the bars in an SHPB experiment shown on the oscilloscope screen is shown in Figure 5.2. This signal can be directly compared to Figure 5.26 [21]. The gains calculated or calibrated in the conditioning amplifiers for incident wave, reflected wave, and transmitted wave were 100 times, respectively. This implies that the strain gauge signals are amplified 100 times and recorded in the oscilloscope. There is a signal conditioner and an amplifier used each for the incident bar and the transmission bar, respectively as shown in Figure 5.3.

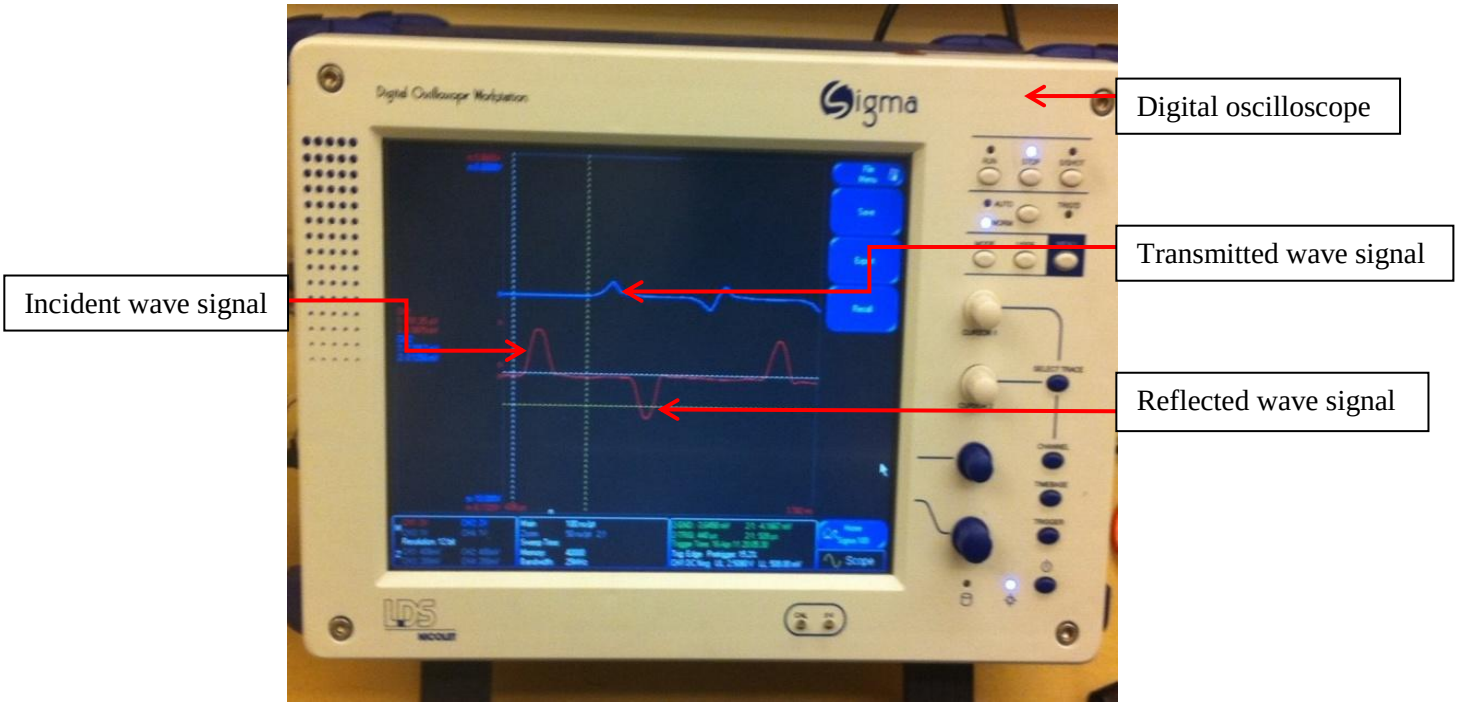

Figure 5.2: Actual signal data obtained from a digital oscilloscope

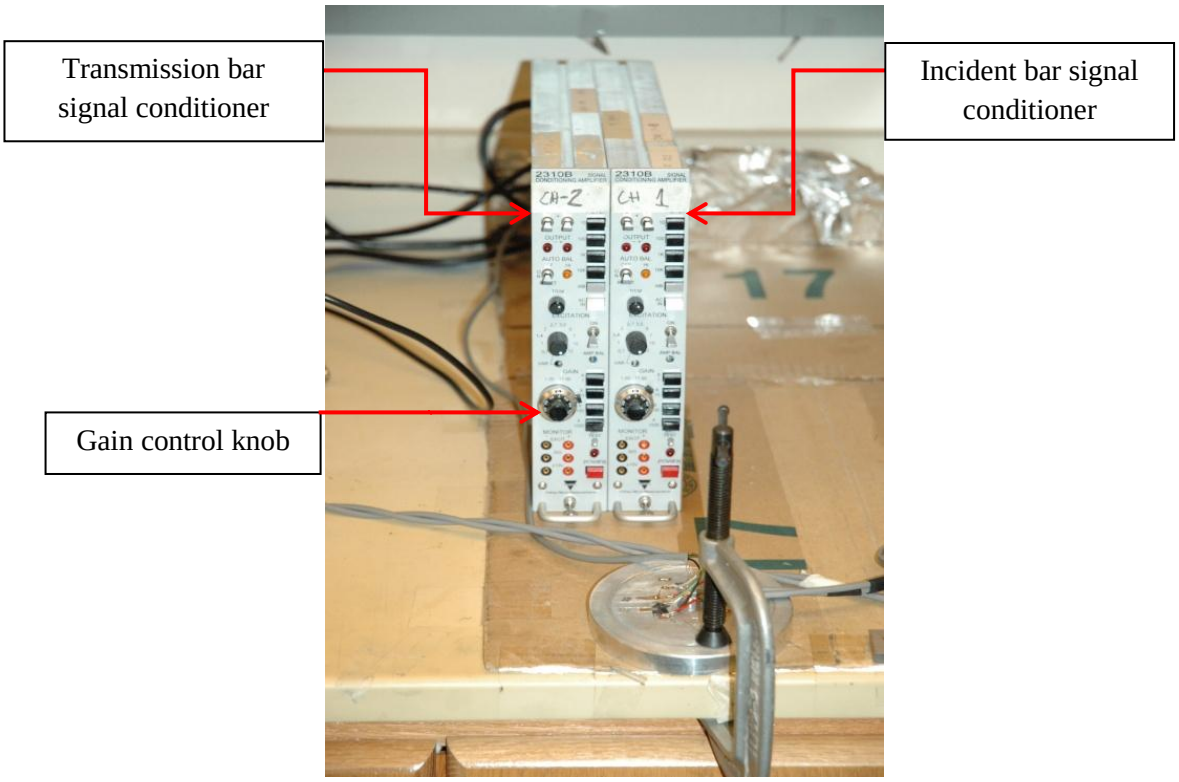

Figure 5.3: Signal conditioners for incident and transmission bars

The bar signals, indicative of the strain history, are acquired by an oscilloscope and plotted. Initially, the incident pulse rises rapidly, which is known as the rising-up phase. It increases then slowly for over a certain period of time, which is known as the loading phase. Finally the pulse decreases, in a phase known as the unloading phase. With this pulse shape, there is no interference between the reflected and the incident pulses, as can be seen in Figure 5.4. The transmitted pulse also has nearly bi-linear characteristics during loading, with only the difference of the yielding of the sample associated to it. In dynamic SHPB tests, when the stresses applied on both ends of the specimen are equal, the dynamic equilibrium state is established. Such an experiment is considered valid and the acquired experimental data are then processed to deduce the dynamic stress-strain curves. To examine the dynamic equilibrium condition, the front stress and back stress on the specimen were calculated following the 1-wave (which is also known as transmitted wave), and 2-wave (also known as a difference between incident wave and reflected wave) method. The stresses at the front face, which is the surface of the specimen in contact with the incident bar, and the back face, which is the surface of the specimen in contact with the transmission bar, are shown in Figure 5.5, plotted together with the strain rate history in Figure 5.6. The front stress is very close to the back stress, indicating that the dynamic equilibrium condition was nearly established and the specimen was nearly uniformly deformed. In traditional SHPB using identical material and dimensions for both the incident and transmission bars, the reflected signals represent usually the strain rate history.

Once the condition of a valid SHPB was identified, the incident, transmitted and reflected signals were processed further using Equations (8) and (9) to determine the

stress-strain relation at high strain rates. In this investigation, the same striker and the same launching pressure and distance were used for the analysis of the similar sample. So, for the aluminum cylindrical sample and the copper cylindrical sample the launching pressure is the same. Whereas for dry Eglin sand, the launching pressure was different compared to the metal samples. The use of different launching pressures in the compressed air allowed the adjustment of striker velocity, which in turn controlled the profile of the shaping pulse.

5.1 Tests on Aluminium cylindrical samples

Test were carried out on different types of aluminum samples, namely, Al 2024, Al 6061, Al 6066 of different length varying from 0.2 in to 0.4 in. In a particular experiment Al 2024 was selected as the sample with an initial length, L_i of 0.2520 in and initial diameter, D_i of 0.4995 in. The pulse shapers used in these experiments were punched out from a sheet to obtain disks of annealed copper (C360) ~ 2 mm thick and 0.25 in. in diameter. The striker bar used in the test is 2 ft long and of the same diameter as that of the incident and transmission bars. The material of the striker bar was also kept the same which is maraging steel. The velocity of the striker bar or impact bar for this test was measured to be 17.7 m/s. The results obtained for this test are shown in Figures 5.4 to 5.7. Tests on aluminum were carried out to have the SHPB setup ready with minimum discrepancies before we move on to the testing of the Eglin sand. The setup was calibrated with the help of these experiments. Calibration include alignment issues, gain on the amplifiers, pulse shaping technique used etc.

Figure 5.4 shows typical signals obtained for the stresses in the incident and transmission bars. The stress value reached in the incident bar was 372 MPa whereas in the transmission bar it was 288 MPa. The pulse width was ~ 400 μs. Figure 5.5 shows the agreement of front stress and back stress, indicating that stress equilibrium was achieved and the sample deformed uniformly. The maximum axial stress achieved in the sample was ~ 680 MPa. Figure 5.6 shows the strain-time plot which gives the maximum value of axial strain achieved in the sample. It was found from this plot that strain value of ~14.25% and strain rate value of 571.43 s^{-1} were achieved in this test. Figure 5.7 shows the stress-strain relation obtained for this test. The final length and final diameter measured after the test was L_f of 0.2220 in and D_f of 0.5360 in . The yield point calculated from this plot was ~ 420 MPa and the breaking point or the fracture point of the sapmle was ~670 MPa. The modulus of elasticity calculated for aluminum was ~ 24 GPa. The measured strain from the deformed sample was ~ 12% whereas from the plots it was ~ 14% a difference of 2% in the strain measurement.

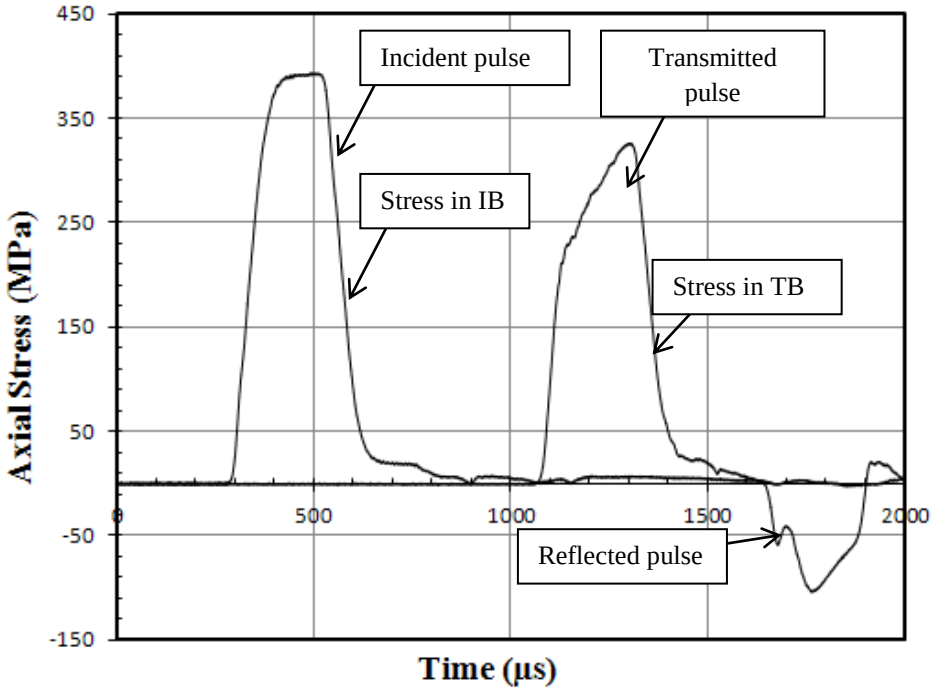

Figure 5.4: Typical signal showing variation of axial stress in the bars v/s time obtained for aluminum cylindrical sample

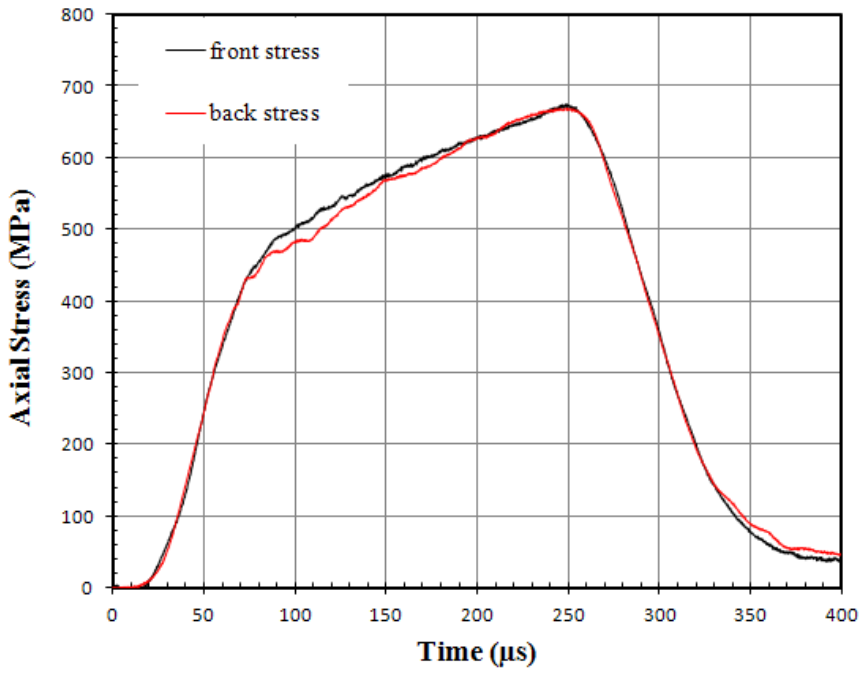

Figure 5.5: Stress equilibrium achieved in the aluminum cylindrical sample

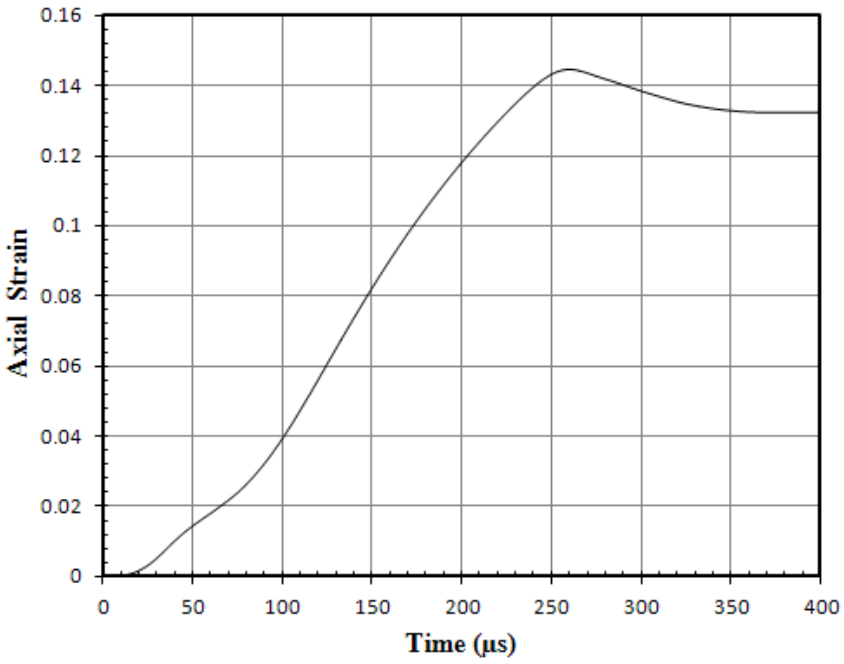

Figure 5.6: Strain achieved in the aluminum cylindrical sample w.r.t time

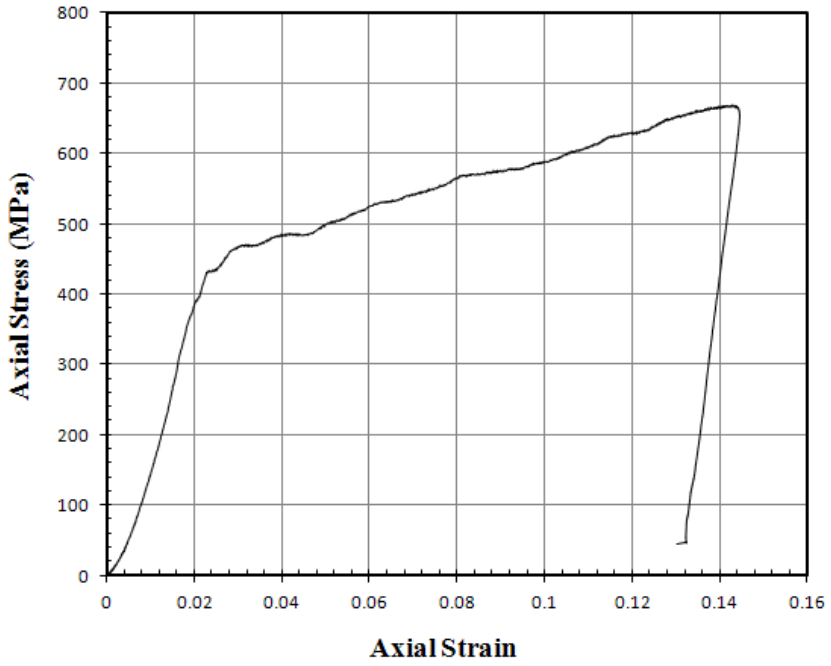

Figure 5.7: Stress-strain relation for aluminum cylindrical sample

5.2 Tests on speckled pattern on cylindrical copper sample

We have obtained some preliminary results on cylindrical copper samples, 0.5 inch in diameter and 0.25-0.4 inch long, deformed over the range of strain rates from 500 to $700s^{-1}$. The material used was 99.999% pure copper, annealed before test to about 800 K in an oven heated at 40 K per minute to achieve recrystallization with little grain growth.

Test were carried out on various samples of copper, namely C110, C360, C101 of length varying from 0.2 in to 0.4 in. For this particular experiment, C360 copper was selected as the sample with an initial length L_i of 0.3625 in and initial diameter D_i of 0.5100 in. The pulse shaper used was punched out from a sheet of annealed copper (C360) in the form a disc ~ 2 mm thick and ~ 0.25 inch in diameter. The striker bar used in the test was 2 ft long, and of the same diameter as that of the incident and the transmission bars. The material of the striker bar was also kept the same, which is maraging steel. The velocity of the striker bar or impact velocity for this test was measured to be 17.3 m/s. The results obtained for this test are shown in Figures 5.8 to 5.11. The tests on copper were carried out in order to have the SHPB setup ready just like those conducted with the aluminum sample earlier. The only thing added to this experiment was the use of high speed photography for DIC analysis to verify the sample actually deformed uniformly and compare the values accordingly.

Figure 5.8 shows typical signals obtained for the stresses in the incident and transmission bars. The stress value reached in the incident bar was 400 MPa whereas that for the transmission bar was 230 MPa. In the case of aluminum it was observed that the stress in the transmission bar was about 50 MPa less than the stress in transmission bar. This implies that most of the incident pulse was reflected back rather than

transmitting making sure that the annealed copper sample is softer than the aluminum sample used. The pulse width was ~ 400 μs. Figure 5.9 shows the agreement between front and back stresses. There are some vibrations associated in this test, and hence some spikes were observed in the plots. This may be due to multiple hitting of the striker bar, improper alignment, friction involved, etc. Further studies have to be made on this issue to avoid oscillations in the bar. There was a mismatch of ~ 30 MPa for some parts of the stress equilibrium. Apart from the oscillations, the plot indicates that the stress equilibrium was achieved and the sample must have deformed uniformly. The maximum axial stress achieved in the sample was about 525 MPa. Figure 5.10 shows the strain-time plot which gives the maximum value of axial strain achieved in the sample. It was found from this plot that strain value of ~ 19% and strain rate value of $650s^{-1}$ were achieved in this test. Figure 5.11 shows the stress-strain relation obtained for this test. The final length and final diameter measured after the test were L_f of 0.2985 in and D_f of 0.5720 in. The yield point calculated from this plot was ~ 345 MPa and the breaking or the fracture stress of the sample ~ 520 MPa. The modulus of elasticity calculated for copper was ~ 35 GPa. When measured, the measured strain from the deformed sample, it was ~ 18%; whereas from the plots it was ~ 19% with a difference of 1% in strain measurement. Further work was done on the sample deformation analysis with the help of high-speed photography to verify that the sample actually deformed uniformly and the strain values obtained were reasonable.

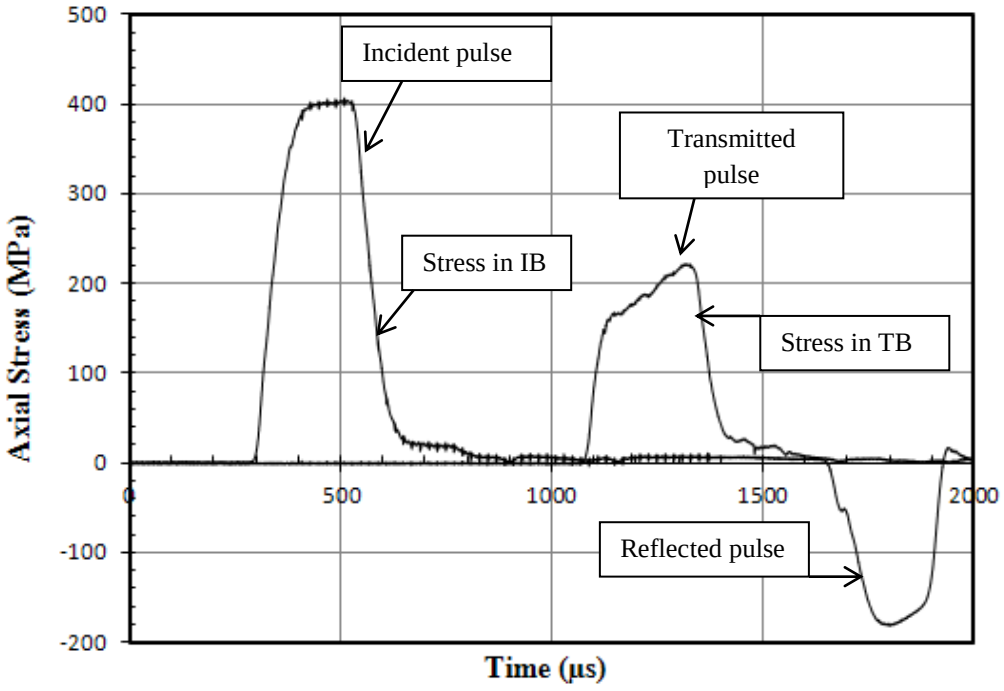

Figure 5.8: Typical signal in SHPB tests obtained for copper cylindrical sample

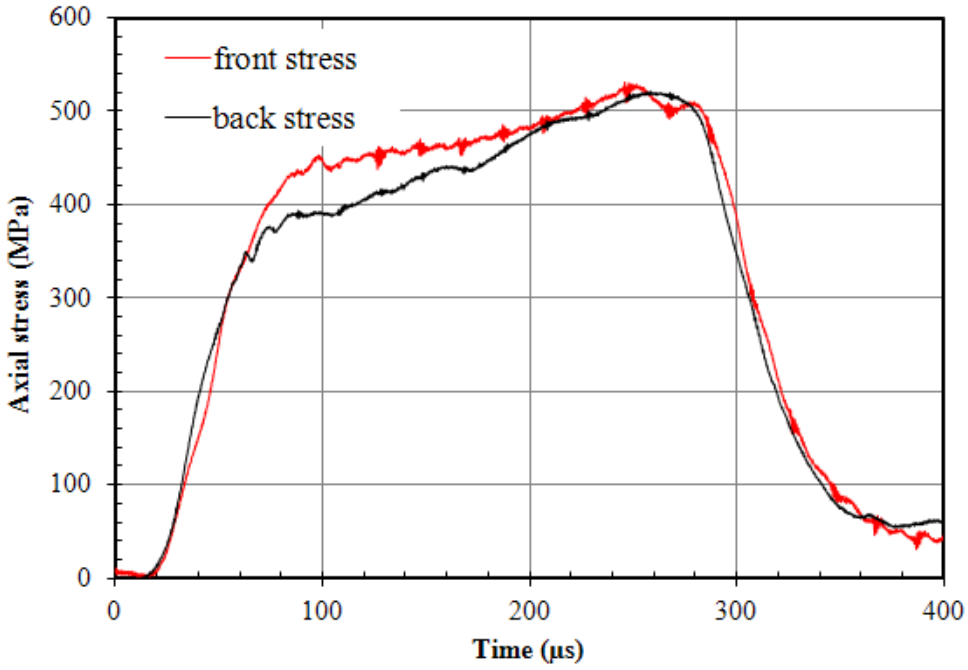

Figure 5.9: Stress equilibrium achieved in the copper cylindrical sample in SHPB test

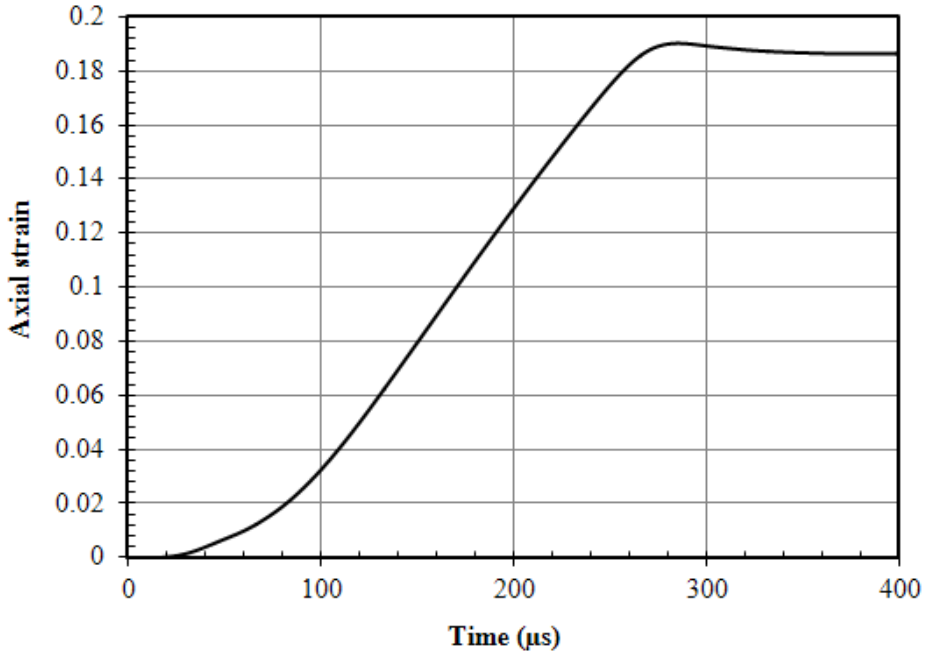

Figure 5.10: Strain achieved in copper cylindrical sample in the SHPB test

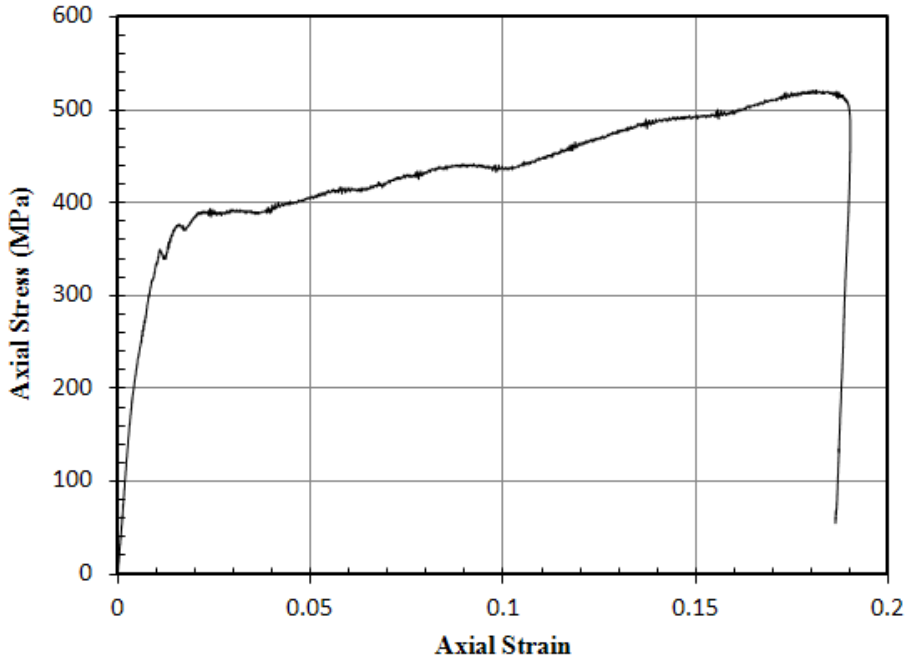

Figure 5.11: Stress-strain relation for copper cylindrical sample in SHPB test

5.2.1 High-Speed Photography and analysis of mechanical behavior of copper sample.

A Cordin (Model 550) 62-frame high speed digital camera was used to acquire images of the same copper sample. Photographs of cylindrical copper surface were taken during deformation to observe deformation and failure behavior at high strain rates. Images were analyzed using Digital Image Correlation (DIC) technique to determine the uniformity in deformation. Five typical images (frames) are shown in Figure 5.12. A paper with a small square grid (1mm × 1mm) was fixed to the surface of the supporting base of the bar on the same plane as the planar surface of the specimen under observation, so that both the specimen surface and the paper could be properly focused at the same time. Since the paper grid is stationary all the time, the motions of the incident bar, transmission bar, and the deformations of a cylindrical specimen with surface grayscale patterns can be visualized clearly. Figure 5.12 (a) shows the image of a specimen prior to loading at time 0 μs. At time 50 μs, the specimen did not show visible failure, as shown in Figure 5.12 (b). At time 99 μs the speckle coating at the center of the imaging surface started to delaminate and split, causing distortion in the black dots on the surface. With increasing deformations, the specimen boundary gradually deformed and bulged out and the speckles at the center of the imaging surface continued to distort and delaminate until unloading. The failed cylindrical specimen remained as one large piece with visible damage at its lateral surface. The grid pattern coating in the specimen delaminated from the substrate and split when observed after the test was conducted. The coated gray scale pattern on all cylindrical surfaces delaminated partially from the substrate after impact. To some extent, the dynamic failure is somewhat similar to the

failure behavior under quasi-static compression, in which the outer layer was distorted due to high lateral tensile strains developed in compression, and in the final stage ~ 75% compressive strain.

Digital image correlation (DIC) was used to determine the surface strain distribution on a specimen. In DIC, the subset size chosen was 60×60 pixels (refer to Figure 5.13). The size of a pixel calculated was ~ 32.2 μm/pixel in both horizontal and vertical directions. Surface deformations were determined at each grid node using Figure 5.12 (a) as the reference image and rest of the figures (Figure 5.12 (b) (c) (d)) as deformed images. The average value of the axial strains (in the horizontal direction in Figures 5.18 and 5.19) determined from all nodes is quoted as the strain at the given deformed state. Five deformed images are processed by DIC to determine strains. Figures 5.14 through 5.21 show the displacement contour in the horizontal and vertical (or transverse) directions as well as the strain fields in horizontal and vertical directions as determined from DIC on the deformed image shown in Figure 5.12 (e), respectively. Two different methods, namely, incremental contour as well as cumulative contour for each displacement and strain field are used to compare the results of DIC analysis. The incremental contour is obtained by comparing the successive deformed images with the previous one. Cumulative contours are obtained by comparing the deformed image with the reference image (in this case Figure 5.12(a)). It is generally recommended to plot and follow the cumulative displacement contours and cumulative strain contours as they are compared to the reference image (undeformed image) at all the time. Cumulative contours are more accurate and uniform compared to the incremental contours. Contours of both axial displacements are straight lines or visible uniform bands, indicating

homogeneous deformations achieved in the copper sample. Figure 5.18 through 5.21 show the strain contours in the axial (horizontal) and transverse directions both incremental and cumulative, respectively. The average axial strain for the strain field as shown in Figure 5.19 is 18% (absolute value), very close to the axial strain 19% (refer to figure 5.10) as determined from measurements by the strain gages attached on the bars. DIC is not sensitive to determine the Poisson's ratio in the linear regime. It may be noted that the standard deviations for the axial strain are small compared to the average value, so that the deformation fields are relatively uniform. However, it may be noted that at some locations, strains are far removed from the average values, but they are localized in small areas so that the global stress-strain relation might not be affected much by these localized strains. The relative uniform axial deformation indicated that localized compaction did not occur at a compressive strain level of ~ 17%. Further investigation is needed in this area of analysis as there is rigid body displacements involved which need to be corrected. It may be noted that in this test, cylindrical samples were used. Results from these tests are comparable with the ones obtained from the stress-strain plots or the signals from the strain gauges in the pressure bars. The length to diameter ratio of cylindrical samples used in this investigation is 1:2.

5.2.2 Digital Image Correlation analysis and results.

Speckle pattern was generated on the annealed copper (C360) sample for DIC analysis. The frame rate on the Cordin camera was ~ 303318 fps. For the DIC analysis frames 1-15-30-45-60 were selected. The measurement of 1 pixel on the grid was calculated to be ~ 32μm/pixel.

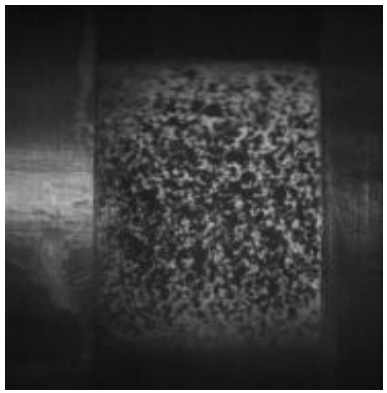

a) Frame 1 (t = 0 µs)

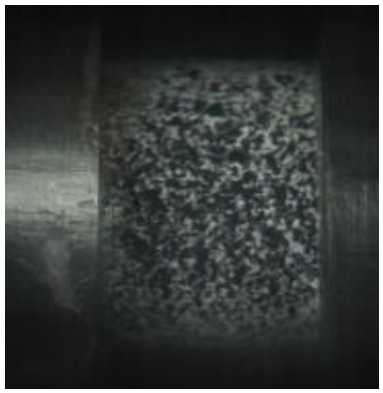

b) Frame 15 (t = 50 µs)

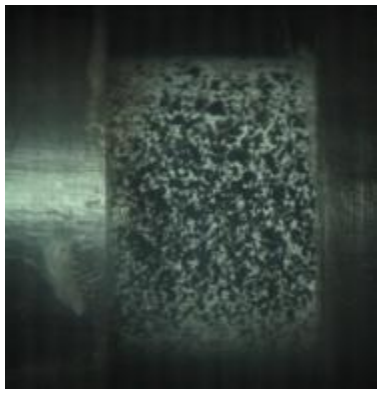

c) Frame 30 (t = 99 µs)

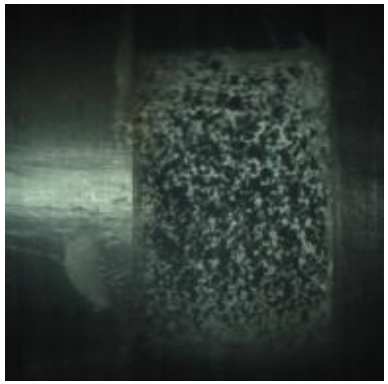

d) Frame 45 (t = 148 µs)

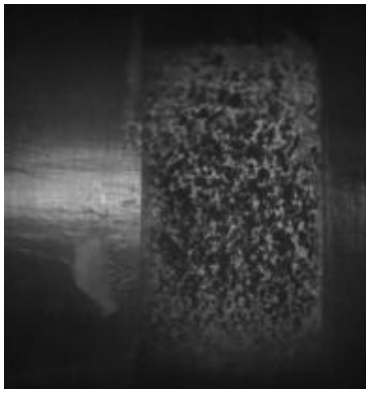

e) Frame 60 (t = 198 µs)

Figure 5.12: Successive images of the copper cylindrical sample in the SHPB test at different stages of compression

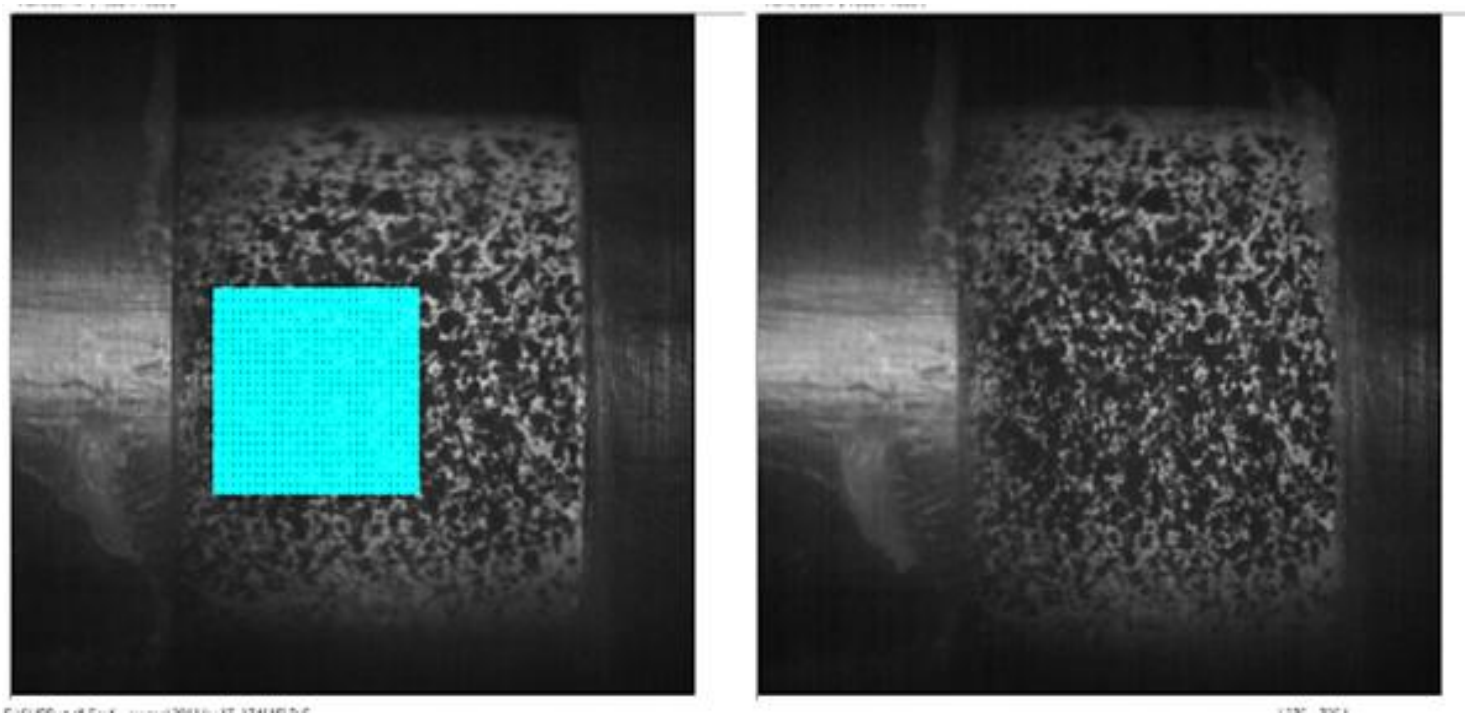

Figure 5.13: Mounting of the DIC grid. A 60 X 60 pixel grid with 5 pixel grid spacing is placed as shown on the specimen.

(a) Frame 1 to 15 (b) Frame 15 to 30

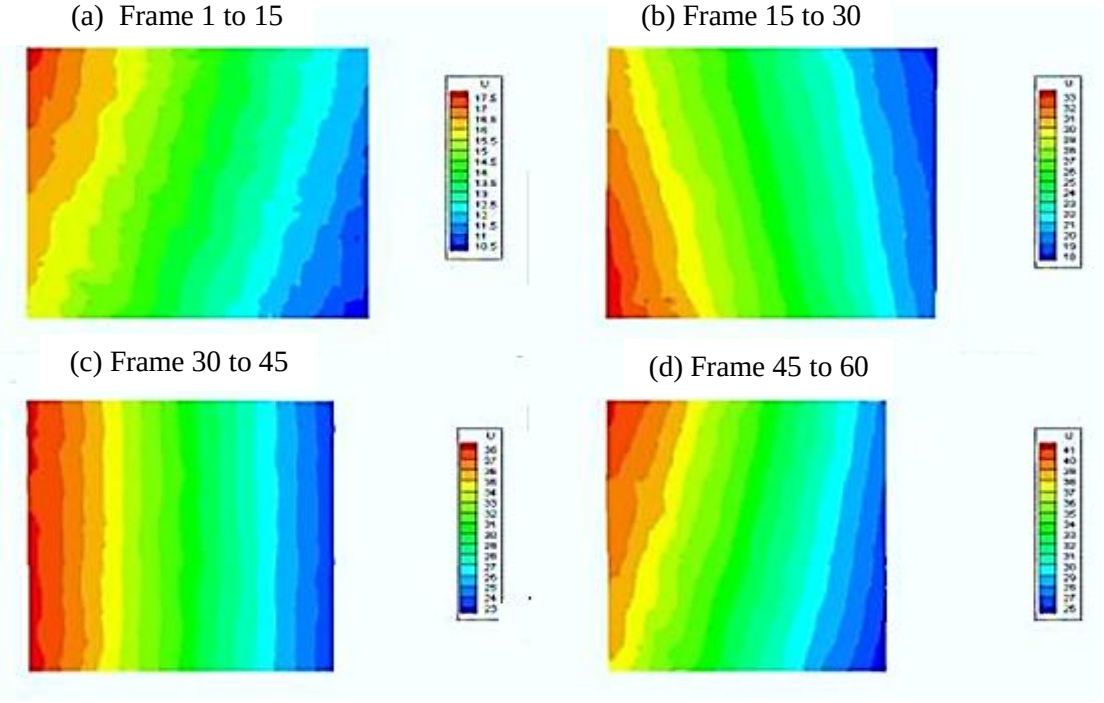

(c) Frame 30 to 45 (d) Frame 45 to 60

Figure 5.14: Incremental displacement contours of u along the X direction

(a) Frame 1 to 15 (b) Frame 1 to 30

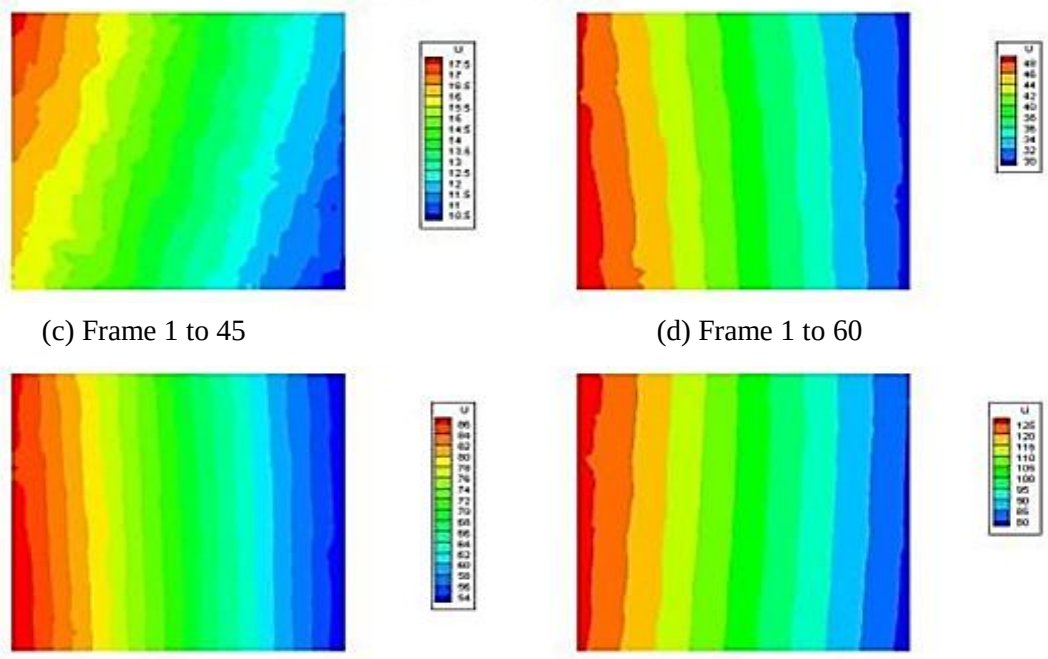

(c) Frame 1 to 45 (d) Frame 1 to 60

Figure 5.15: Cumulative displacement contours of u along the X direction

(a) Frame 1 to 15

(b) Frame 15 to 30

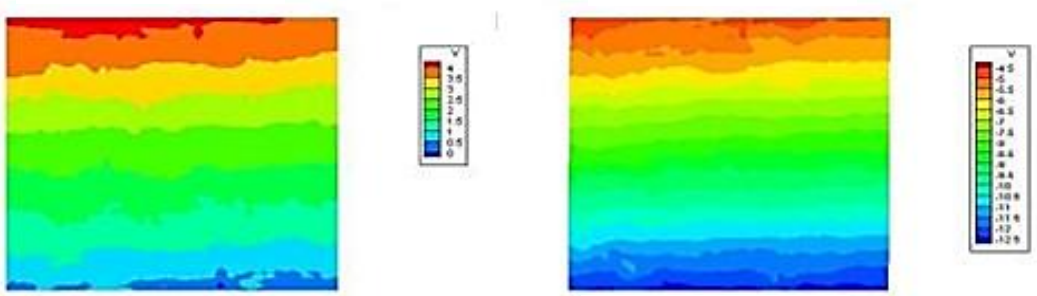

(c) Frame 30 to 45

(d) Frame 45 to 60

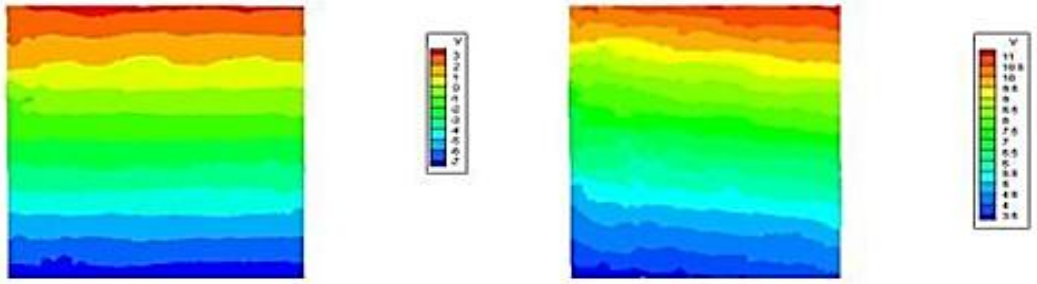

Figure 5.16: Incremental displacement contours of v along the Y direction

(a) Frame 1 to 15

(b) Frame 1 to 30

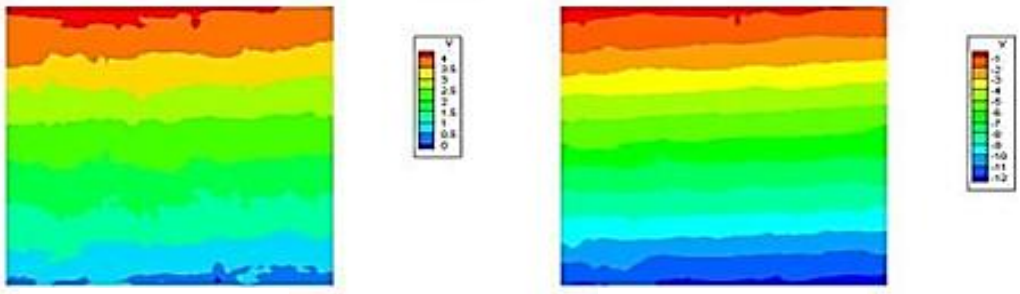

(c) Frame 1 to 45

(d) Frame 1 to 60

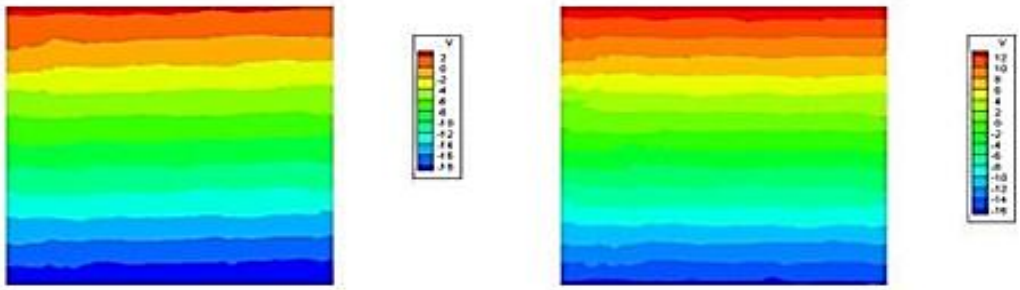

Figure 5.17: Cumulative displacement contours of v along the Y direction

(a) Frame 1 to 15

(b) Frame 15 to 30

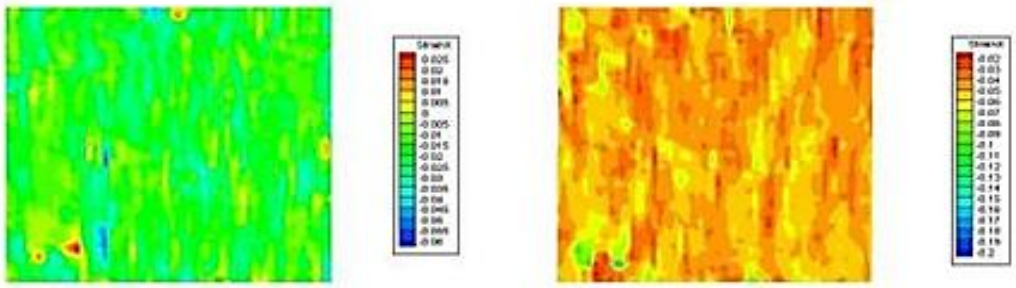

(c) Frame 30 to 45

(d) Frame 45 to 60

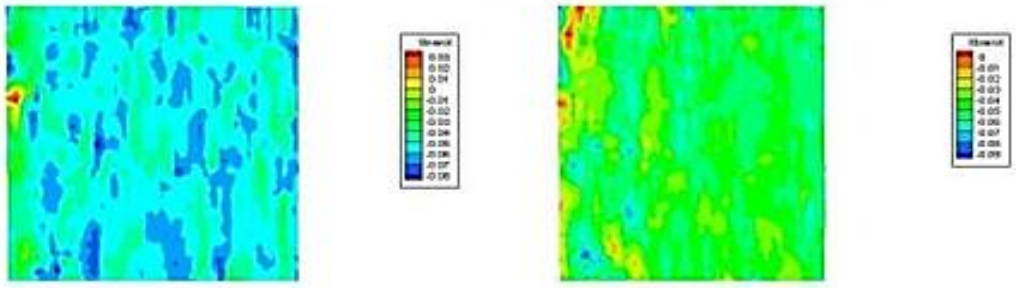

Figure 5.18: Incremental strain contours of ε_{xx} along the X-direction

(a) Frame 1 to 15

(b) Frame 1 to 30

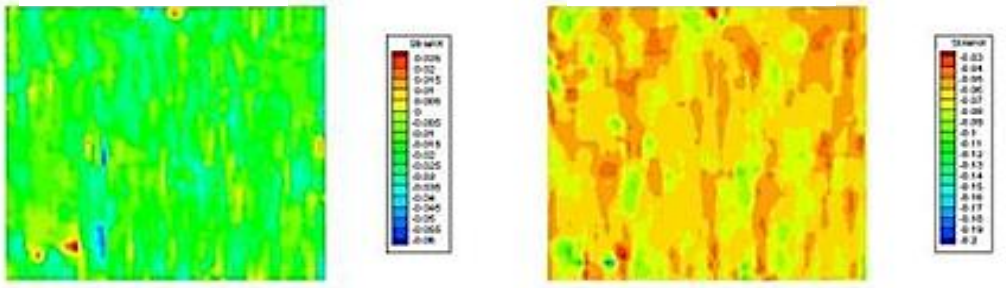

(c) Frame 1 to 45

(d) Frame 1 to 60

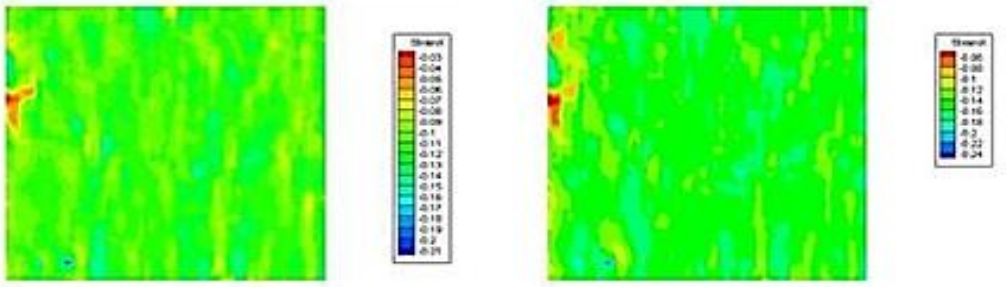

Figure 5.19: Cumulative strain contours of ε_{xx} along the X-direction

(a) Frame 1 to 15

(b) Frame 15 to 30

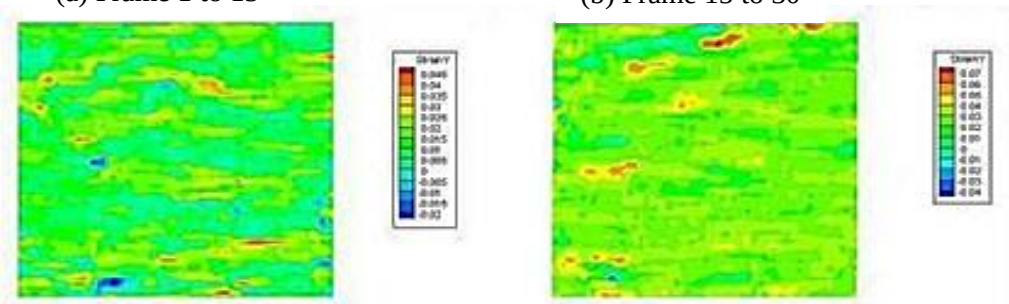

(c) Frame 15 to 45

(d) Frame 45 to 60

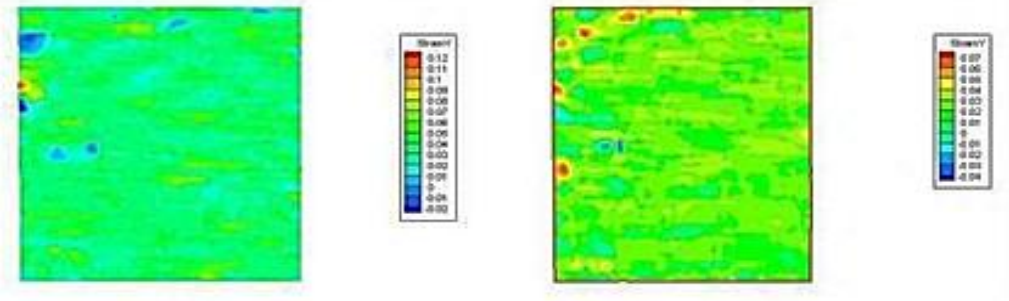

Figure 5.20: Incremental strain contours of ε_{yy} along the Y-direction

(a) Frame 1 to 15

(b) Frame 1 to 30

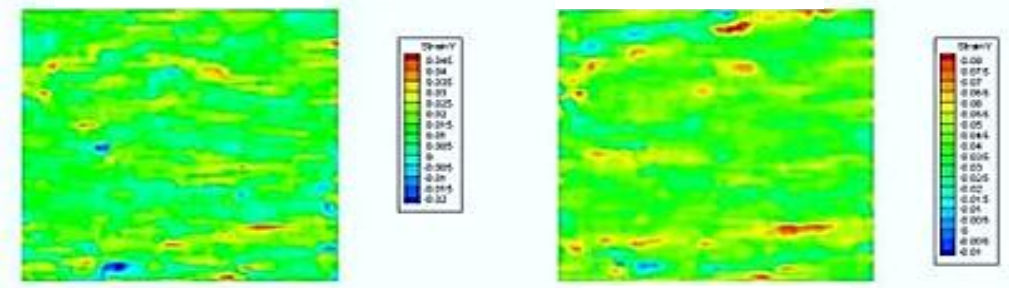

(c) Frame 1 to 45

(d) Frame 1 to 60

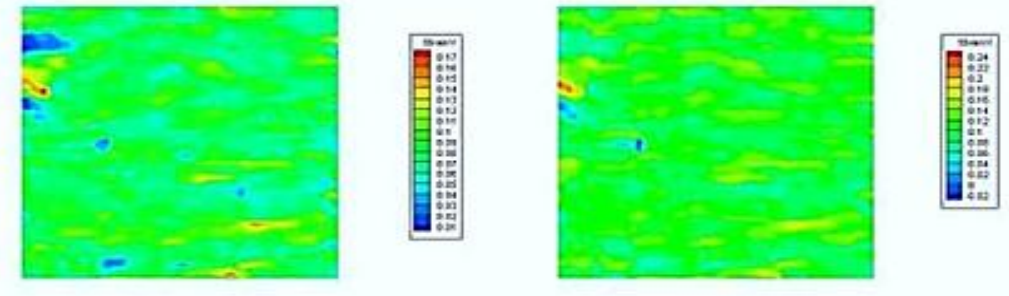

Figure 5.21: Cumulative strain contours of ε_{yy} along the Y-direction

5.3 Tests conducted on Dry Eglin Sand

The dry sand specimens used for all the tests conducted was received from Eglin Air Force Base (Eglin AFB), Florida. The sand received was silica-based, fine grain washed and dried. By naked eye the sand looks like beige in color but when observed under an optical microscope, the color of the sand appeared to be yellow. The sand appears to be part transparent and part translucent. The Eglin sand sample also showed void space between grains with smaller grains between larger grains. As the void space between the sand grains reduces, some smaller sand grains become visible on the surface. There are a few sand grains showing red, grey, and black colors due to inclusions in the sand. All sand used in this work was kept in sealed plastic bags to prevent moisture effect prior to testing. It may be noted that Eglin sand has been characterized by the Air Force Research Laboratory at Eglin Air Force Base extensively and is widely used by researchers in the U.S. and Europe.

5.3.1 Eglin Sand - Particle Size Analysis

The particle size distribution of dry Eglin sand was conducted according to the ASTM standard (D2487). Sorting of sand is done through utilization of set of sieves with different mesh sizes. The particle size distribution was measured for the as-received sand as shown in Figure 5.22. In our investigation we used eleven sieve sizes, namely, 14, 18, 20, 30, 35, 40, 50, 70, 100, 140, and 270 in the particle size analysis. Each sieve is 3 inch in diameter (manufactured by Dual Mfg. Co.) following the ASTM E-11 specifications. Hundred grams of sand was taken and passed on the largest sieve and the assembly of stacked sieves was shaken for about 20 minutes using a mechanical shaker (Dual Mfg.

Co., Model # D-4326). Table 5.1 gives the values recorded from the particle size analyzer. The cumulative plot of % mass of sand passed through each sieve is plotted against the corresponding sieve size. The grain size distribution of Eglin sand is shown in Figure 5.22. The values of D_{10} and D_{60} are obtained from the grain size distribution plot. D_{10} and D_{60} are the diameters of sand grains for which 10% and 60% of the particles are finer, respectively. The co-efficient of uniformity, was calculated as

$$C_U = D_{60}/D_{10}$$

C_U value of less than 4 indicates uniform particle size, as is the case with Eglin sand indicating that Eglin sand grains have a narrow size distribution. Poorly graded sands have a steep size distribution curve. Based on Unified Soil Classification System (USCS), Eglin sand is categorized as SP-SM. The symbol 'S' represents sand and, 'SP-SM' refers to poorly graded sand with silt. Table 5.2 describes briefly the physical properties of Eglin sand obtained from the sieve analysis and from the previous literature review [31].

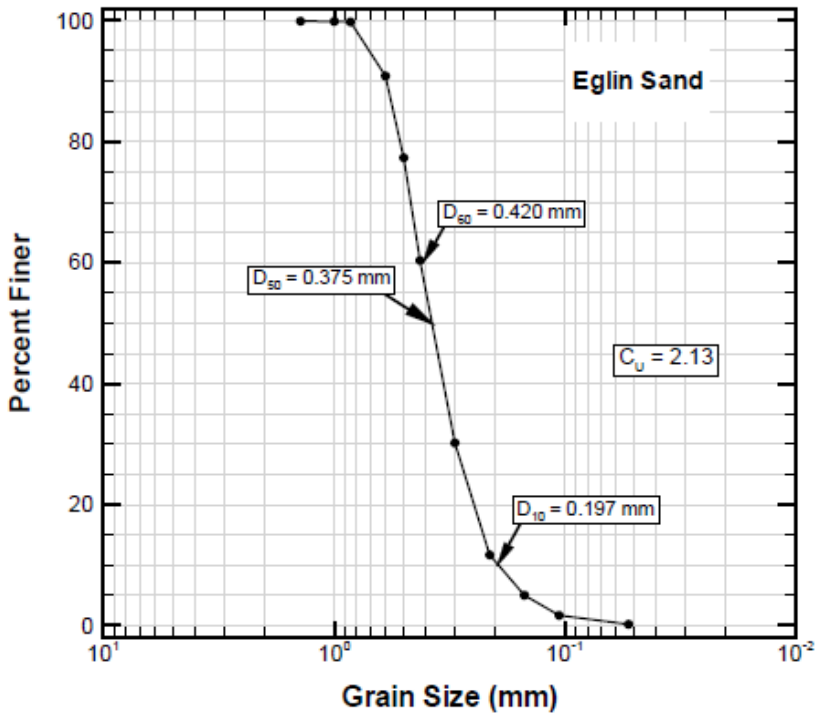

Figure 5.22: Particle size distribution of Eglin sand [32]

Table 5.1; Particle size analysis of Eglin sand [32]

Sieve Size	Sieve opening (mm)	Mass of sand collected (gm)	Mass of sand passed (gm)	Percent finer by weight
14	1.400	0.087	99.913	99.91
18	1.000	0.044	99.870	99.87
20	0.850	0.075	99.795	99.79
30	0.600	8.873	90.922	90.92
35	0.500	13.430	77.492	77.49
40	0.425	16.852	60.640	60.64
50	0.300	29.956	30.684	30.68
70	0.212	18.374	12.310	12.31
100	0.150	6.623	5.687	5.69
140	0.106	3.313	2.374	2.37
270	0.053	1.456	0.918	0.92
Pan		0.231	0	0.00

Table 5.2: Physical properties of Eglin sand [32]

USCS Classification	SP-SM
Specific gravity	2.65
D_{50} or average grain size (mm)	0.375
D_{60} Particle size (mm)	0.420
D_{10} Particle size (mm)	0.197
Uniformity, $C_u = D_{60}/D_{10}$	2.13

After impact, most sand grains (Figure 5.23 (a)) were crushed into tiny powder with only occasional larger sand grains remaining, as shown in Fig 5.23 (b).

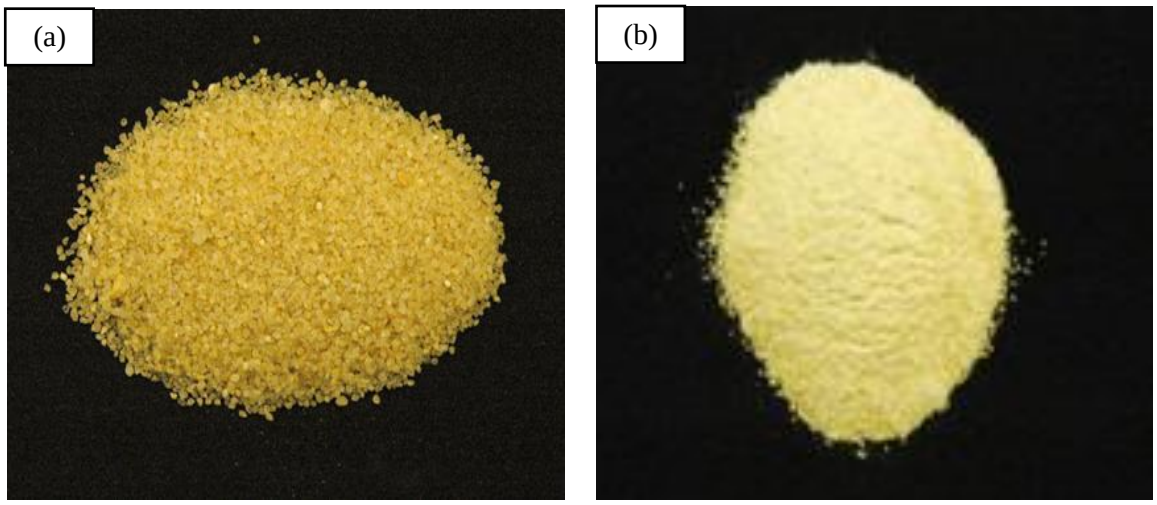

Figure 5.23: Macrographs of Eglin sand (a) before (b) after the compression test

In general, the observation of sand grains after impact requires loading once in a SHPB experiment under a given set of testing conditions. However, during SHPB impact, the reflected wave in incident bar will reflect back and forth, which may allow potentially

multiple reflected compressive waves to load a sand sample for several times, until the wave is fully dissipated, if the specimen is still sandwiched between the incident bar and the transmission bar after the first impact. To collect sand sample for observation after the SHPB test, the sand sample must experience only a single impact loading, which can be achieved through the use of a momentum trapper [24-26]. Another approach for ensuring loading only once is to use an incident bar twice as long as the transmission bar. The incident bar used in our setup is 24 ft long which is twice the transmission bar length of 12ft. This 1:2 ratio of incident bar length to transmission bar length allows the specimen and transmission bar to separate before the subsequent compressive waves in the incident bar hit the specimen again, so that multi-loading is avoided [16].

5.3.2 Confinement used for Sand tests

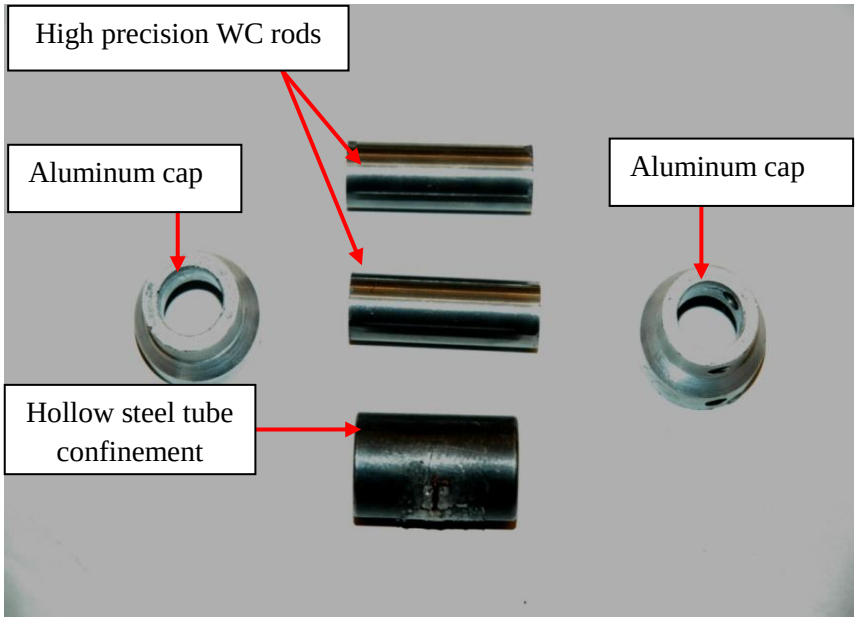

Figure 5.24: Components of the confinement fixture used in the SHPB tests for Eglin sand

Figure 5.24 is a photograph of various components of fixture. The main aim for having such a design for the fixture is: a) to reach high axial stresses in the sand sample, b) to prevent non-uniform stresses along the cross-section of the sand sample arising from the rotation of the sample while testing and misalignments in the test frame, c) to measure displacements independent of the system compliance, and d) to place the confined sample at the same location between the pressure bars for each test to maintain repeatability. At the ends of the transmission bar and the incident bar which are in contact with the WC rods, an end cap made of aluminum was press-fitted as shown in Figure 5.25. The sole purpose of these two caps at the end was to make sure the specimen was intact within the steel hollow tubing and the sample always aligned axially.

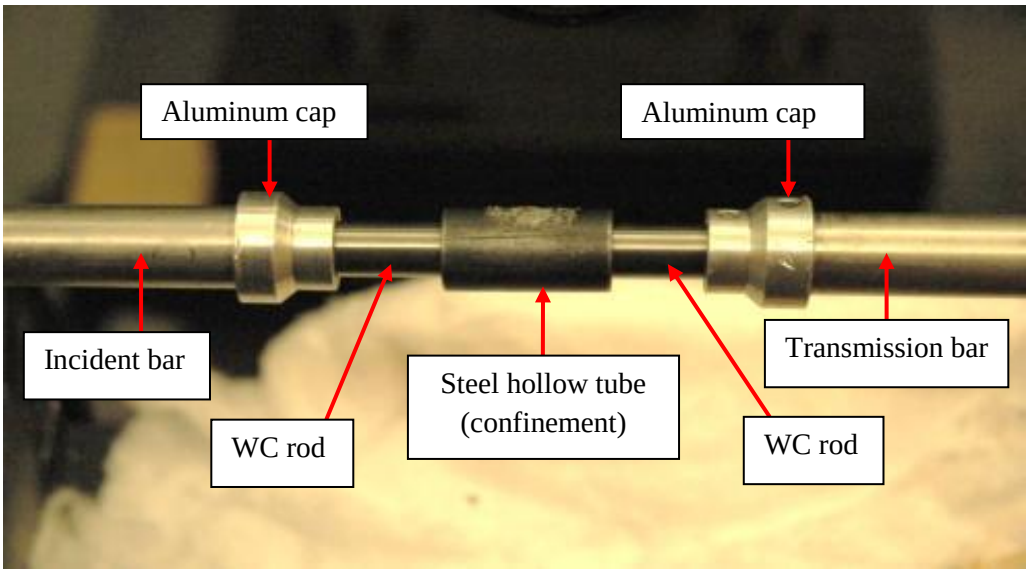

Figure 5.25: Assembly showing the components of the confinement fixture on the SHPB setup

Tests were conducted on an SHPB uniaxial testing apparatus equipped with a pneumatic system and data acquisition unit. The maximum pressure that can be achieved

in this pressure system is 150 psi. With restrictions in the pneumatic piping we could go only upto 120 psi; the sample diameter was fixed at 0.5 in for both metal and sand. The aim is to achieve axial stress of 400 MPa and above. The sample is confined in a hollow steel tube with internal diameter of 12.7 mm (0.5 in.). The aluminum caps were designed so as to hold the sample together with the WC rods on the pressure bars (refer to Figure 5.25). A 0.50 in diameter tungsten carbide (WC) rods were inserted from both ends of the hollow steel tube filled with the sand sample. The length of the confinement was 31.826 mm (1.253 in). It was heat-treated in an oven to a temperature of 1100±10°C and air-quenched. Tempering was performed at 180±10°C to relieve stresses and to increase the toughness. Rockwell hardness measurements, made after heat treatment, gave an average hardness of HRC 58 on the outer surface of the confinement. After heat treatment, the inner bore was re-finished with a120 grit (silicon carbide abrasive) flex-hone tool at 1200 rpm for 60 seconds. A smooth bore is necessary to minimize friction between the inner walls of the confinement and the sand sample. Determination of friction between the sand particles and the walls of the confinement is not possible. In order to reduce friction, the length of the sand sample was kept small (10 mm for the least dense samples). Tungsten carbide rods were used to compress the sample in the confinement. The WC rods are 12.7 mm in diameter (0.5+0.0000 −0.0005 in.) and 38.1 mm (1.5 in.) long. To accommodate for the expansion of the WC rods in the confinement during the tests, the WC rods were smaller than the bore diameter of the confinement. The WC rods were cut from a longer stock rod using a diamond saw. The WC rods had 10% cobalt content (binder) with submicron grain size. This grade of WC rods has an estimated hardness of HRA 92, modulus of elasticity of 580 GPa and compressive strength of 5.5 GPa (information

provided by the manufacturer, Kennametal Inc.). High strength, good surface finish, and high hardness of cemented WC rods make it an ideal choice of material for compression of sand to high pressures. The rods exhibited resistance to abrasion and wear by the sand grains even after numerous rounds of tests.

5.3.3 Sample Preparation

In all of the Eglin sand compression tests conducted in this investigation, 2 gm of sand was used, irrespective of the parameters used. Whether it is the effect of initial mass density, effect of pulse shapers, or effect of particle size, 2.0000±0.0010 gram of sand was always weighed using a balance (Denver Instruments APX-200 with 0.1 mg resolution), and poured into the confinement with the bottom WC rod in place. Care was taken to prevent loss of sand grains during the transfer. The top WC rod was inserted into the confinement and the assembly was compacted. Since no standard methods for compaction exist, the assembly was gripped firmly in hand and gently tapped on a rubber pad. The assembly was rotated after every few taps to prevent settling of smaller sand grains. This was done to maintain the heterogeneous distribution of sand grains. The length of the rods was measured from time to time to check if the sand specimen was compacted to the desired density based on Equation (10).

$$\rho = \frac{m}{\Pi/4 \; D^2 \; L_s} \tag{10}$$

In this work, the length of the incident bar (24ft long) is 2.0 times of the length of the transmission bar (12ft long); thus the sand assembly was separated from the ends of the incident and transmission bars so that a sand specimen was only loaded once in an

experiment. The sand specimen assembly was stacked in a steel confinement tube, with tungsten carbide rods inserted in it to prevent it from falling, for ease of collection of the sand after impact. The required length of the sand sample was achieved by tapping the steel confinement tube in order to achieve the desired mass density.

5.3.4. Dynamic Equilibrium and Repeatability of SHPB Data

Typical recorded input and output signals from strain gages attached to the bars in a SHPB test are plotted in Figure 5.26. Initially, the incident pulse rises rapidly during the first 50 μs, then increases slowly for ~ 450 μs during the loading phase, and finally decreases in the last 100 μs during the unloading phase. Similar trend was observed in the experiments conducted on sand in this investigation, as shown in Figure 5.27. The difference between the two graphs are Figure 5.26 is obtained directly from the oscilloscope whereas Figure 5.27 is a graph showing the processed signal data and provides the stresses obtained in the pressure bars. It may be noted that the nature of both the graphs remains the same.

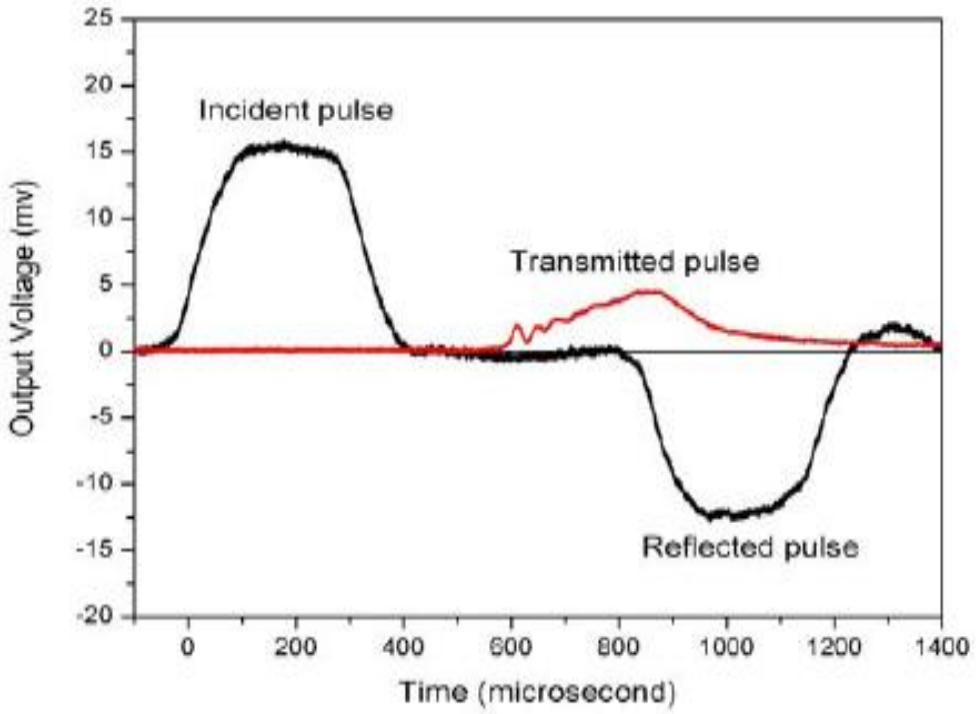

Figure 5.26: Typical signals obtained from the oscilloscope for Eglin sand in SHPB test [21]

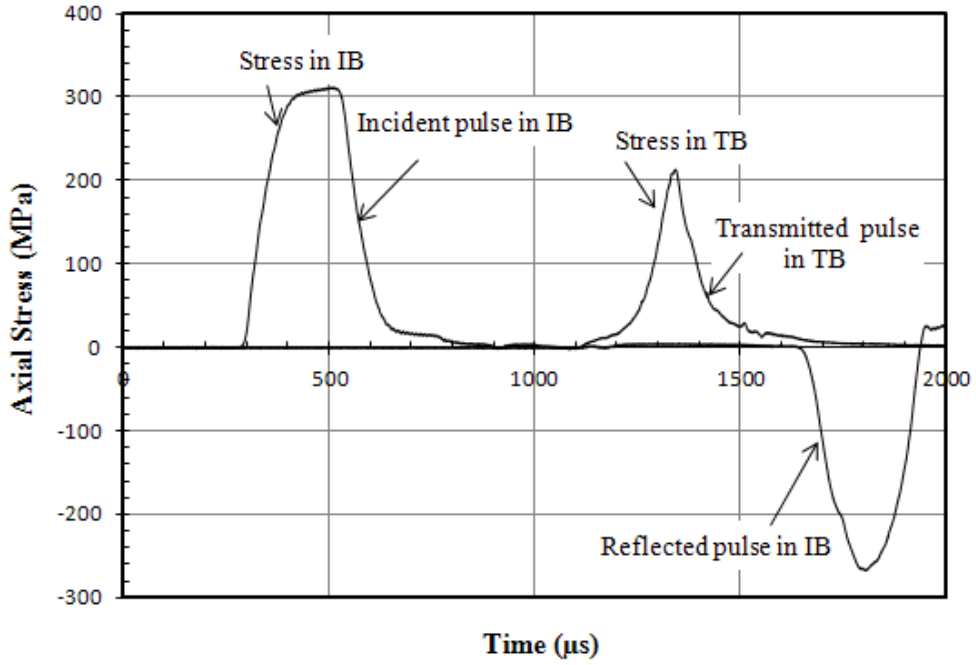

Figure 5.27: Typical stress signals obtained for the Eglin sand in SHPB test

In the dynamic compaction testing of sand using SHPB apparatus, when the stresses applied on both ends of the specimen are equal, dynamic equilibrium state is established. The experiment is then considered valid, and the acquired experimental data are processed further to determine the stress-strain relationship. To examine the dynamic equilibrium condition, the front stress and the back stress on the specimen are calculated following the 1-wave, and 2-wave methods. The stress at the front face (end of the specimen in contact with the incident bar) and the back face (end of the specimen in contact with the transmission bar) with time are shown in Figure 5.28 for the examination of dynamic stress equilibrium. Similar kind of trend, if not better of the stress equilibrium was achieved in our experiments as shown in Figure 5.29. The front stress was very close to the back stress during loading, indicating that the dynamic equilibrium condition has nearly been established and the specimen was uniformly loaded. In a valid SHPB experiment, the incident, transmitted, and reflected signals are processed further to determine the stress-strain relationship at high strain rates.

The average relative deviation of the stress-strain curves (Figures 5.30 to 5.37), is in the range of 3.57% to 8.6% for the three densities of sand used, each tested with a minimum of 5 specimens. This indicates that the percentage variation in stress-strain curves is not solely due to density variation. The dynamic behavior of sand is sensitive to the packing conditions and the morphology of sand grains. An Eglin sand specimen is comprised of sand grains primarily in the range of 0.1 to 1 mm with an irregular shape.

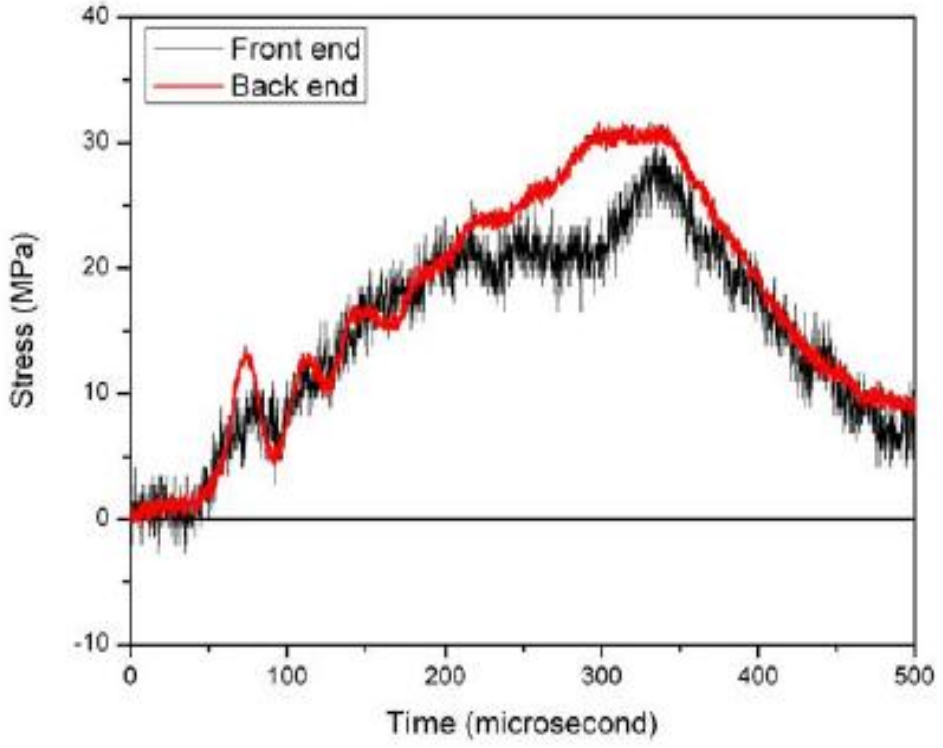

Figure 5.28: Dynamic stress equilibrium achieved for uniaxial experiment [21]

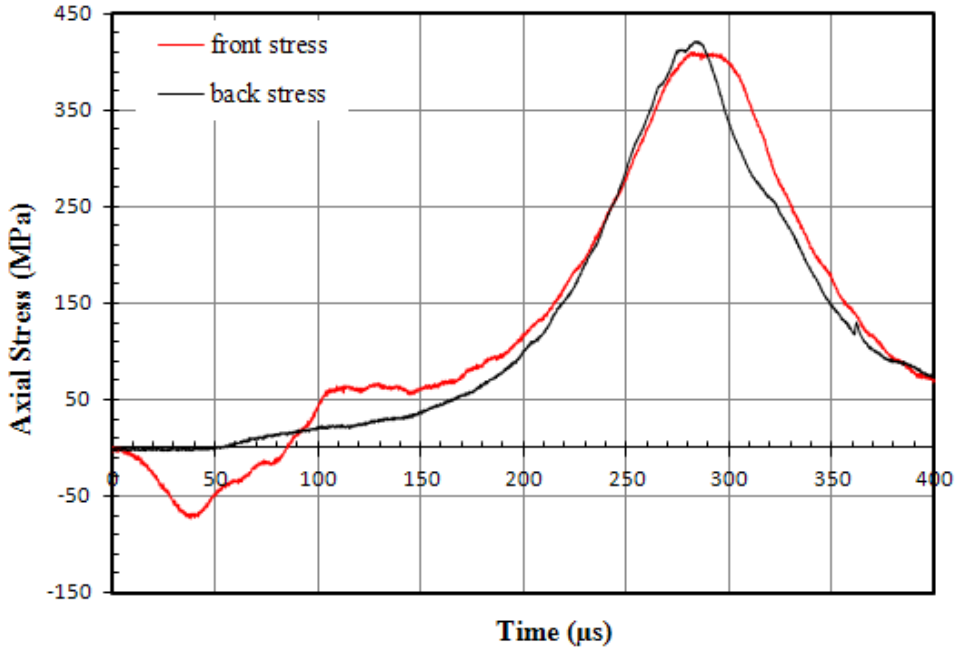

Figure 5.29: Dynamic stress equilibrium achieved in SHPB tests on dry Eglin sand

As previously mentioned, sand sample at a density of 1.51 g/cm^3 was formed by filling in the cavity enclosed by hollow cylinder and WC rod ends with a small amount of tapping and shaking. Different sand grains are randomly stacked together, giving large variation in the sand packing, including variation in the end contact conditions with WC rods, from one sample to another, potentially leading to large variation in data, up to 8% as observed. When sand was consolidated through shaking to reach a density of 1.63 g/cm^3, all the fine sand grains were allowed to move and rotate to fill the cavities between large sand grains, giving much lower porosity with less variation from sample to sample in packing configuration than the case with a density of 1.51 g/cm^3. As a result, higher density sand (e.g., 1.63 g/cm^3) gives much better reproducibility than lower density sand (1.51 g/cm^3).

5.3.5 Effect of initial mass density on stress-strain relationship of dry Eglin sand

The mechanical behavior of dry Eglin sand depends on its initial mass density. Its effect on the stress-strain relations was investigated at strain rates from ~ 500s^{-1} to 1100s^{-1}. To determine the effectiveness and improving mechanical properties, we also used dry Eglin sand sample in compression to determine the stress-strain relation at high strain rate to compare with the results of dry Eglin sand used by Luo *et al's* [5] under the same conditions.

Results of the tests conducted to investigate the effect of initial density of dry sand on its mechanical behavior are given in Figures 5.30 to 5.37. Minimum density of 1.51 g/cm^3 was attained by pouring the sand sample into the confinement and gently tapped a few times to reach a sample length of 10.45 mm. Maximum density of 1.63

g/cm^3 was attained gently tapping the assembly for an extended period of time to reach a length of 9.7 mm. Minimum of five tests were conducted at each packing density for repeatability. Figures 5.30 to 5.37 show good repeatability in the axial stress-strain behavior for the lowest and highest initial densities. Particle size of 150 - 180 μm (sieve size 100) was used in all tests for initial mass density. The reason behind this was to densely pack the sand sample at higher densities. Also, we were restricted by the confinement length, as using coarser sand would not allow achieving a density of ~1.63 g/cm^3 and above. All experiments were conducted up to a maximum axial strain of ~ 27%. Tests conducted on the densest configuration of sand, namely, 1.63 g/cm^3 reached maximum axial stress of 315 MPa at corresponding axial strain of 23.8%. Three nominal densities of Eglin sand, namely, 1.51, 1.57, and 1.63 g/cm^3 were compressed to 28% axial strain at 780 s^{-1} strain rate. Figure 5.37 shows the axial stress-strain plots. It can be seen that the slope of the axial stress strain curves increases as the initial density increases. As the initial density increases, the axial stress also increases.

The linear plot of axial stress-strain curves in Figures 5.30 to 5.37 exhibit two linear trends in the loading region followed by a linear unloading curve. The curves follow the general three phase behavior proposed by Hagerty *et al* [40]. The first linearity is observed in the initial portion of the loading curve, between 0% and 0.5% axial strain. Hagerty *et al* [40] defined the slope of the initial portion of the loading curve as the secant modulus (M_i). The initial linear slope for the three different densities experimented is found to be almost same, as seen in Figure 5.37. This is likely due to the elastic compression of the sand grains during initial loading. The slopes of all the curves for different densities of Eglin sand are found to be similar. There is no apparent

influence of initial density on the secant modulus. The initial linear region is terminated at the break-point stress, after which particle crushing begins. This region is marked by a drastic drop in the slope of the stress-strain curve. The axial stress-strain plot shows the dependence of the onset of particle crushing on the initial density.

The break-point stress is found to increase with increase in initial density. This is found to be in agreement with the results of Luo *et al's* [5]. The break-point stress becomes less distinguishable as the initial density increases. The crushing and rearrangement of sand particles are found to be gradual in loosely packed sand than in dense sand. The higher packing density of the densely packed sand constrains the rearrangement of the sand grains which lead to the build-up of higher stresses. Thus the duration of grain crushing in densely packed sand is shorter than that of loosely packed sands. The transitional phase of grain crushing is gradually followed by the pseudoelastic compression phase, where the crushed grains behave much stiffer than in the initial uncrushed phase. The extent of elastic recovery is similar for all densities, indicating that the elastic strain energy accumulated in the pseudoelastic phase is recovered during unloading [32]. The trends observed in the axial stress-strain curves in Figure 5.37 agree closely with the previous results obtained by Luo *et al's* [5] as shown in Figure 5.36. Overall, the stiffness of the stress-strain curves is found to increase with higher initial density. Dynamic tests conducted by Luo *et al's* [5] on the Split Hopkinson Pressure bar (SHPB) up to axial stresses of 350 MPa, show similar trends in the curves of axial stress-axial strain. It can be inferred from the experimental results, that the densely packed sand has lesser amount of voids than loosely packed sand. Hence, densely packed sand can easily obtain higher stress value than the loosely packed sand. The difference of stress

value achieved for the densely packed sand and the loosely packed sand was of the magnitude of ~ 60MPa.

5.3.5.1 Tests on Eglin sand at nominal density $\rho = 1.51 g/cm^3$

Tests were conducted on dry Eglin sand of sieve size 100 (150 -180 μm) at a constant nominal density of $\rho = 1.51 g/cm^3$. A minimum of 5 tests were conducted to check the repeatability and accuracy of the results. An average velocity of the striker impact was calculated for all the tests to be 14.3 m/s. Results of stress-strain plots are shown in Figure 5.31 and compared with Luo *et al's* [5] results testing of Eglin sand at the same density. The strain rate achieved in our experiments on an average of all the tests was ~ 805 s^{-1}.The results of Luo *et al's* [5] at same density were conducted with unsorted sand i.e. with the as-received sand. Whereas, in our experiments, we chose a sieve size of 100 of sand for conducting and analyzing the results of initial mass density, to be more precise. Lead was used as the pulse shaper in all the experiments as it gave highest stress values and constant strain rate over a sustained period of time. The diameter of the sample in all the tests was 12.7 mm and the mass of sand used was 2gms. The length of the sample was controlled accordingly to achieve the desired density of 1.51 g/cm^3.

It was found that ε_{max}= 27.4% was achieved in our experiments compared to 27.8% in Luo *et al's* [5] tests. Also, the σ_{max} = 255 MPa was achieved compared to 295 MPa in Luo *et al's* [5] work. The standard deviation calculated for these tests was 14.74 MPa. Figures 5.30 and 5.31 can be compared for further analysis.

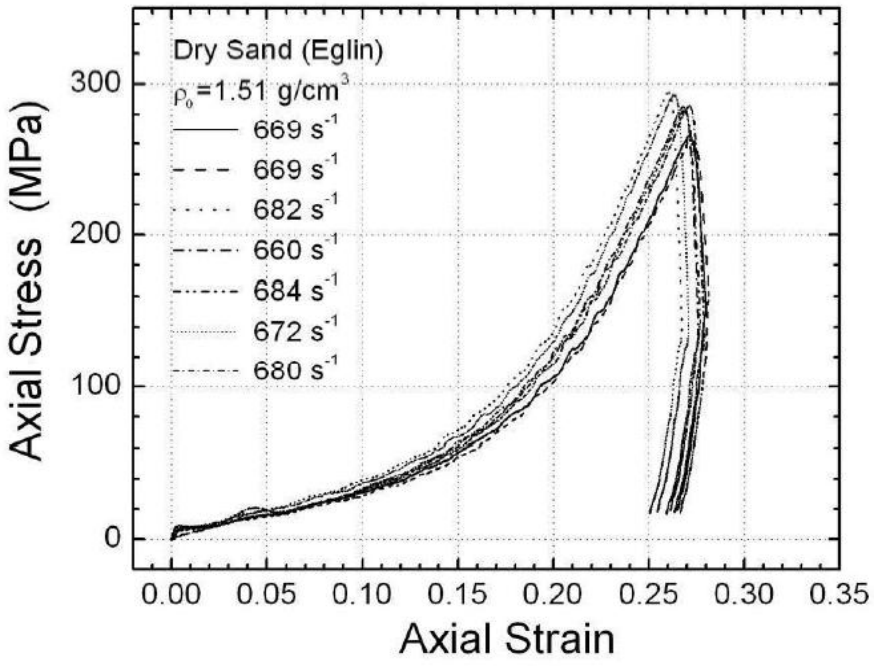

Figure 5.30: Reproducibility of SHPB test data of dry sand; axial stress vs. axial strain for $\rho = 1.51$ g/cm^3 [5]

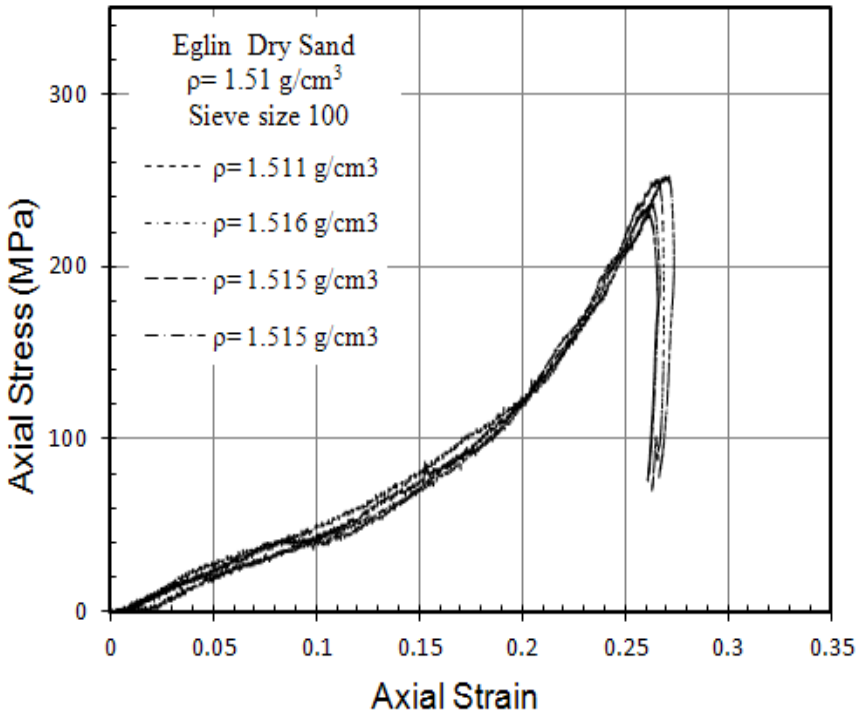

Figure 5.31: Reproducibility of SHPB test data of dry sand; axial stress vs. axial strain of sand for $\rho = 1.51$ g/cm^3

5.3.5.2 Tests on Eglin sand at nominal density $\rho = 1.57 g/cm^3$

Similar to the tests carried out for $\rho = 1.51 g/cm^3$, tests were conducted on dry Eglin sand of sieve size 100 (150 -180 μm) at a constant nominal density ρ of $1.57 g/cm^3$. Except for the change in the initial mass density, all other parameters were kept the same. Results of stress-strain plots are shown in Figure 5.32 and compared with Luo *et al's* [5] results using the same density. The strain rate achieved in our experiments on the average for all the tests was ~ $765 s^{-1}$. The results of Luo *et al's* [5] at the same density were conducted with the as-received sand (unsorted sand). In our tests, we chose sand of sieve size 100 for conducting and analyzing the results of initial mass density, to be more precise. The diameter of the sample for all the tests was 12.7 mm and the mass was 2 gms. The length of the sample was controlled accordingly to achieve the desired density of 1.51 g/cm^3.

It was found that ε_{max}= 26.2% was achieved in our experiments compared to 25.5% in Luo *et al's* [5] tests. Also, the mean stress value (σ_{mean}) from these seven tests was calculated to be 287 MPa. Luo *et al's* [5] test results gave a value of 265 MPa as the mean stress value. The standard deviation was found to be 10.14 MPa. Figures 5.32 and 5.33 can be compared for further detail analysis if needed.

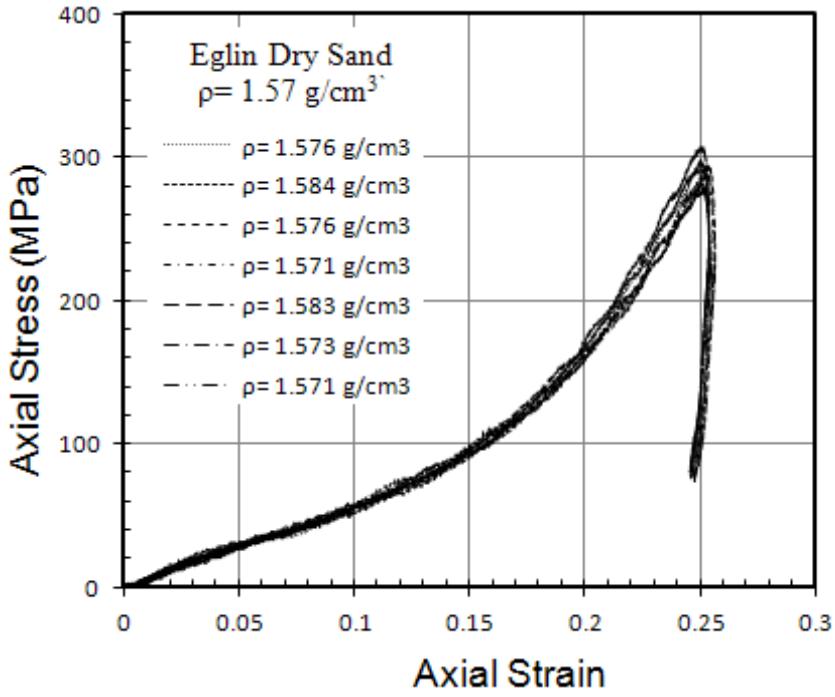

Figure 5.32: Reproducibility of SHPB test data for dry sand in SHPB test; axial stress vs. axial strain for ρ = 1.57 g/cm^3

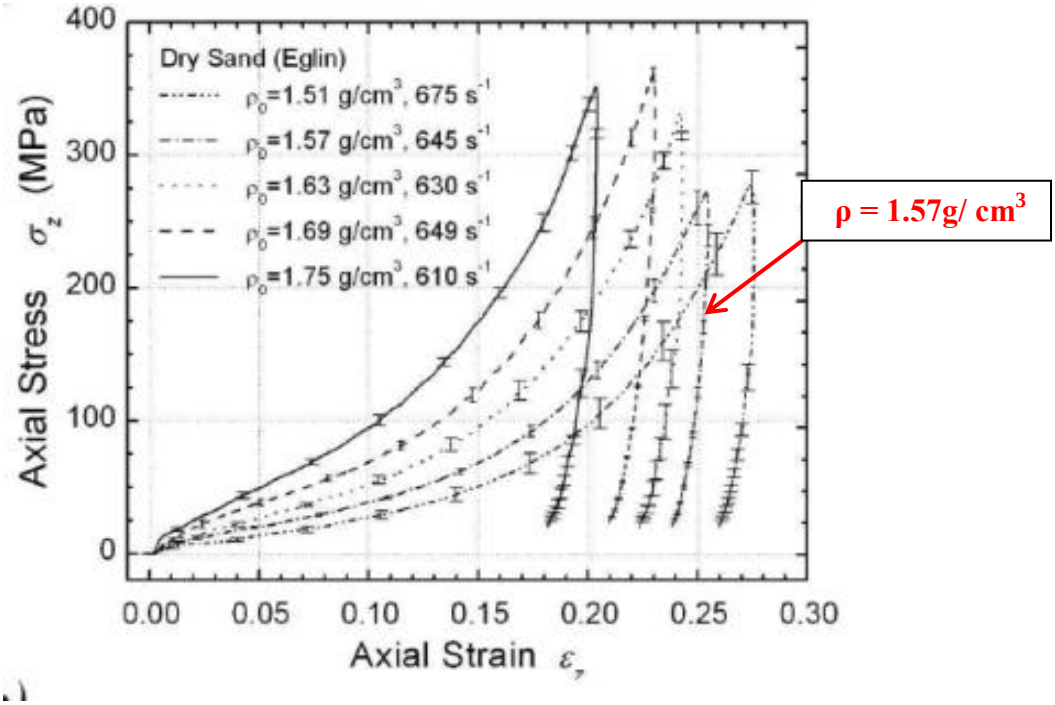

Figure 5.33: Variation of axial stress-strain for different nominal densities of dry sand at constant strain rate [5]

5.3.5.3 Tests on Eglin sand at nominal density $\rho = 1.63$ g/cm^3

Similar to the tests carried out for $\rho = 1.51$ g/cm^3 and $\rho = 1.57$ g/cm^3, tests were conducted on dry Eglin sand of sieve size 100 (150 -180 μm) at a constant nominal density ρ of 1.63 g/cm^3. Except for the change in the initial mass density, everything else was kept the same as in the previous cases. Results of stress-strain plots are shown in Figure 5.34 and compared to Luo *et al's* [5] results of testing of Eglin sand at same density. The strain rate achieved in our experiments on an average of all the tests was ~ 730s^{-1}.

It was found that $\varepsilon_{max} = 23.8\%$ was achieved in our experiments compared to 23.5% in Luo *et al's* [5] tests. Also, the mean stress values from these five tests was calculated to be $\sigma_{mean} = 307.50$ MPa. Luo *et al's* [5] test results gave a value of 325 MPa as the mean stress value. The standard deviation calculated for all these tests was 7.20 MPa. Figure 5.34 and 5.35 can be compared for further analysis.

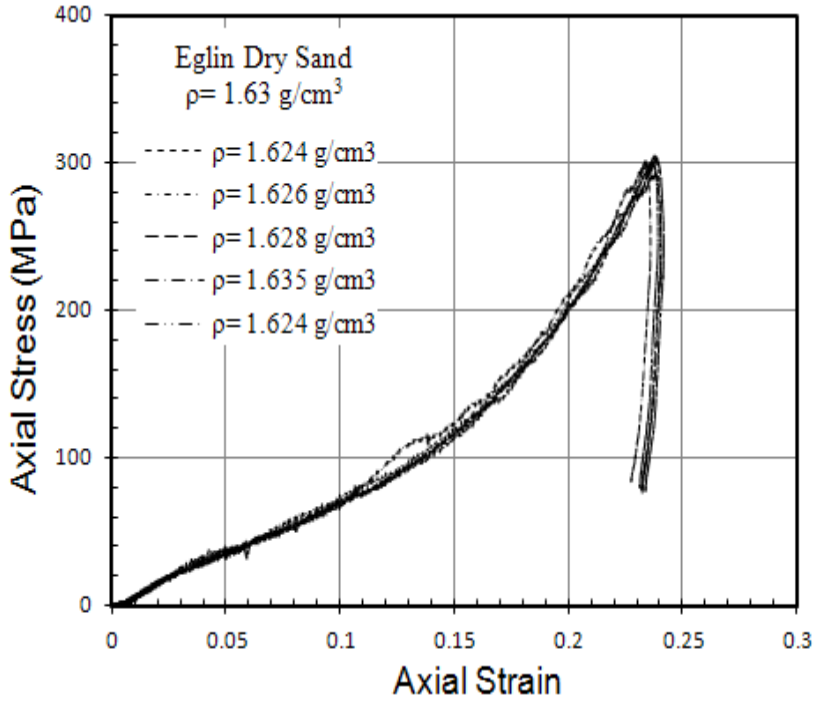

Figure 5.34: Reproducibility of SHPB test data of dry sand in SHPB test; axial stress vs. axial strain for ρ = 1.63 g/cm^3

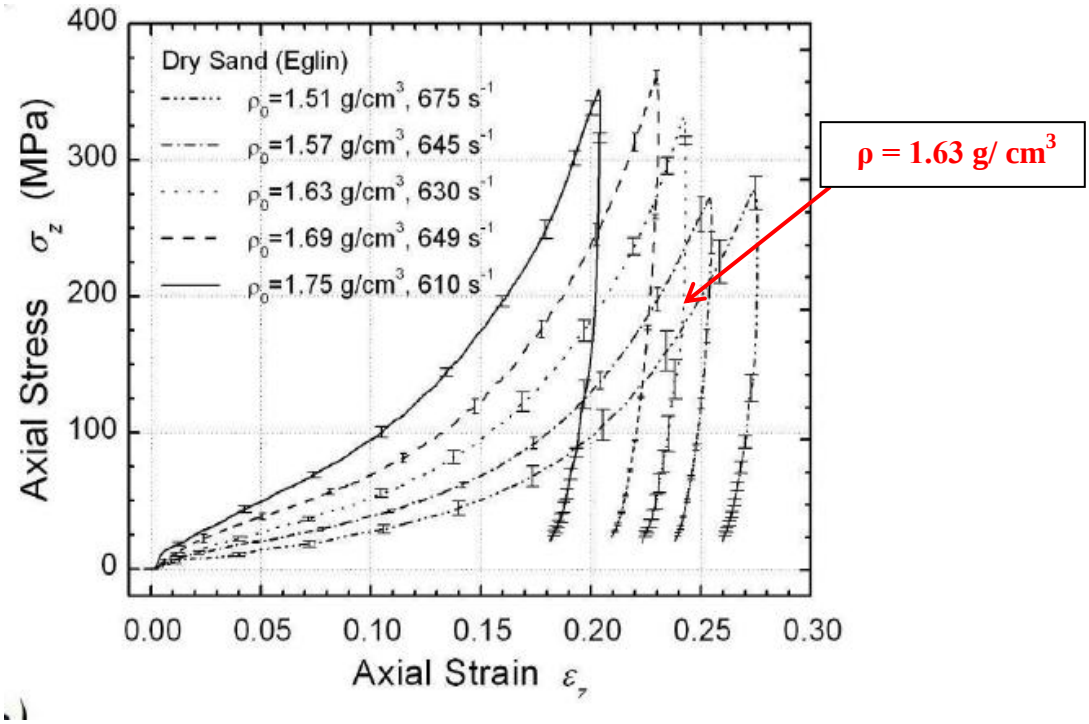

Figure 5.35: Variation of axial stress-strain for different nominal densities of dry sand at constant strain rate [5]

5.3.5.4 Comparison of effect of initial mass densities on dynamic behavior of Eglin sand

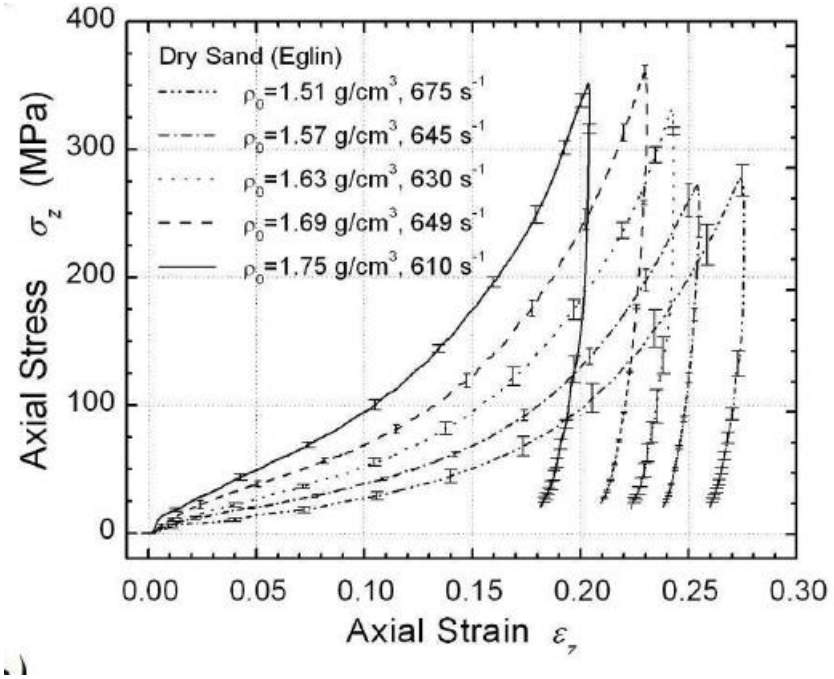

Figure 5.36: Variation of axial stress-strain for different nominal densities of dry sand at constant strain rate [5]

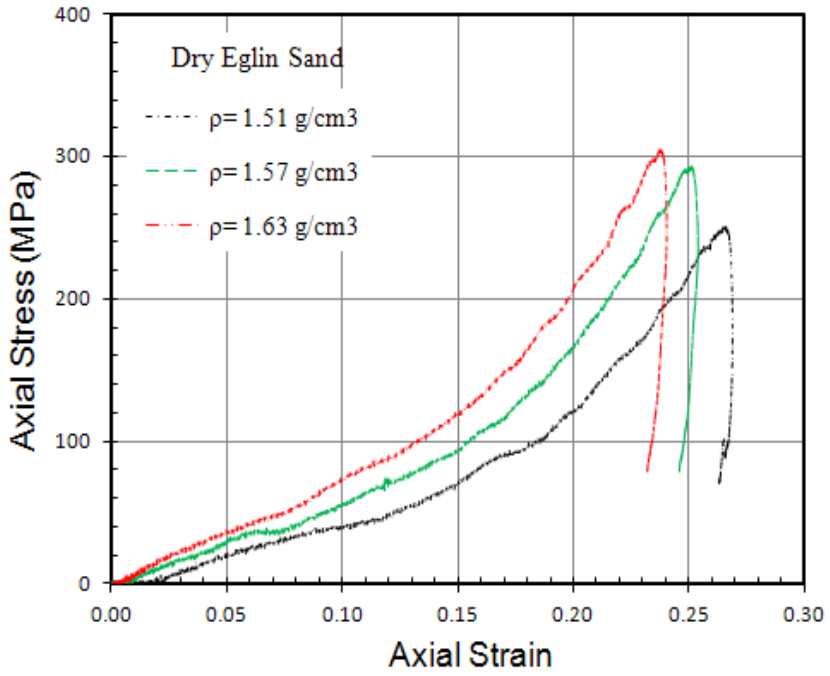

Figure 5.37: Axial stress-strain experimental plots of dry sand at different sand densities in SHPB tests

Figure 5.36 and 5.37 can be compared one on one for further analysis. Table 5.3 gives you the values of the stress and strain achieved in our test conducted on effect of initial mass density.

Table 5.3: Variation of max axial stress and max axial strain values obtained for different initial mass densities

Initial mass density (g/cm^3)	Max Axial Stress (MPa)	Max Axial Strain
1.51	260	26.50%
1.57	282	25.25%
1.63	315	23.8%

5.3.6 Effect of using different Pulse Shapers at constant density (ρ= 1.57 g/cm^3)

Pulse shapers play an important role in shaping the pulse. Pulse shaping techniques are developed for both loading and unloading paths of SHPB tests to obtain valid dynamic stress-strain relationships for engineering materials. Determining and using the proper pulse shaper ensures the precise control of the profiles of the loading and unloading portions of the incident pulse.

Assuring a constant strain rate during dynamic testing is highly desirable to develop physics based predictive, constitutive material models. Incident pulse shaping has not been fully developed or successfully demonstrated over a wide range of strains in high work hardening materials. To shape an incident pulse for a constant strain rate in a split-Hopkinson pressure bar (SHPB) test, a very soft material was selected to fabricate the pulse shaper. Several test sample materials with pulse shapers, namely, aluminum

(Al2024), annealed copper (C360), and lead (Pb) were tested in SHPB with and without a sample in between the bars at different strain rates and pressure. The current experiments demonstrated that lead (Pb) pulse-shaper is ideally suited to shape the incident pulse to achieve constant strain rates and achieve stress equilibrium, while inherently dampening high frequency oscillations in the incident pulse.

Until now, most of the work associated with the pulse shaper has focused on the experimental method to shape an incident pulse [1,3,7,10,12] and theoretical analysis to model pulse-shaper material response [9,10]. The effect of the pulse shaper on the stress-strain response of the materials investigated has not received much attention. In the current study, three typical pulse shaper results are produced using the same sand grain size at the same density, to illustrate the effect of the pulse shaper on the stress-strain response of the sand material under investigation. In Ellwood *et al.'s* [41] work, in order to shape the incident pulse for a constant strain rate, they recommended employing a dummy sample of the same material as the test sample in their SHPB equipped with a preloading bar. It was also reported that the pulse-shaper material is often the same material as the sample and the pulse shaper is a disc slightly larger in diameter than the bar [7] a work-hardening characteristic similar to the test material is required for the pulse shaper material [20] and the pulse-shaper material is typically selected to have the same strength as the sample [6]. However, from the current work, it appears that the preceding limitations are not necessary for pulse-shaper materials, and that the requirements may not always be applicable for different classes of materials. In particular, when testing some very brittle materials, such as ceramic, and composites, and rock, if these materials were selected to fabricate pulse shapers, such pulse shapers may

fail completely prior to the achievement of tailored incident pulse and stress equilibrium due to their small failure strains. A tailored incident pulse, with a relatively long rise time, is unlikely to be obtained. Our current work shows that it is not necessary to choose the same material as the test sample for a pulse shaper, or to choose similar strength level materials as the test sample. However, a high-work hardening rate is a necessary property for pulse-shaper materials employed for high-work-hardening test materials. Furthermore, it appears that pulse-shaper materials should not necessarily be limited to soft materials. Clearly, soft materials (such as brass, plexiglass, polymer, copper, and low-strength stainless steel), which are not similar to the test samples, can be employed for shaping incident pulses, because they can easily deform plastically to a relatively large strain without fracture. However, these soft material pulse shapers, which display relatively modest work-hardening rates and often flat or modest hardening stress strain responses (particularly at high strain rates) are limited in their ability to maintain the constant amplitude reflected pulses required to achieve constant strain rates, when the samples exhibit high-work-hardening rates. Mostly, all the soft materials have low impedance, and it is difficult to obtain dynamic equilibrium. Generally, in such case a pulse shaper is used to shape the loading profile of the incident pulse and to achieve the desired effect.

In this part of the research significant results of stress v/s strain behavior of dry Eglin sand at constant density at $\rho = 1.57$ g/cm^3 using different pulse shapers are presented (Figures 5.38 to 5.41). A minimum of three tests were conducted using three different kinds of pulse shapers each for repeatability and accuracy. The pulse shapers which were used were lead (Pb), aluminium (Al2024) and annealed copper (C360). These

tests were conducted with a Eglin sand of sieve size 40 (425-500 μm) for all cases. The pulse shapers were punched out to a disk of 2mm thickness and 0.25 inch in diameter. It was observed that lead pulse shaper gave the highest amount of stress values compared to others (refer Figure 5.41 and Table 5.4 for values). Also, Pb pulse shaper gave higher strain rate values compared to other over a sustained period of time. Hence, in the further research work it was recommended to use Pb pulse shapers.

5.3.6.1 Tests using Lead (Pb) pulse shapers

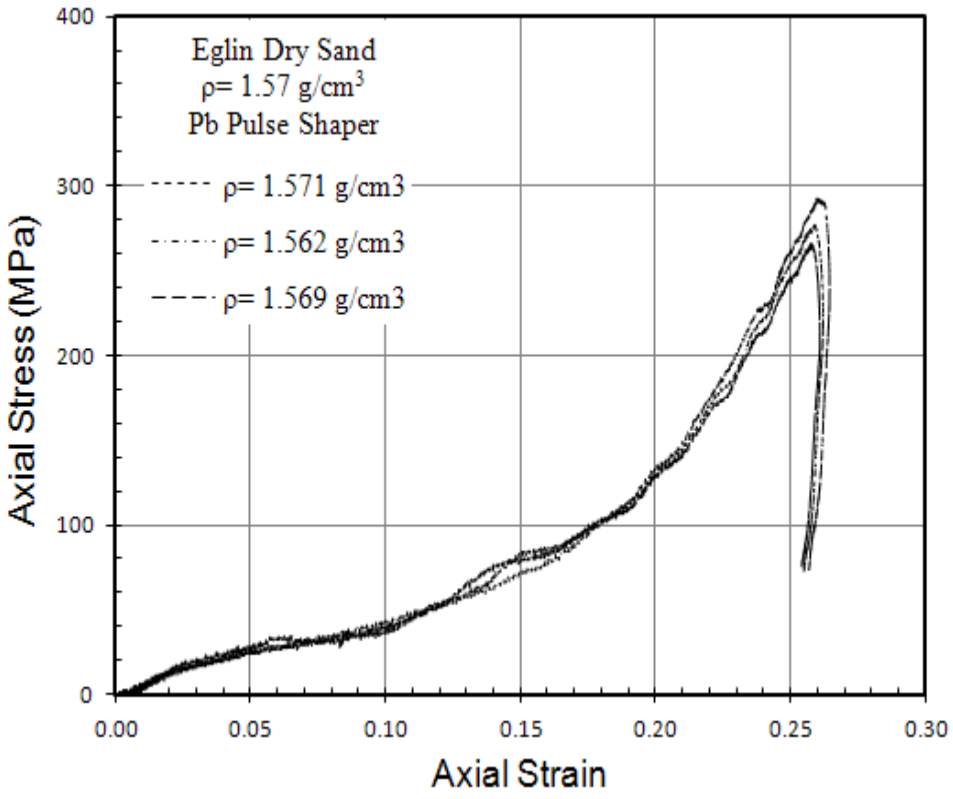

Figure 5.38: Reproducibility of SHPB test data of dry Eglin sand at nominal density of ρ= 1.57 g/cm^3; axial stress-strain of sand using Pb pulse shaper

5.3.6.2 Tests using annealed Copper disk pulse shapers

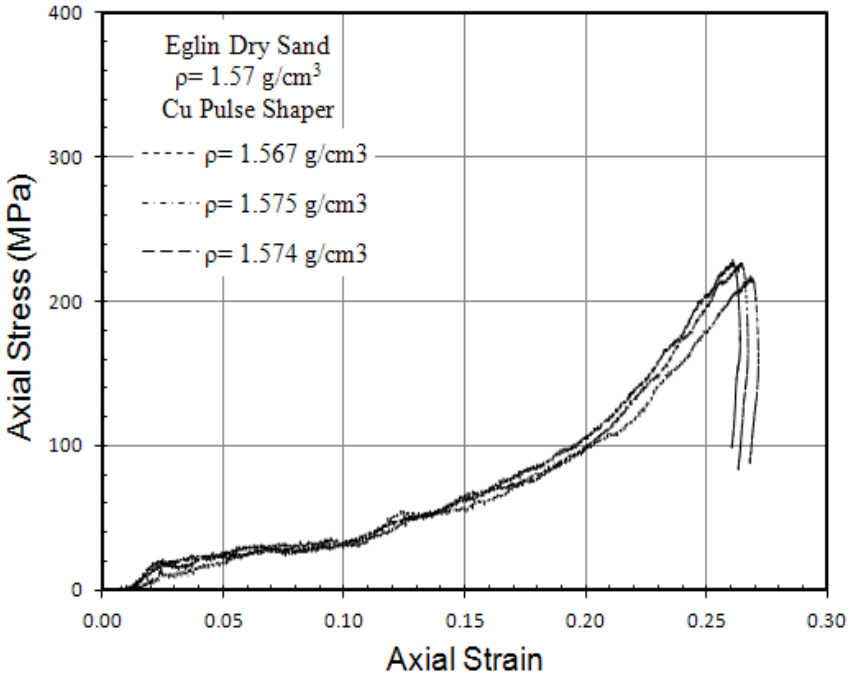

Figure 5.39: Reproducibility of SHPB test data of dry Eglin sand at nominal density of ρ= 1.57 g/cm^3; axial stress-strain of sand using an annealed Cu pulse shaper

5.3.6.3 Tests using aluminum disk pulse shapers

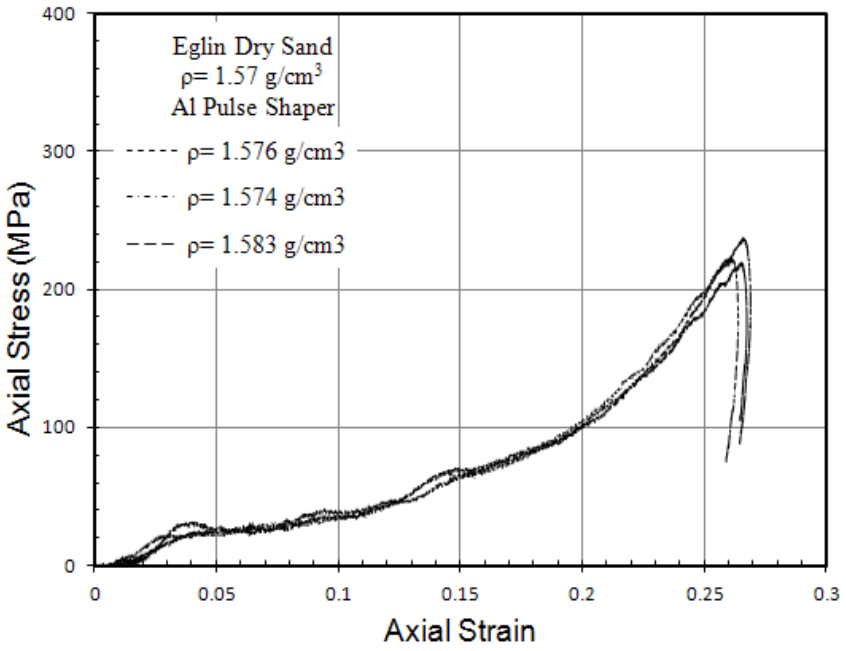

Figure 5.40: Reproducibility of SHPB test data of dry Eglin sand at nominal density of ρ= 1.57 g/cm^3; axial stress-strain of sand using Al pulse shaper

5.3.6.4 Stress-strain relationship using different kind of pulse shapers

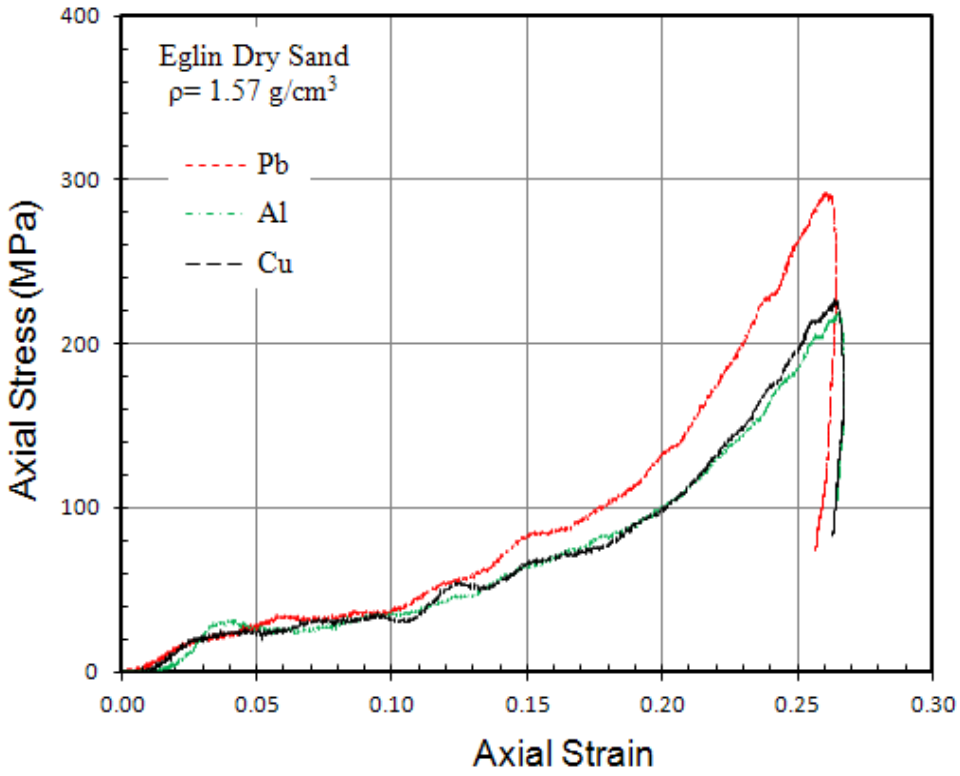

Figure 5.41: Results of axial stress-strain experimental plots of dry sand in SHPB tests with different pulse shapers (Pb,Al, and annealed Cu)

Table 5.4 provides us with the values of the maximum stress and maximum strain achieved in our test conducted on effect of using different pulse shapers at constant density of Eglin sand.

Table 5.4: Maximum stress and maximum strain values obtained for three different pulse shapers

Pulse Shaper	Max Stress (MPa)	Max Strain
Annealed Cu	230	26.2%
Al	225	26.2%
Pb	292	25.5%

5.3.7 Effect of Particle size of sand at constant nominal density ($\rho = 1.57$ g/cm^3)

For the study on the effect of particle size on the dynamic behavior of Eglin sand, experiments were conducted on dry Eglin sand of four grain sizes, namely, (a) passing sieve size #20 but stopped by sieve size #30 (20-30) (b) passing sieve size #40 but stopped by sieve size #50 (70-100) (c) passing sieve size #70 but stopped by sieve size #100 and (d) passing sieve size #100 but stopped by sieve size #150. These sand sizes are sieve sizes 20, 40, 70 and 100 given in the graphs of stress strain plot respectively. The particle size varied from 150 μm to 850 μm. All tests were conducted at approximately a constant density of $\rho = 1.57$ g/cm^3. At least five tests were conducted for each particle size at $\rho = 1.57$ g/ cm^3 to achieve repeatability and accuracy. Lead (Pb) pulse shaper was used for all the tests as Pb gives the highest stress values and higher strain rates compared to aluminum pulse shaper or annealed copper pulse shapers. This was concluded from the observation mentioned earlier. Figures 5.42 to 5.45 show the axial stress-strain responses of sand particles. The smaller particles or fine sand of sieve size #70-100, showed a stiffer response as compared to the larger particles or coarser sand of sieve sizes #20-40. Another thing to notice was the maximum strain values obtained in all of these tests for respective particle sizes. The finer sand (sieve size #100) had an increased value of slope giving high stress values (stiffer in nature) but on the other hand had the deformation lowest of all. The coarser sand (sieve size #20) had the least value of slope giving the lowest stress values but on the other hand had the largest deformation or largest strain rates (refer to Figure 5.46 and Table 5.5 for more details)

The results of tests conducted on the effect of particle size on the stress-strain behavior of sand are presented in Figures 5.42 through 5.46. Eglin sand was mechanically

separated into coarse and fine grains using various sieves sizes in the mesh. The coarser grains attain lower stresses at the maximum axial strain of 27.2% as compared to the finer sand grains. About 50% by weight of Eglin sand contains particles in the sieve size of 40 through 50. The 20-30 and 70-100 particles constitute 9% and 7% of Eglin sand by weight, respectively. Test results show that the fine grains exhibit the highest stiffness, while the coarse grains show the least stiffness. This is explained by the distribution of stresses between the sand particles. In coarse sand, the average numbers of inter-particle contacts are higher than that in loosely packed sand. The high inter-particle contacts correspond inversely to the stresses arising between the particles. Thus, coarse sand has higher inter-particle stresses leading to particle fracture at lower axial stresses. The fracture of sand particles also aid in the rearrangement and rotation of sand grains, leading to collapse of voids. Fine grain sand breaks down at higher stresses while coarse grain sand start collapsing at lower stresses. The high stiffness of fine grain sand is due to restricted rearrangement of the sand grains and rapid collapse of voids. The radial, hydrostatic and shear stress-strain curves show similar trends.

5.3.7.1 Tests using Dry Eglin Sand particle size = 150 -180 µm (sieve size 100)

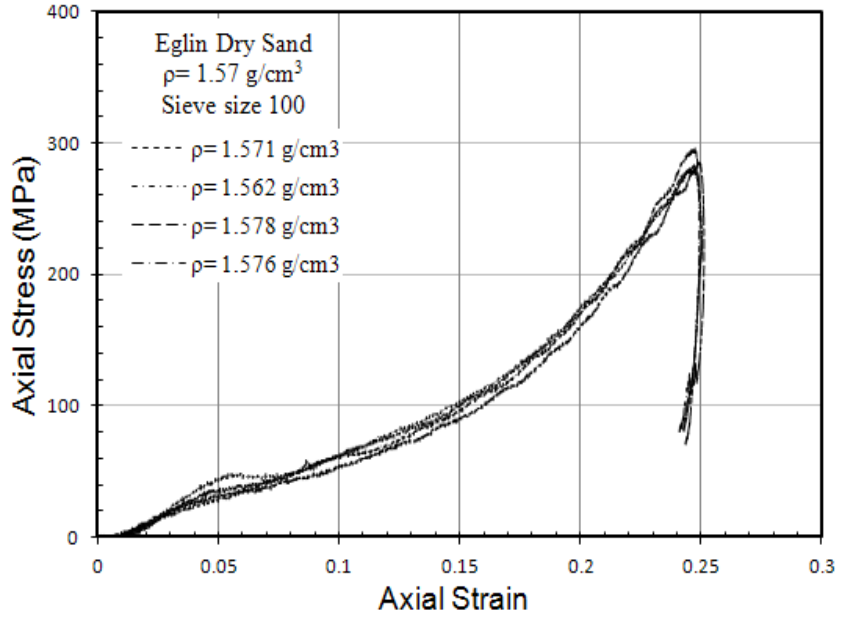

Figure 5.42: Reproducibility of SHPB test data of dry Eglin sand in SHPB tests at nominal density of ρ = 1.57 g/ cm^3; axial stress-strain of sand for particle of sieve size 100

5.3.7.2 Tests using Dry Eglin Sand particle size = 212 µm (sieve size 70)

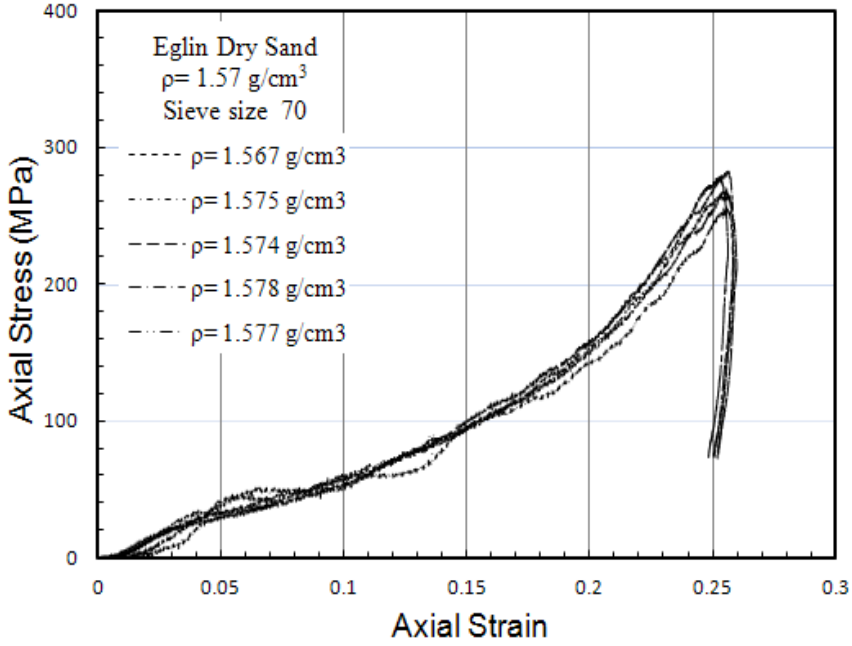

Figure 5.43: Reproducibility of SHPB test data of dry Eglin sand in SHPB tests at nominal density of ρ = 1.57 g/ cm^3; axial stress-strain of sand for particle of sieve size 70

5.3.7.3 Tests using Dry Eglin Sand particle size = 425-500 µm (sieve size 40)

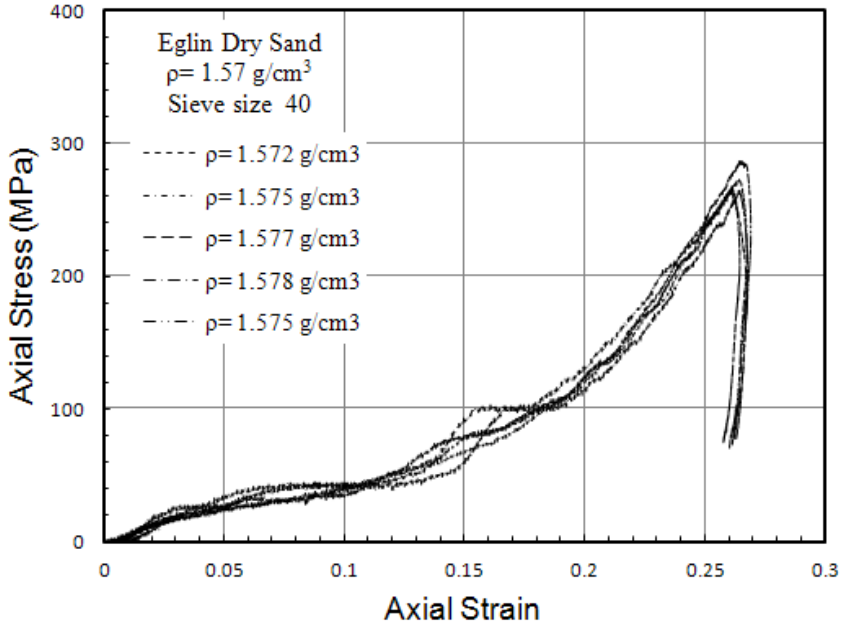

Figure 5.44: Reproducibility of SHPB test data of dry Eglin sand in SHPB tests at nominal density of ρ = 1.57 g/ cm^3; axial stress-strain of sand for particle of sieve size 40

5.3.7.4 Tests using Dry Eglin Sand particle size = 850 µm (sieve size 20)

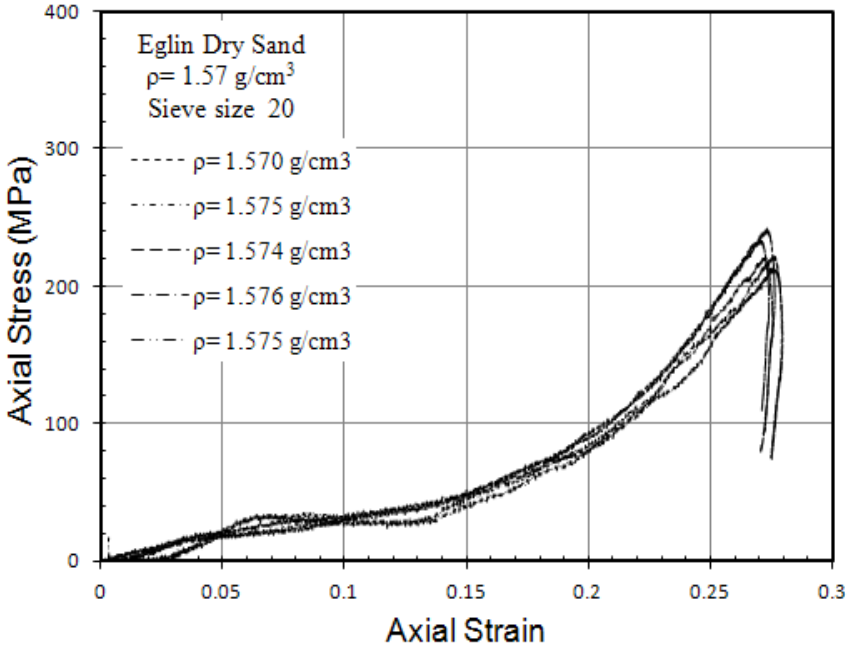

Figure 5.45: Reproducibility of SHPB test data of dry Eglin sand in SHPB tests at nominal density of ρ = 1.57 g/ cm^3; axial stress-strain of sand for particle of sieve size 20

Figure 5.46 shows the result of four different particle sizes used at same constant density of dry Eglin sand ($\rho = 1.57$ g/cm^3)

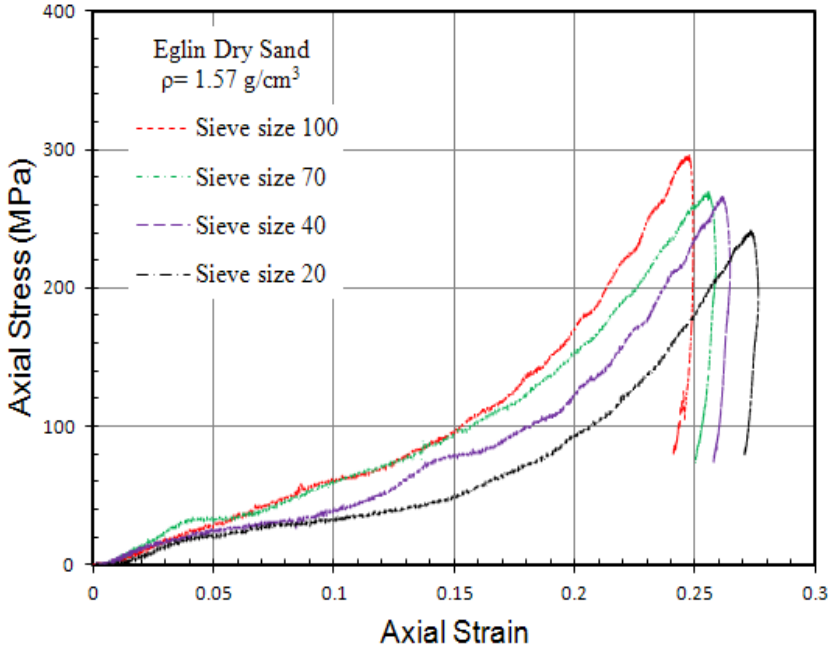

Figure 5.46: Results of axial stress-strain experimental plots of dry sand at a nominal density of $\rho = 1.57$ g/ cm^3 and different sieve sizes (20 to 100)

Table 5.5: Maximum stress and maximum strain values obtained for each particle size at constant density of $\rho = 1.57$ g/ cm^3

Sieve sizes	**Max Stress (MPa)**	**Max Strain**
20	242	27.2%
40	269	26.1%
70	272	25.8%
100	298	24.9%

Table 5.5 provides us with the values of the maximum stress and maximum strain achieved in the tests conducted on effect of using different particle sizes at constant density of Eglin sand. Clearly, fine sand gave higher stiffness values compared to coarse sand.

CHAPTER VI

CONCLUSIONS

In SHPB tests, the mechanical behavior of materials, such as aluminum, copper, and sand have been investigated using high-speed photographic images of the deformation using DIC analysis. The results obtained from DIC analysis of copper sample are directly compared to the stress-strain plots of copper ensuring the validity of the SHPB setup designed and built at OSU.

The dynamic compressive behavior of dry sand (from Eglin AFB) under stiff confinement, namely, sand particle in a steel cylindrical tube was investigated using a modified long split Hopkinson pressure bar (SHPB) at high strain rates (650~800 s^{-1}) and compressive stress of up to 400 MPa. A sand specimen assembly consists of a steel tube with ends covered by WC inserts. The assembly allows shaking of the sand to consolidate it with consistent initial mass densities. Sand samples of three initial mass densities (1.51, 1.57, and 1.63 g/cm^3) were compressed upto axial strains of 30% at high strain rates. The deviation of sand axial stress-strain curves is in the range of 3.27% ~ 10.3% indicating highly repeatable SHPB data, especially at higher initial mass density. The curves of axial stress-axial strain of sand are determined up to compressive strain of 29%, and up to 360 MPa axial compressive stresses at high strain rates. Significant density effects and particle size effects have been identified.

An experimental investigation was conducted to determine the uniaxial stress-strain behavior of Eglin sand up to axial pressure of ~ 400 MPa. Dynamic uniaxial tests were conducted to primarily investigate three parameters that affect the behavior of sand, namely, initial mass density, effect of particle size, and effect of pulse shapers. Investigations of these parameters on sand consolidation have not been reported in the literature. All tests were conducted up to a axial strain of 30% at constant strain rate of ~ $750s^{-1}$. Three tests were conducted for each test parameter to ensure repeatability. The results show that dense sand is less compressible than loosely packed sand. The slope of the stress-strain curves show that dense sand exhibit higher stiffness compared to less dense sand. The void ratio curves of different densities merge along a single path as the grain crushing approaches completion. Tests conducted on coarse and fine sand grains at 1.57 g/cm^3 show a significant effect of particle size on the stress-strain behavior of sand. Fine grain sand showed significantly higher stiffness values as compared to coarse grain sand. Also, deformation of sand was observed using the high speed photography unit.

CHAPTER VII

FUTURE WORK

Suggestions for further tests on Dry Eglin sand includes a better understanding of the stress-strain behavior, or mechanical characterizations under dynamic loads. They include

a) Use of a high pressure pneumatic system to attain higher stresses and higher strain rates values. Going up in pressure will ensure that the velocity of the striker bar is varied accordingly to achieve higher stresses and higher strain rate values.
b) The effect of different confinement materials such as PMMA tube, PVC tube and different geometries can be investigated.
c) The role of particle size can be further investigated by mixing sand particles of different sizes in known proportions. The resulting stress-strain behavior can be characterized and compared with samples of individual sand particle grain size.
d) Effect of pulse shapers can be further explored using different pulse shapers at different sand densities. Also, in this research round disk shaped pulse shapers were used, and it would be very interesting to see if changing the geometry of the shape of pulse shaper makes any difference in the mechanical behavior of the sample.

e) High speed photography and DIC analysis on the dry Eglin sand is probably the biggest and most challenging future work that needs to be done. If we could capture the fracturing of sand particle with the help of high-speed photography, then it will enable a better understanding of the sand behavior.

f) Varying the moisture content in the dry Eglin sand sample and investigating the effect of it on the mechanical behavior of sand would be immediate next research topic of significance to this project.

REFERENCES

1. Gama, B.A., *Split Hopkinson Bar Technique: Experiments, Analyses and Applications.*Ph.D dissertation, University of Delaware, Spring 2004.
2. Chen. W, Song. B, *Loading and Unloading SHPB Pulse shaping Techniques for Dynamic Hysterectic Loops* Society for Experimental Mechanics, december 2004. 44: p. 622-627.
3. Kolsky. H, *An Investigation of the Mechanical Properties of Materials at Very High Rates of Strain.* Proc. Roy. Phys. Soc, 1949. B 62: p. 676-700.
4. Kaiser, M.A., *Advancements in the Split Hopkinson Bar Test.*M.S. Thesis, Virginia State University, May 1998.
5. Luo H, Lu. H, Cooper W, Komanduri R, *Effect of Mass Density on the Compressive Behavior of Dry Sand under Confinement at High Strain Rates.* Experimental Mechanics, 2010.
6. Charlie, W.A., Ross, C.A., Pierce, S.J., *Split-Hopkinson pressure bar testing of unsaturated sand.* Geotechnical Testing Journal GTJODJ 1990. 13 (4): p. 291–300.
7. Semblat. J.F, *Soils under dynamic and transient loadings : dynamic response on Hopkinson bars, wave propagation in centrifuged medium.* Laboratoire Central des Ponts & Chaussées, Paris, March 1995: p. 212 p.

8. Semblat J.F, Gary. G., Luong M.P., *Dynamic response of sand using 3D-Hopkinson Bar.* 1st International Conf. on Earthquake Geotechnical Engineering, Tokyo, November 1995: p. 14-16

9. Shibusawa. S., Oida. A., *Dependency of observation parameters on soil dynamic parameters in unconfined impact compression tests.* Jal of Terramechanics, 1992. 29: p. 289-306.

10. Mitchell, J.K., Soga. K., *Fundamentals of Soil Behavior.* John Wiley & Sons, Hoboken, NJ, 2005. 3rd Edition.

11. Li, H., Yang, H., Chang, C. and Sun, X, *Experimental Investigation on Compressive Strength of Frozen Soil versus Strain Rate.* Journal of Cold Regions Engineering, 2001. 15: p. 125-133

12. Li. X, Yang. W. L, *Effects of Vibration History on Modulus and Damping of Dry Sand.* Journal of Geotechnical and Geoenvironmental Engineering, 1998. 124 (11): p. 1071-1081

13. Bragov, A.M., Grushevsky, G. M., Lomunov, A.K., *Use of the Kolsky Method for Confined Tests of Soft Soils.* Exp. Mech, 1996. 36(3): p. 237-242.

14. Bragov, A.M., Lomunov, A. K., Sergeichev, I. V., Tsembelis, K., Proud, W.G, *Determination of physiomechanical properties of soft soils, from medium to high strain rates.* Int. J. Imp. Eng., 2008. 35: p. 967-976.

15. Ross, C.A., Nash, P. T., Friesenhahn, G. J., *Pressure Waves in Soils Using a Split-Hopkinson Pressure Bar.* ESL-TR-86-29, Air Force Engineering and Services Center, Engineering and Services Laboratory, Tyndall AFB, FL, 1986.

16. Pierce, S.J., *High Intensity Compressive Stress Wave Propagation through Unsaturated Sands.* Review of Scientific Instruments 1989. 70 (10): p. 4055-4058.

17. Felice, C.W., Brown, J. A., Gaffney, E. S., Olsen, J. M, *An Investigation into the High Strain rate behavior of Compacted Sand Using the Split-Hopkinson Pressure Bar Technique.* Proceedings of the 2nd Symposium on the Interaction of Non-Nuclear Munitions with Structures, 1987b: p. 391-396.

18. Veyera, G.E., *Uniaxial Stress–Strain Behavior of Unsaturated Soils at High Strain Rates.* Wright Laboratory, 1994.

19. Felice, C.W., Gaffney, E.S., Brown, J. A., Olsen, J. M, *Dynamic High Stress Experiments on Soil.* Geotechnical Testing Journal GTJODJ, 1987a. 10(4): p. 192-202.

20. Veyera, G.E., Hampton, D., Wetzel, R. A., , *Stress Wave Propagation in Confined Soils.* American Society for Testing and Materials, 1988: p. 421-459.

21. Song, B., Chen, W., Luk, V., *Impact Compressive Response of Dry Sand.* Mech. Mater, 2009. 41 (6): p. 777–785.

22. Chen, W., Lu, F., Frew, D. J., and Forrestal, M. J, *Dynamic Compression Testing of Soft Materials.* Journal of Applied Mechanics, 2002. 69 [3]: p. 214-223

23. Frew, D.J., Forrestal, M. J., and Chen, W, *Pulse-Shaping Techniques for Testing Brittle Materials with a Split Hopkinson Pressure Bar.* Experimental Mechanics, 2002. 42 (1): p. 93-106

24. Frew, D.J., Forrestal, M. J., and Chen, W, *Pulse Shaping Techniques for Testing High- Strength Steel with a Split Hopkinson Pressure Bar*. Experimental Mechanics, 2005. 45 (2): p. 186- 195

25. Brown, J.L., Vogler, T.J., Chhabildas, L.C., Reinhart, W.D., Thornhill, T.F., *Shock Responses of Dry Sand.* Sandia National Laboratories, 2007.

26. Hopkinson, B., *A method of measuring the pressure produced in the detonation of high explosives or by the impact of bullets.* Philos. Trans. R. Soc. Lond. Ser. A 213, 1914: p. 437–456.

27. Follansbee, P.S., . *The Hopkinson Bar*. ASM Handbook, Materials Park, OH, 1985: p. 198–207.

28. Lindholm, U.S., *Some Experiments with the Split Hopkinson Pressure Bar.* J. Mech. Phys. Solids, 1964. 12: p. 317-335.

29. Nemat-Nasser, S., Isaacs, Jon B., Starrett, John E., *Hopkinson techniques for dynamic recovery experiments.* Proc. R. Soc. Lond.Ser. A A435, 1991: p. 371–391.

30. Gray III, G.T., *Classic Split-Hopkinson Pressure Bar Testing.* Mechanical Testing and Evaluation, Metals Handbook, American Society for Metals, 2000: p. 462-476.

31. Follansbee, P.S., and Franz, C. E., *Wave Propagation in the Split Hopkinson Pressure Bar*. Trans. ASME, J. Eng. Mat. Technol, 1983. 105: p. 61-66

32. Subramanian, V., *Quasi static compression of Granular materials (sand) at High pressure(3GPa).* M.S. Thesis, Oklahoma State University, December 2010.

33. Gray III, G.T., *High-Strain-Rate Testing of Materials: The Split-Hopkinson Pressure Bar*. Los Alamos National Laboratory, 1997.

34. Gray III, G.T., Blumenthal, W. R, *Split-Hopkinson Pressure Bar Testing of Soft Materials.* Mechanical Testing and Evaluation, Metals Handbook, American Society for Metals, 2000.: p. 488-496.

35. Saouma.V., Cintron .R., *Strain Measurements with the Digital Image Correlation System Vic-2D.* Center for Fast Hybrid Testing; Department of Civil Environmental and Architectural Engineering; University of Colorado, sept 2008.

36. Luo H., Lu.H., Leventis N., *The compressive behavior of isocyanate-crosslinked silica aerogel at high strain rates.* Mech Time-Depend Mater, 2006(10.1007/s11043-006-9015-0).

37. Lu, H., Vendroux, G., Knauss, W.G, *Surface deformation measurements of a cylindrical specimen by digital image correlation.* Exp. Mech. 37(4), 2000: p. 433–439.

38. Lu, H., Cary, P.D., *Deformation measurements by digital image correlation: Implementation of a second-order displacement gradient.* Exp. Mech. 40(4), 2000: p. 393–400.

39. Knauss, W.G., Zhu, W, *Nonlinearly viscoelastic behavior of polycarbonate. I. Response under pure shear.* Mech. Time. dep. Mater. 6(3), 2002: p. 231–269.

40. Hagerty M.M., H.D.R., Ullrich C.R., and Hagerty D.J., *One dimensional high-pressure compression of granular media.* Journal of Geotechnical Engineering, 1993. 119(1): p. 1–18.

41. Ellwood S., Griffiths L.J., Parry D.J., J Phys. E: Sci Instrum., 1982(15) p280-82

VITA

SWAPNIL SANKAYE

Candidate for the Degree of

Master of Science

Thesis: DYNAMIC TESTING TO DETERMINE SOME MECHANICAL PROPERTIES OF ALUMINUM, COPPER, AND DRY EGLIN SAND USING SPLIT HOPKINSON PRESSURE BAR (SHPB), HIGH SPEED PHOTOGRAPHY, AND DIGITAL IMAGE CORRELATION (DIC).

Major Field: Mechanical Engineering

Biographical:

Personal Data: Born in Aurangabad, Maharashtra, India, on June 17, 1986 son of Late Mr Shivling Sankaye and Mrs Mangala Sankaye.

Education: Received Bachelor of Engineering degree in Mechanical Engineering from Government Engineering College of Aurangabad (GECA), India, in June 2008.

Experience: Graduate Research Assistant in Mechanical and Aerospace Engineering Department, Oklahoma State University, Stillwater, Oklahoma, May 2009-May 2011

Teaching Assistant in Mechanical and Aerospace Engineering Department, Oklahoma State University, Stillwater, Oklahoma, August 2009 – December 2010.

Name: SWAPNIL SANKAYE Date of Degree: July, 2011

Institution: Oklahoma State University Location: Stillwater, Oklahoma

Title of Study: DYNAMIC TESTING TO DETERMINE SOME MECHANICAL PROPERTIES OF ALUMINUM, COPPER, AND DRY EGLIN SAND USING SPLIT HOPKINSON PRESSURE BAR (SHPB), HIGH SPEED PHOTOGRAPHY AND DIGITAL IMAGE CORRELATION (DIC).

Pages in Study: 100 Candidate for the degree of Master of Science

Major Field: Mechanical Engineering

Scope and Method of Study: This investigation presents the results on dynamic behavior of aluminum, copper, and dry Eglin sand the later confined in a hollow steel tube. The sand from Eglin Air Force Base was subjected to axial compressive stresses of up to 400 MPa. A high-speed camera is used to capture digital images of the deformation of the copper sample. Digital image Correlation (DIC) analysis was used to compare the strain values obtained from wave propagation theory. Strain gages were mounted on the pressure bars to measure the axial stresses and axial strains in the sample. Using these axial stress, axial strain, and DIC analysis, the dynamic behavior of the confined sand and metal samples were investigated.

Findings and Conclusions: Compression tests were conducted up to axial strains of 30%. The dynamic response of the dry sand was tested at three initial mass densities, namely, 1.51, 1.57 and 1.63 g/cm^3. Effect of particle size (primarily classified as coarse and fine) were investigated. The effect of pulse shaper was also investigated using three different pulse shapers, namely, Al, Cu, and Pb at a nominal sand density of 1.57 g/cm^3. Dense sand provided a much stiffer response than the loosely packed ones. It was observed that coarse sand grains to crush to smaller particles and this were followed by compression of sand into powder sand.

ADVISER'S APPROVAL: RANGA KOMANDURI